KINETIC VASCULOGENIC ANALYSES OF ENDOTHELIAL COLONY FORMING CELLS EXPOSED TO INTRAUTERINE DIABETES

Kaela Margaret Varberg

Submitted to the faculty of the University Graduate School
in partial fulfillment of the requirements
for the degree
Doctor of Philosophy
in the Department of Cellular & Integrative Physiology,
Indiana University

July 2017

Accepted by the Graduate Faculty, Indiana University, in partial fulfillment of the requirements for the degree of Doctor of Philosophy.

Doctoral Committee

Laura S. Haneline, M.D., Chair

Matthias A. Clauss, Ph.D.

Richard N. Day, Ph.D.

May 11, 2017

Maureen A. Harrington, Ph.D.

Edward F. Srour, Ph.D.

DEDICATION

This thesis is dedicated to the many teachers and mentors that have been a part of my educational journey. I am grateful for the patience you have shown me, and the knowledge and wisdom you have shared with me. I am continually inspired to reimagine my professional goals because of your unwavering confidence and support.

> “Teaching is more than imparting knowledge, it is inspiring change.”
>
> –William Arthur Ward

ACKNOWLEDGEMENTS

I would like to start by recognizing and thanking my mentor, Dr. Laura Haneline. I am grateful to have had the opportunity to be mentored by you. It's no secret that taking on a graduate student is risky business, so I thank you for taking a chance on me, and welcoming me into the lab as first-year student. I have truly enjoyed our meetings and discussions over the years, and I know it has helped shape me as a scientist, critical thinker, presenter, and writer. Your leadership skills are truly admirable, and I know the example you have set will serve as a long-lasting guide for me as I continue to develop in my career. It has been an honor to work for you and with you, and I hope to make the most of the opportunities you have provided for me.

To members of my research committee, including Dr. Richard N. Day, Dr. Maureen A. Harrington, Dr. Edward F. Srour, and Dr. Matthias A. Clauss. Thank you for generously giving your time and attention to overseeing the successful completion of my research projects and, ultimately, my degree over the last four years. Your support, guidance, and mentorship have helped me develop as a professional and an independent investigator. The feedback you have provided has made invaluable contributions to this research.

I would like to recognize the contributions of the lab mates I have had throughout my time in the Haneline lab. Emily, thank you for training me and for providing feedback and input throughout my time in the lab. Cassie, thank you for going through graduate school with me and for providing feedback and support along the way. I would also like to acknowledge my lab mentee, Rashell Garretson, for providing a positive experience for me as I worked to develop mentoring and training skills in the lab. Kim and Shelly, thank you for training me in my early days in the lab. Several other students and fellows have

enhanced and contributed to my lab experience over the years and they include: Zia Nuss, Dr. Bre Sheehan, Cavya Chandra, Dr. Sarah Rust, Amna Sohail, Dr. Lauren Kneller, and Lauren Gilliland.

I have had the great fortune throughout my time at the Indiana University School of Medicine to collaborate with several individuals across campus. First, I would like to thank members of the Simon Cancer Center Flow Cytometry Facility for their services and expertise. I would especially like to thank Sue Rice and Kim Stoner for their help with single cell flow sorts. I would also like to recognize the Indiana Center for Biological Microscopy at the Indiana University School of Medicine for their services and imaging expertise. All confocal and overnight imaging experiments highlighted in this dissertation were carried out at the ICBM. Ken, thank you for the scholarly discussion and brainstorming sessions. Gosia, thank you for patiently training me on the microscopes and for providing support as well as constructive feedback. Seth, thank you for the countless hours you have devoted to successful completion of the microscopy experiments in this project. It should be noted that much of the new methodology used to perform these studies was made possible by the software (including KAV and VTEA) that you developed. I have greatly enjoyed collaborating with you, and I know the technical and critical thinking skills you have taught me will continue to make me a better scientist throughout my career.

I have benefitted from working with several labs in my home department, the Department of Cellular & Integrative Physiology, and would, therefore, like to recognize those labs and individuals who have specifically contributed to my training. I thank Dr. Sturek and Dr. Anderson for giving me the opportunity to rotate in their labs first year. I enjoyed all my rotations, and am grateful for the opportunities to work in different model systems. I would

like to recognize Dr. Day, Dr. Gunst, Dr. Angelia Lockett, Rita O'Riley, and Dr. Pavalko for graciously providing support and resources for experimental development. I would also like to recognize Dr. Tune for being a great advisor and resource, especially during the qualifying exam and thesis writing processes. To Dr. Basile, Dr. Elmendorf, Dr. Obukhov, Dr. Herring, and Dr. Gallagher, thank you for teaching memorable courses, and for providing constructive feedback over the years.

I would also like to thank the IU School of Medicine Graduate Office for providing critical support and resources to help me be successful throughout my time in the program. I appreciate the efforts you have made to improve the program, such that the resources and workshops you offer are relevant and reflect current challenges facing students in the biomedical sciences today. Your support of student groups, like networkIN, have made it possible for me to develop important leadership skills during my time at IUSM. Tara and Brandy, thank you for encouraging me to get involved and give back to the IBMG program. I enjoyed participating in recruitment and educational sessions for new students, and I know that these experiences and soft skills will serve me well in the future. Lauren, thank you for supporting networkIN and for providing valuable programming opportunities. Tricia, thank you for helping me craft my application materials so that I could successfully secure a job after graduation. Val, thank you for being a bright, shining presence in the office.

There are several other individuals who have contributed, in a variety of ways, to the completion of this work. I would like to recognize Lucy Miller, Leanne Hernandez, Dr. David Haas, and Brittany Yeley from Eskenazi Health and the Indiana University School of Medicine for their contribution to consenting patients for studies and obtaining umbilical cord blood samples. Members of the Angio BioCore at the Indiana University Simon

Cancer Center, including Dr. Karen Pollok, Julie Mund, Matthew Repass, and Emily Sims, were instrumental in isolating ECFCs from umbilical cord blood samples. Acquisition of patient data was made possible by contributions from previous doctoral fellows that rotated in the laboratory, including Dr. Bre Sheehan, Dr. Riddhi Shukla Dr. Sarah Rust, and Dr. Lauren Kneller. I would like to thank members of the Yoder laboratory, including Dr. Mervin Yoder, Mike Ferkowicz, and Yang Lin, for scholarly discussion and technical assistance. I would also like to recognize Elizabeth Rybak and Janice Walls for outstanding administrative support. Byron Varberg, my brother-in-law, should be recognized for saving me countless hours of image processing by graciously designing image merging software. Importantly, his contribution not only benefitted me, but others in the laboratory, who still use it to this day.

Finally, I would like to thank my husband, Joe, for his love and support throughout the pursuit and completion of this degree. Working toward a PhD together created new challenges and times of great stress, however, your support and encouragement made it manageable. I have felt very fortunate to share in this experience with you. And, to our families, thank you for supporting us throughout this process and for constantly encouraging us to be the best people we can be.

The research outlined in this dissertation was made possible by a T32 Training Fellowship from the National Heart, Lung, and Blood Institute of The National Institutes of Health granted to Dr. Hal Broxmeyer in the Department of Microbiology and Immunology at the Indiana University School of Medicine (Award #T32HL007910). In addition, this research was supported by the National Institutes of Health in grants awarded to Dr. Laura Haneline (R01 HL094725, P30 CA82709, and U10 HD063094) as well as the Riley Children's Foundation.

Kaela Margaret Varberg

KINETIC VASCULOGENIC ANALYSES OF ENDOTHELIAL COLONY FORMING CELLS EXPOSED TO INTRAUTERINE DIABETES

Vasculogenesis is a complex process by which endothelial stem and progenitor cells undergo *de novo* vessel formation. Quantitative assessment of vasculogenesis is a central readout of endothelial progenitor cell functionality. However, current assays lack kinetic measurements. To address this issue, new approaches were developed to quantitatively assess *in vitro* endothelial colony forming cell (ECFC) network formation in real time. Eight parameters of network structure were quantified using novel Kinetic Analysis of Vasculogenesis (KAV) software. KAV assessment of structure complexity identified two phases of network formation. This observation guided the development of additional vasculogenic readouts, including a tissue cytometry approach to quantify the frequency and localization of dividing ECFCs within cell networks. Additionally, FIJI TrackMate was used to quantify ECFC displacement and speed at the single cell level during network formation. These novel approaches were then applied to determine how intrauterine exposure to maternal type 2 diabetes mellitus (T2DM) impairs fetal ECFC vasculogenesis, and whether increased Transgelin 1 (TAGLN) expression in ECFCs from pregnancies complicated by gestational diabetes (GDM) was sufficient to impair vasculogenesis. Fetal ECFCs exposed to maternal T2DM formed fewer initial network structures, which were not stable over time. Correlation analyses identified that ECFC samples with greater division in branches formed fewer closed network structures and that reductions in ECFC movement decreased structural connectivity. To identify specific cellular mechanisms and signaling pathways altered in ECFCs following intrauterine GDM exposure, these new techniques were also applied in TAGLN expression studies. Similarly, ECFCs from GDM

pregnancies and ECFCs overexpressing TAGLN exhibited impaired vasculogenesis and decreased migration. Both ECFCs from GDM pregnancies as well as ECFCs over-expressing TAGLN exhibited increased phosphorylation of myosin light chain. Reduction of myosin light chain phosphorylation via Rho kinase inhibition increased ECFC migration; therefore, increased TAGLN was sufficient to impair ECFC vasculogenic function. Overall, identification of these novel phenotypes provides evidence for the molecular mechanisms contributing to aberrant ECFC vasculogenesis. Determining how intrauterine exposure to maternal T2DM and GDM alters fetal ECFC function will enable greater understanding of the chronic vascular pathologies observed in children from pregnancies complicated by diabetes mellitus.

Laura S. Haneline, M.D., Chair

TABLE OF CONTENTS

LIST OF TABLES

LIST OF FIGURES

LIST OF ABBREVIATIONS

ADAM: A Disintegrin and Metalloproteinase

ANOVA: Analysis of Variance

BMI: Body Mass Index

CI: Confidence Interval

CO_2: Carbon Dioxide

CFI: Chrome Free Infinity

CPDL: Cumulative Population Doublings

DAPI: 6-Diamidino-2-Phenylindole

DAPT: *N*-[(3,5-Difluorophenyl)acetyl]-L-alanyl-2-phenyl]glycine-1,1-dimethylethyl ester

DLL(4): Delta-like Ligand (4)

DM: Diabetes mellitus

DMEM: Dulbecco's Modified Eagle Medium

DNA: Deoxyribonucleic Acid

EBM2: Endothelial Basal Medium 2

EC: Endothelial Cell

ECFC: Endothelial Colony Forming Cell

EGM2: Endothelial Cell Growth Medium 2

EPC: Endothelial Progenitor Cell

EV: Empty Vector

FACS: Fluorescence Activated Cell Sorting

FBS: Fetal Bovine Serum

FDR: False Discovery Rate

FIJI: Fiji is just (a newer versio of) ImageJ

FOAD: Fetal Origins of Adult Disease

FRET: Förster Resonance Energy Transfer

GDM: Gestational Diabetes Mellitus

GFP: Green Fluorescent Protein

HbA1c: Hemoglobin A1c

hESC: Human Embryonic Stem Cell

HES: Hairy/Enhancer of Split gene family

HESR1: Hairy/Enhancer of Split gene receptor 1

HEY1: Hairy/Enhancer of Split-related with YRPW motif 1

hiPSC: Human Induced Pluripotent Stem Cell

HPP: High Proliferative Potential

HPRT: hypoxanthine phosphoribosyltransferase

IF: Immunofluorescence

INF-γ: Interferon gamma

JPEG: Joint Photographic Experts Group

KAV: Kinetic Analysis of Vasculogenesis

LAP: Linear Assignment Problem

LPP: Low Proliferative Potential

MEOX2: Mesenchyme Homeobox 2

MGCV: Mixed GAM Computational Vehicle

MLC: Myosin Light Chain

MLCK: Myosin Light Chain Kinase

MLPC: Myosin Light Chain Phosphatase Complex

MMP9: Matrix Metalloproteinase 9

MODY: Maturity Onset Diabetes of the young

MOI: Multiplicity of Infection

mRNA: Messenger Ribonucleic Acid

NICD: Notch Intracellular Domain

NOD-SCID: Non-obese Diabetic-Severe Combined Immunodeficiency

NP25: Neuronal-Specific Protein 25

PBS: Phosphate Buffered Saline

PDGF: Platelet-derived Growth Factor

PDT: Population Doubling Time

PLAC8: Placenta-specific 8

pMLC: Phosphorylated Myosin Light Chain

qRT-PCR: Quantitative Real-Time Polymerase Chain Reaction

R: A programming language and software environment for statistical computing

RIPA: Radio-immunoprecipitation Assay

ROI: Region of Interest

ROS: Reactive Oxygen Species

RT: Room Temperature

SEM: Standard Error of the Mean

SD: Standard Deviation

SM22α: Smooth Muscle Protein 22-Alpha

SM22β: Smooth Muscle Protein 22-Beta

SORP: Special Order Research Product

TAGLN: Transgelin 1

TAGLN2: Transgelin 2

TAGLN3: Transgelin 3

TC: Tissue Cytometry

TIFF: Tagged Image File Format

TNF-α: Tumor Necrosis Factor Alpha

T1DM: Type 1 diabetes mellitus

T2DM: Type 2 diabetes mellitus

UC: Uncomplicated

UCB: Umbilical Cord Blood

UT: Untreated

VEGF: Vascular Endothelial Growth Factor

VEGFA: Vascular Endothelial Growth Factor A

VEGFR1: Vascular Endothelial Growth Factor Receptor 1

VEGFR2: Vascular Endothelial Growth Factor Receptor 2

VTEA: Volumetric Tissue Exploration and Analysis

VTD: Venous Thromboembolic Disease

VWF: von Willebrand factor

2D: Two-dimensional

3D: Three-dimensional

CHAPTER 1: INTRODUCTION

Vasculogenesis

Vasculogenesis is the dynamic process by which angioblasts in the developing embryo differentiate into endothelial cells and form new vessels in the absence of preexisting vascular structures [1]. Following vasculogenesis, the process of angiogenesis occurs, which involves the expansion of the pre-existing vascular network. Finally, angiogenesis is followed by arteriogenesis, a process where pericytes and vascular smooth muscle cells cover the endothelial vessels to provide stability and modulate vessel perfusion. Vasculogenesis can, therefore, be differentiated from these other modes of vessel formation, as outlined by Carmeliet and Jain (Figure 1) [2]. The establishment of the vascular network is a complex process regulated at several different stages by coordinated molecular mechanisms. Two of the key signaling pathways regulating endothelial cell vasculogenesis are the Notch and vascular endothelial growth factor (VEGF) pathways [3].

Notch signaling is implicated in cell fate determination and differentiation in numerous physiologic processes including limb development, neurogenesis, arterio-venous specification, and vasculogenesis [4,5]. In the vasculature, Notch signaling regulates the dynamic selection of endothelial tip cells, which guide the process of angiogenesis [6]. Four Notch receptors have been identified (NOTCH 1-4) as well as five ligands [JAGGED 1-2 and Delta-like ligand 1, 3, 4 (DLL1, DLL3, DLL4)]. In the endothelium, vascular endothelial growth factor A (VEGF-A) signaling through vascular endothelial growth factor receptor 2 (VEGFR2) up-regulates expression of DLL4 (Figure 2) [7]. Increasing the DLL4 ligand leads to subsequent activation of Notch signaling through binding to NOTCH1 or NOTCH4 on adjacent “stalk” cells. Activation of Notch signaling in adjacent cells restricts tip cell formation, allowing for appropriate tip to stalk cell ratio, which promotes effective

branching [8]. Following Notch receptor activation, the Notch intracellular domain is cleaved by the gamma secretase/presenilin complex and A Disintegrin and Metalloproteinase family proteases [9,10]. The Notch intracellular domain subsequently translocates to the nucleus where it interacts with the CBF1/Su(H)/Lag-1 transcription factor complex and regulates expression of genes such as *MYC, p21, HESR1*, and the Hairy/Enhancer of Split gene family [11]. Downstream Notch effector proteins then act as a feedback loop to modulate VEGF receptor expression. For example, HESR1 decreases VEGFR2 expression in endothelial cells [11]. In addition, the "stalk" cells adjacent to DLL4-expressing cells, undergo NOTCH1-mediated upregulation of vascular endothelial receptor 1 (VEGFR1), also known as Flt-1, and JAGGED1 [12–14]. VEGFR1 is a receptor with high affinity but low activity and acts primarily as a competitive inhibitor of VEGF signaling [13]. Importantly, VEGF signaling occurs in both tip and stalk cells but is thought to induce migration in tip cells, while causing proliferation in stalk cells [15]. Overall, Notch and VEGF signaling are critical to endothelial sprouting in angiogenesis.

In addition to modulating endothelial sprouting, Notch and VEGF are key regulators of cell fate determination. In endothelial progenitor cells (EPCs), Notch signaling is a primary mediator of the negative feedback loop that links VEGF activation with maturation to fully differentiated endothelial cells [16]. These signaling pathways aren't just important in developmental vasculogenesis. Recent studies suggest that some progenitor cells are also capable of undergoing 'postnatal vasculogenesis'. Establishment of neo-vasculature postnatally is an important mechanism for vascular homeostasis and for new vessel formation in response to disease [17]. Therefore, EPCs not only undergo *de novo* vessel formation to establish embryonic vasculature during development, but they also participate in postnatal vasculogenesis. Investigation is ongoing to understand EPC function during vascular development as well as their potential therapeutic use for postnatal vascular

repair [18–22]. The goals of this work are to identify the molecular mechanisms underlying endothelial colony forming cell vasculogenesis, and to determine how intrauterine exposure to maternal diabetes mellitus disrupts these processes and alters endothelial colony forming cell function.

Endothelial Colony Forming Cells

In 1997, Asahara et al. first reported that circulating EPCs incorporate into active sites of angiogenesis. In addition, Asahara et al. were the first to suggest EPCs for use in angiogenic therapies to augment vessel growth in ischemic tissues and to deliver angiogenic regulatory agents [23]. Since that initial report, many attempts have been made to define and characterize EPC populations [24–27]. Currently, the term, 'endothelial progenitor cell,' describes a diverse collection of cell types defined by clonogenic potential and cell surface markers such as CD133, KDR, VE-cadherin, and CD34 [28–30].

One EPC subset, endothelial colony forming cells (ECFCs), is a well-defined cell population that displays key characteristics of an immature EPC. These characteristics include high proliferative potential, self-renewal capacity, and *de novo* vessel formation *in vivo* [17,31,32]. ECFCs reside in endothelium to maintain vascular integrity and circulate in the peripheral blood to facilitate vessel formation or repair [17,33–35]. Moreover, ECFCs are enriched in umbilical cord blood, a non-invasive source for cell acquisition with therapeutic potential [36]. ECFC cord-blood enrichment occurs at 33-36 weeks gestational age and is maintained through the term of the pregnancy [37]. Importantly, umbilical cord blood-derived ECFCs are fetal cells. Thus, initial studies to characterize cord-blood-derived ECFCs focused on functional comparisons with ECFCs isolated from adult peripheral blood [38].

In 2004, a hierarchy of endothelial stem and progenitor cells in adult and umbilical cord blood was identified based on clonogenic and proliferative potential [31]. The hierarchy includes high proliferative potential ECFCs (HPP-ECFCs), low proliferative potential ECFCs (LPP-ECFCs), endothelial cell clusters, and fully differentiated endothelial cells (ECs) (Figure 3). HPP-ECFCs are defined not only by their ability to form large colonies upon initial plating, but also the ability to form secondary and tertiary colonies upon re-plating. Importantly, colonies produced by HPP-ECFCs include all other differentiated cell stages of the hierarchy (LPPs, cell clusters, and ECs). Interestingly, umbilical cord-blood contains a higher frequency of ECFCs with robust clonal proliferative potential compared to adult peripheral blood [31,36]. In two week, single cell colony formation assays, cord blood-derived ECFCs form significantly more HPP-ECFC colonies (2000+ cells) and fewer cell cluster colonies (2-50 cells) compared to adult peripheral blood-derived ECFCs [31]. During 60 days of culture, cord blood-derived ECFCs undergo approximately 40 cumulative population doublings compared to adult peripheral blood-derived ECFCs, which achieve about half as many [31]. Therefore, the population doubling time for cord-blood-derived ECFCs is approximately 1.5 days compared to nearly 4 days for adult peripheral blood ECFCs. Thus, cord blood-derived ECFCs have greater therapeutic potential since the acquisition of sufficient cell numbers affects ECFC efficacy in regenerative medicine applications [39].

Despite differences in clonogenic and proliferative potential, ECFCs isolated from adult peripheral blood and umbilical cord blood have similar surface marker expression, including CD31, CD141, CD105, CD146, CD144, von Willebrand factor, and Flk-1 [31]. Neither population contains cells that express the lymphocyte markers CD45 or CD14. Interestingly, both populations contain a subset of cells expressing hematopoietic progenitor markers such as CD34, CD133, and CD117. However, the implications of

differential progenitor surface expression remain unclear. Based on these results, cord blood and adult peripheral blood-derived ECFCs exhibit similar endothelial and hematopoietic surface marker expression patterns. The common surface markers analyzed in these studies, however are not sufficient to discern proliferative differences identified in population doubling assays. Therefore, the implications of differential surface marker expression on ECFC clonogenicity are yet to be elucidated. Overall, the clonogenic hierarchy assay is an important measure of individual cell clonogenic potential and of cell differentiation content in an entire ECFC sample. Importantly, the hierarchy assay is considered a gold standard assessment in the field and can be applied to identify how ECFC samples are altered in different pathologic states.

Assessments of ECFC Function: Modeling Vasculogenesis

In addition to their high clonogenicity, ECFCs are capable of *de novo* vessel formation *in vivo*, making them an attractive cell source for engineered blood vessel models [36,40–42]. Modeling vasculogenesis by seeding cells in extracellular matrix is a standard quantitative measurement to assess cell function both *in vitro* and *in vivo* [43,44]. In addition, modeling provides an opportunity to identify the impact of fundamental properties, such as the physical properties of the extracellular matrix, on the process of vessel formation. Since ECFCs have been explored extensively for use in regenerative vascular therapies, optimized conditions have been established to enhance ECFC vasculogenesis in 3D matrices [40]. Specifically, increasing collagen concentration in gel matrices decreases the number of ECFC-derived vessels, but increases average vessel size following implantation *in vivo*. Optimization of transplant matrices will improve ECFC transplant efficacy *in vivo*.

Blood vessels formed by ECFCs exhibit normal blood flow, are selectively permeable to macromolecules, and are capable of leukocyte-endothelial interactions in response to cytokine activation [45]. Not surprisingly, the ability of ECFCs to form neo-vasculature following implantation is dependent on the tissue source from which they are derived. In a vasculogenesis model where ECFCs were embedded in collagen gels with 10T1/2 (mouse embryonic fibroblast) cells and transplanted into severe combined immunodeficient mice, adult peripheral blood-derived ECFCs formed blood vessels four days after transplantation with perfusion occurring around 11 days post-transplant [45]. However, the vessels formed by the adult ECFCs were unstable and were almost completely gone 21 days after transplantation. In contrast, cord-blood derived ECFCs formed dense vessel networks that were stable *in vivo* for more than 120 days [45]. Therefore, it is evident that not all ECFCs populations have the same functional capabilities, and that cord-blood-derived ECFCs may be more efficacious for therapeutic use.

The outcomes from ECFC functional assessments are similar to previous studies examining hematopoietic stem progenitor cells. Similar to ECFCs, hematopoietic progenitor cells are enriched in umbilical cord blood compared to bone marrow [46]. Hematopoietic progenitor cell division also creates a hierarchy, such that population subsets can be discerned based on proliferation and differentiation capabilities [47,48]. Moreover, cord blood-derived hematopoietic progenitor cells exhibit enhanced proliferative capacity and re-plating, or self-renewal capacity, *in vitro* [46,47,49–51]. Thus, ECFC enrichment and functional capabilities closely mirror previously established characteristics of hematopoietic progenitor cells.

Fetal Origins of Adult Disease

In 1989, the fetal origins of adult disease (FOAD) hypothesis was first proposed by Dr. David Barker in the Lancet [52]. His proposition, which was supported by strong epidemiologic data, was that environmental influences impairing growth and development early in life could be risk factors for ischemic heart disease later in life. The basic premise of Dr. Barker's initial assertion is still maintained today in the current FOAD hypothesis, which states that events transpiring during early development significantly impact the risk for developing multiple diseases later in life [53]. However, since Dr. Barker's initial assertion, the FOAD hypothesis has been expanded to include additional morbidities, such that low birth weight is now associated with coronary artery disease, hypertension, obesity, and insulin resistance [53–55].

Low birth weight, resulting from abnormal developmental environments, is not the only clinical measure associated with long-term health outcomes. Acute and chronic morbidities resulting from exposure to maternal diabetes mellitus during development have also been associated with poor health outcomes in children. Type 2 diabetes mellitus (T2DM) occurs when the body is not able to use insulin produced by the pancreas to lower blood glucose, resulting in subsequent development of hyperglycemia [56]. Maternal glucose can consequently cross the placenta, leading to fetal exposure to hyperglycemia during development [57]. Importantly, clinical diagnosis of maternal hyperglycemia during pregnancy is classified into two subgroups depending on the timing of diagnosis. Pre-gestational diabetes, most commonly T2DM, is defined as maternal hyperglycemia diagnosed prior to pregnancy. Alternatively, the diagnosis of gestational diabetes mellitus (GDM) is defined as diabetes first diagnosed during pregnancy. Although GDM is most often diagnosed in the third trimester, the duration and severity of the glucose intolerance can vary. Therefore, different treatment strategies are

implemented to maintain blood glucose levels. Specifically, GDM may be conservatively managed by alterations in diet and exercise. Alternately, GDM may require pharmacologic treatment to maintain normal glucose levels. Typically, women receiving insulin therapy have more severe hyperglycemia, and/or are unable to manage glucose levels with diet and exercise. Access to clinical information, including treatment strategies utilized during gestation, enables further differentiation of GDM samples during functional analysis.

Early studies of the Pima Native Americans were the first to identify that fetal exposure to maternal T2DM enhances the risk of an offspring to develop T2DM during childhood [58–63]. The Pima are an especially informative population to study because they have the highest reported prevalence of T2DM in the world [58]. The high prevalence in T2DM in this population is due to abrupt diet and lifestyle changes following infringement on Native American reservations during settlement of, what is today, Arizona in 1859. In addition to high prevalence, the onset of T2DM in this population occurs early, at approximately 5-10 years of age. Due to the combination of high prevalence and early onset, a large percentage of women in the tribe develop diabetes prior to childbearing years. This population, therefore, offers a unique opportunity to understand how maternal T2DM impacts fetal development.

In the Pima tribe, children born to mothers with T2DM have a higher prevalence of the disease in early adulthood compared to children of non-diabetic mothers [62]. Moreover, intrauterine exposure to maternal diabetes results in higher systolic blood pressure and hemoglobin A1c in childhood [61,62]. Importantly, the observation that maternal T2DM impacts child health outcomes is not limited to the Pima population. Similar findings have been confirmed in populations outside of the Pima tribe as well [64–68]. In non-Pima populations, maternal obesity and T2DM during pregnancy alters offspring weight, glucose

tolerance, and blood pressure [64]. Specifically, maternal T2DM exposure *in utero* increases body mass index in late childhood, which correlates with a long-standing risk of developing obesity [65,68]. Therefore, individuals exposed to T2DM *in utero* are at an increased risk for developing chronic diseases, such as high blood pressure, later in life.

Increasing Pregnancies are Complicated by Maternal Diabetes Mellitus

Widespread increases in obesity due to Western lifestyle and diet has produced a steadily increasing prevalence of T2DM the past several decades. Notably, worldwide prevalence of obesity has more than doubled since 1980 [69]. According to 2014 global estimates by the World Health Organization, more than 1.9 billion adults (aged 18+) were overweight or obese [69]. Overall, approximately 13% of the world's population were considered obese in 2014 [69]. Not only are more adults developing obesity and T2DM, but they are developing these complications at an earlier age, like in the Pima population [70]. Early-onset T2DM has proven especially important for women, because the age at diagnosis now coincides more frequently with child-bearing years [71,72]. Although women are having children later in their lives than ever before, age during pregnancy can only account for a portion of the increased prevalence [73].

In addition to increasing T2DM diagnoses and maternal ages, the rising rate of obesity alone has contributed to increasing pregnancy complications. Rates of obesity in American pregnant women has been reported between 18.5 and 38.5% [71,74]. Importantly, obesity is a known risk factor for the development of GDM [75,76]. Analyses completed by the Centers for Disease Control and Prevention in 2014 suggest that GDM currently impacts 9.2% of all pregnancies [77]. Despite shorter disease duration compared to T2DM, GDM also has a significant impact on fetal development [78]. Exposure to GDM *in utero* leads to both acute and chronic morbidities in children [63,67].

Recent studies suggest that intrauterine GDM exposure increases the likelihood for a child to develop high blood pressure, cardiovascular disease, T2DM and the metabolic syndrome [67]. Presently, no 'cure' for GDM exists, but lifestyle guidelines assist with disease management to minimize long-term fetal effects. Current prevention strategies include regulating diet and exercise, monitoring blood glucose levels, and, in some cases, administering insulin injections [76]. Unfortunately, these strategies rely heavily on patient compliance, which is very difficult to control. Although maternal GDM is often resolved following birth, women diagnosed with GDM have increased risk for developing T2DM following pregnancy. Based on the number of individuals affected, the numerous health risks associated with the disease, and a lack of successful intervention thus far, it is evident that GDM will be a significant health concern for decades to come. Therefore, understanding how the GDM intrauterine environment impacts fetal development will contribute to future treatment strategies and preventative therapies. Specifically, the research outlined in this thesis provides novel approaches to identify molecular mechanisms altered, following GDM exposure, in a fetal vascular cell population critical for vessel formation during development and angiogenesis/vascular repair postnatally. Identification of specific mechanisms or gene targets altered in GDM-exposed ECFCs through studies such as those presented in this work will guide the development of future prevention and treatment strategies.

Maternal T2DM Negatively Alters Endothelial Progenitor Cell Number and Function

Previously, our lab has demonstrated that exposure to maternal pre-gestational diabetes mellitus *in utero* negatively impacts fetal progenitor cell number and function [79–81]. These observations are the result of several studies in which primary cell samples were either obtained directly from diabetic pregnancies or exposed *in vitro* to conditions intended to recapitulate a component of the diabetic intrauterine environment (i.e.

hyperglycemia). To mimic physiologic hyperglycemia resulting from maternal diabetes, umbilical cord blood-derived ECFCs from non-diabetic pregnancies were exposed to high concentrations of dextrose (10-30mmol/l) compared to a normoglycemic concentration (5mmol/l) for seven days. Following dextrose treatment, ECFCs incurred dose-dependent reductions in colony forming abilities, with a 50% reduction in colony number at the highest dextrose concentration tested (30mmol/l) compared to untreated controls [79]. Additionally, high dextrose treatment (15mmol/l) reduced ECFC vasculogenesis, as measured *in vitro,* by 30% [79]. Thus, exposure to hyperglycemia, at levels comparable to those observed in mothers with T2DM, is sufficient to impair ECFC function. To determine if these observations translated *in vivo*, functional studies were performed using ECFC samples derived from T2DM pregnancies. Similar to the functional deficits observed following dextrose treatment, ECFCs exposed to T2DM *in utero* exhibited reduced colony formation, clonogenic capacity and proliferative potential [79]. In addition, ECFCs from T2DM pregnancies had altered vasculogenic potential, forming 66% fewer networks i*n vitro* compared to samples from uncomplicated pregnancies (Figure 4). To more rigorously assess vessel forming ability, ECFCs from uncomplicated and T2DM pregnancies were embedded in gel plugs and transplanted into immunodeficient, NOD-SCID mice. Consistent with differences observed *in vitro*, ECFCs from diabetic pregnancies formed 50% fewer perfused vessels compared with ECFCs from uncomplicated pregnancies (Figure 5) [79]. Therefore, exposure to a maternal diabetic intrauterine environment, and specifically to hyperglycemia, impairs the ability of ECFCs to proliferate and undergo vasculogenesis.

To begin to identify the mechanisms underlying the differences in ECFC clonogenic capacity and network formation following exposure to hyperglycemia *in vitro* or intrauterine maternal T2DM, senescence and apoptosis were assessed. Following exposure to *in vitro*

hyperglycemia, a greater percentage of ECFCs underwent cellular senescence compared to untreated controls [79]. Similarly, ECFCs isolated from T2DM pregnancies had an increased percentage of senescent cells compared to ECFCs from uncomplicated pregnancies [79]. No differences were observed in the percentage of ECFCs undergoing apoptosis. Together, these data indicate that senescence is an important mechanism by which ECFCs from diabetic pregnancies may incur functional deficits.

Gestational Diabetes Mellitus Alters ECFC Proliferation and Senescence

In addition to T2DM, GDM, a more common, later-onset form of maternal hyperglycemia, also impacts pregnancy outcomes. Therefore, additional studies were necessary to determine if GDM exposure negatively impacts fetal ECFC function to the same extent as T2DM. Similar to ECFCs from T2DM pregnancies, low passage (<5) ECFCs isolated from GDM pregnancies exhibited impaired network forming abilities, forming 50% fewer networks in Matrigel assays [81]. Interestingly, despite similar defects in network formation, low passage ECFCs exposed to GDM do not maintain all phenotypic deficits. Specifically, exposure to GDM did not impact ECFC colony formation or senescence at low passage, however GDM exposure increased ECFC proliferation compared to ECFCs from uncomplicated pregnancies [81].

Since senescence was identified as an important mechanism impacting ECFC function following exposure to maternal T2DM, an *in vitro* model of ECFC aging was implemented to evaluate higher passaged GDM-exposed ECFCs for a predisposition towards a senescent phenotype. To model cell “aging” ECFCs were serially passaged by re-plating. Serially passaged GDM-exposed ECFCs were no longer hyper-proliferative, but had an increased frequency of senescent cells compared to uncomplicated controls [81]. Additionally, in the setting of hyperglycemia (15mmol/l glucose), approximately 10% of

ECFCs from non-diabetic pregnancies become senescent while GDM-exposed ECFCs were resistant with only 2% of cells staining positive for senescence-associated β-galactosidase [79,81]. Resistance to hyperglycemia-induced senescence is indicative of an adaptive response in the ECFCs, enabling them to survive the abnormal intrauterine environment. Thus, the duration and severity of exposure to maternal diabetes, whether pre-gestational or gestational, impacts ECFC function differently. Therefore, it is important to identify mechanisms, including differential gene expression and signaling pathway activation, that could be underlying these functional differences. In the work presented in this thesis, a combination of quantitative Real-Time Polymerase Chain Reaction (qRT-PCR), western blotting, and immunofluorescence techniques are used to identify differential gene expression and pathway activation in ECFCs from uncomplicated, T2DM, and GDM pregnancies.

Maternal Diabetes-induced Alterations in Fetal ECFC Gene Expression and Epigenetic Regulation

Vascular progenitor cell populations, including ECFCs, display significant functional impairments as a result of exposure to maternal diabetes *in utero* [79,80]. However, the molecular mechanisms underlying the observed phenotypic differences in number and function are unknown. Therefore, an increasing number of studies have focused on the identification and confirmation of differentially expressed genes in vascular progenitor cells obtained from diabetic pregnancies [82,83]. Previously, the Haneline laboratory identified that ECFCs isolated from GDM pregnancies exhibit alterations in gene expression [83]. Out of nearly 28,000 genes assessed using microarray analysis, 596 mRNAs were significantly altered ($p<0.01$) in ECFCs from GDM pregnancies compared to uncomplicated controls [83]. Of the 596 genes identified, only 38 genes had at least a 50% increase or decrease in expression. Interestingly, placenta-specific 8 (PLAC8) was

one of the most highly upregulated genes in GDM samples, while ALX homeobox 1 and endothelial nitric oxide synthase were significantly down-regulated (described in detail below).

Since exposure to intrauterine diabetes produces long-term changes in ECFC gene expression, alterations in epigenetic regulation is postulated as the underlying mechanism given the stability of these changes over time [84]. Thus, in addition to gene expression, the impact of epigenetic regulation on cell fate determination has been increasingly studied to understand how suboptimal conditions during development, such as maternal diabetes, lead to increased metabolic morbidities later in life [85–88]. Nomura et al. identified that global methylation levels in the placenta are lower in women with GDM and preeclampsia compared to women without those risk conditions [86]. Similarly, in a study by Hajj et al. methylation of genes such as Mesoderm Specific Transcript, and NR3C1 glucocorticoid receptor were significantly reduced in cord blood and placental tissue from GDM patients compared to controls [87]. Finally, in a study by del Rosario et al., pathway analysis identified pathways, including the NOTCH signaling pathway, with differentially methylated promoters in offspring of diabetic mothers such as Maturity Onset Diabetes of the Young (Figure 6) [85]. In combination, these pathway results support the hypothesis that altered β-cell function could be the mechanism by which offspring of diabetic mothers have an increased risk for developing T2DM later in life. In general, epigenetic and pathway analyses provide insight into how offspring with suboptimal development are at increased risk for developing future metabolic morbidities.

Epigenetic studies using fetal ECFCs have produced strong evidence that epigenetic reprogramming occurs following GDM exposure in humans [83]. Specifically, critical regions of the PLAC8 promoter and first intron had reduced CpG methylation in GDM-

exposed ECFCs compared to uncomplicated controls. Additionally, DNA methylation status of 17 CpG sites in *PLAC8* negatively correlated with mRNA expression [83]. Similar to PLAC8, correlations between RNA expression and DNA methylation have also been identified in the promoter regions of other genes, including Transgelin 1 (r= -0.72, p=0.02, FDR =0.28, Emily Blue, unpublished data). These findings suggest that the alterations in gene expression observed in ECFCs from GDM pregnancies could be regulated, in part, by epigenetic mechanisms such as DNA methylation.

Implications of Elevated Transgelin 1 in ECFCs from GDM Pregnancies

Gene expression studies conducted on umbilical cord blood-derived ECFCs identified Transgelin 1 (TAGLN) as one of the genes significantly increased in fetal ECFCs exposed to GDM. This is surprising, as TAGLN was initially thought to be smooth muscle-specific when discovered in 1987 in chicken [89]. However, TAGLN expression has been identified in other cell types, including mesenchymal cells, fibroblasts, and epithelial cells [90,91]. Interestingly, this is not the first report of elevated TAGLN in the setting of GDM. Increased TAGLN has also been identified in placentas from GDM pregnancies [92]. It is speculated that increases in TAGLN, along with other genes associated with chronic stress and inflammatory pathways, could link inflammation to GDM-associated insulin resistance. Overall, GDM is a multi-faceted disease with intrauterine exposure likely resulting in numerous changes to the developing infant [65,66,93].

Since the initial discovery, three different Transgelin genes have been identified (Transgelin1-3). TAGLN, also known as SM22α, is an early marker of smooth muscle cell differentiation [94]. Transgelin 2 (TAGLN2), otherwise known as SM22β, is a homolog of TALGN, but has not been studied to the same extent as TAGLN [95]. The third gene, Transgelin 3 (NP25) is primarily expressed in neuronal cells [96]. Abundant literature

outlines the function of TAGLN in smooth muscle cells, since expression was thought to be specific for that differentiated cell population. In smooth muscle cells, TAGLN down-regulation may be an indicator of cellular transformation [91]. Vascular smooth muscle cells in a contractile state express high levels of TAGLN and have reduced migration and proliferation [97,98]. Upon injury or disease, however, vascular smooth muscle cells can switch to a synthetic state, with decreases in TAGLN expression and increases in cell migration and proliferation [99–101]. Cellular differentiation studies have not been limited to vascular smooth muscle cells. Recent studies using endothelial stem progenitor cells to form vascularized tissue utilized TAGLN as a marker of vascular smooth muscle cell differentiation [102,103]. Thus, TAGLN represents an important marker of cellular differentiation.

All three Transgelin genes contain the conserved Calponin homology domain and Calponin Family Repeat [104]. The Calponin homology domain is an actin-binding domain commonly found in cytoskeletal and signal transduction proteins [105]. In this regard, TAGLN primarily localizes in the cytoplasm near actin filaments and aids in the formation of actin bundles via induction of polymerization of globular actin (G-actin) to filamentous actin (F-actin) in addition to promoting F-actin cross-linking [106–109]. Therefore, TAGLN is involved in the dynamic process of actin cytoskeletal rearrangement.

The ability of the cells that comprise the vasculature to reorganize their cytoskeleton in response to external stimuli is a critical function. Endothelial cells respond to mechanical forces, including fluid shear stress, by modulating intracellular signaling pathways and gene expression [110]. Although few studies have assessed the functional role of the Transgelin genes in endothelial cells, TAGLN and TAGLN2 have been implicated in regulating endothelial cell migration via modulation of matrix metalloproteinase 9 (MMP9)

and phosphorylation of myosin light chain, respectively [111,112]. Specifically, TAGLN is a regulator of MMP9, such that overexpressing TAGLN in HT1080 (human fibrosarcoma line) cells decreased MMP9 expression, and reduced cell invasion in Matrigel trans-well assays [112]. Importantly, HT1080 cell migration was rescued by addition of exogenous MMP9, suggesting that not only is MMP9 regulated by TAGLN, but, as a Type IV collagenase, it is a key component of cell migration [112]. In another study by Xiao et al., siRNA-mediated reductions of TAGLN2 were sufficient to increase human umbilical vein endothelial cell migration following lovastatin (10μM) treatment [111]. Moreover, TAGLN2 knockdown was associated with increased in myosin light chain phosphorylation, thereby implicating myosin light chain activation in TAGLN2-regulated cell migration.

TAGLN is not highly expressed in fetal ECFCs isolated from uncomplicated pregnancies. However, exposure to GDM during development increases TAGLN levels in ECFCs. Interestingly, elevated TAGLN transcripts were identified in the placenta from GDM pregnancies previously [92]. In addition to TAGLN, differentially expressed genes associated with chronic stress and inflammatory pathways were also identified. This is an interesting finding, as the authors postulate that it could provide a link between inflammation and GDM-associated insulin resistance [92].

ECFC Functional Assessments Limited by Current Experimental Approaches

Although several studies have demonstrated that intrauterine exposure to maternal T2DM and GDM have long-term effects on child health outcomes, the mechanisms responsible are not fully understood. Improving functional assessment of fetal vascular progenitor cells will allow for an understanding of how intrauterine diabetic exposure imparts long-term vascular complications. Currently, limited clinical tools are available to assess severity of diabetic exposure in children from mothers with T2DM and GDM.

Unfortunately, these morbidities often go undiagnosed until children present with disease later in life, at which time the opportunity for prevention has ended. Therefore, in-depth analyses of ECFC vasculogenesis are needed to identify how and why functional deficits are incurred *in utero*. Studies conducted to complete this thesis work address the need for in-depth analyses of ECFC vasculogenesis through the development of novel microscopic approaches to rigorously assess vessel formation kinetics.

Modeling vasculogenesis enables rapid analysis of cells to perform basic tasks of network or vessel formation [113,114]. However, standard methods are limited in scope and fail to capture many aspects of this highly dynamic process (Figure 4). Though attempts have been made to apply quantitative analyses, current methods are insufficient for dynamic studies [115–117]. Therefore, kinetic assessments are needed to identify mechanisms of impaired vasculogenesis. Specifically, improved assessment of ECFC function following intrauterine diabetes exposure, will improve infant risk assessment and inform future preventative strategies.

Major Aims

1. To develop innovative methods to quantitatively assess the kinetics of ECFC vasculogenesis *in vitro*.

2. To identify novel phenotypic differences in ECFC vasculogenesis following exposure to intrauterine diabetes.

3. To determine if increased Transgelin 1 expression in ECFCs from gestational diabetic pregnancies impairs vasculogenesis.

Figures (1-6)

Figure 1. Modes of Vessel Formation

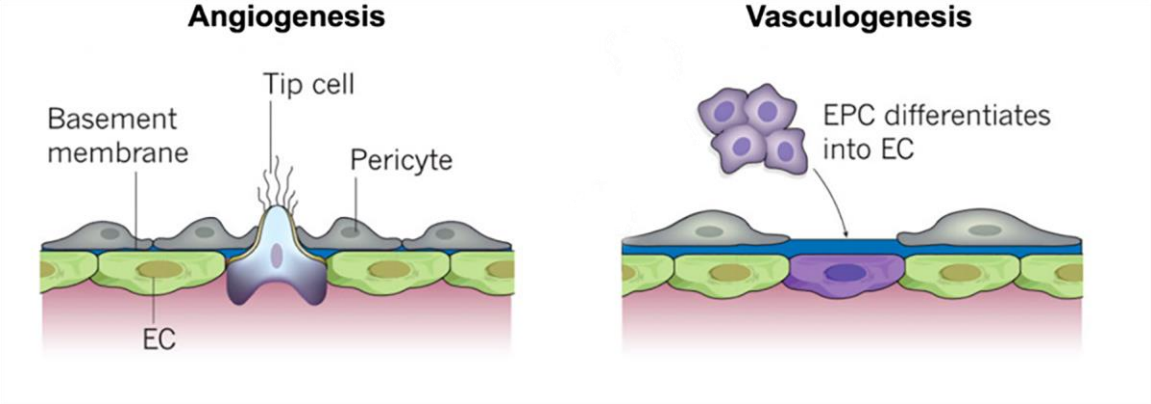

Vessel formation can occur by angiogenesis where new vessels sprout from pre-existing vascular networks. New vessels can also be formed by vasculogenesis where endothelial progenitor cells (EPCs) can differentiated into endothelial cells (ECs) to form new vessels in the absence of preexisting vascular structures. *Figure adapted from Carmeliet et al. (2011)* [2].

Figure 2. Notch and VEGF Signaling Regulate Endothelial Tip Cell Formation

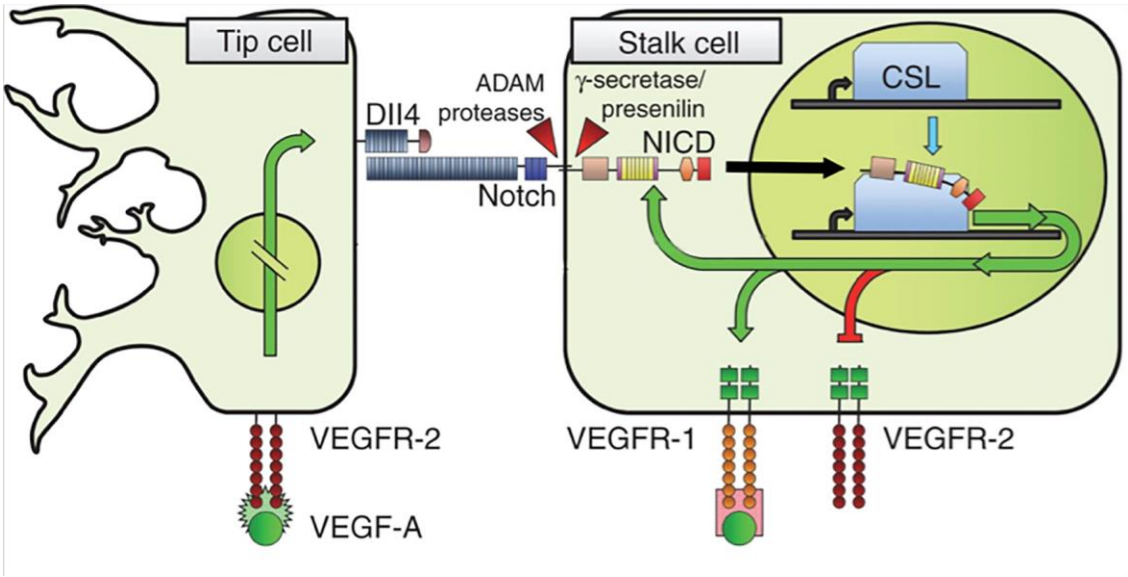

In future tip cells, VEGF-A signaling via VEGFR-2 causes up-regulation of Dll4. Dll4 binds Notch molecules on the membranes of adjacent endothelial cells and facilitates receptor cleavage by ADAM and γ-secretase/presenilin. Cleavage untethers the Notch intracellular domain (NICD) from the membrane, which then translocates to the nucleus and complexes with CSL, turning the transcriptional repressor into a transcriptional activator. Transcriptional activation has several downstream effects, including the creation of a positive feedback loop via increased Notch expression, inhibition of VEGFR-2 expression, and up-regulation of VEGFR-1, a receptor with high affinity for VEGF-A but low signaling activity. Thus, endothelial cells adjacent to tip cells have greatly reduced sensitivity to VEGF-A, and adopt a stalk cell character. *Figure adapted from Tung et al.,* (2012) [4].

Figure 3. Schematic of the ECFC Single-cell Assay

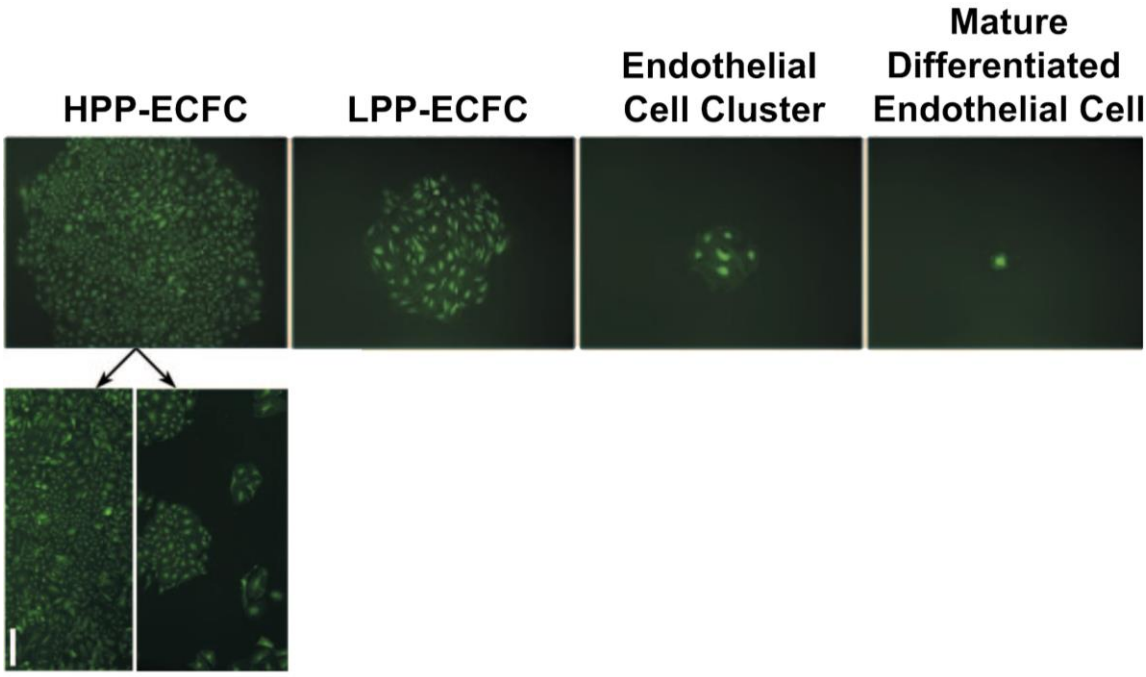

HPP-ECFCs are large colonies that form secondary and tertiary colonies on re-plating. HPP-ECFCs give rise to all subsequent stages of endothelial progenitors in addition to re-plating into secondary HPP-ECFCs. LPP-ECFCs form colonies that contain more than 50 cells but do not form secondary colonies or LPP-ECFCs on re-plating. Endothelial cell clusters can arise from a single cell but contain fewer than 50 cells that are typically larger than the smaller cells found in HPP-ECFC and LPP-ECFC colonies. Mature, terminally differentiated endothelial cells do not divide. The scale bar represents 100μm. *Figure adapted from Ingram et al., (2004)* [31].

Figure 4. Exposure to Maternal Diabetes Mellitus Reduces Fetal, Cord Blood-derived ECFC Network Formation

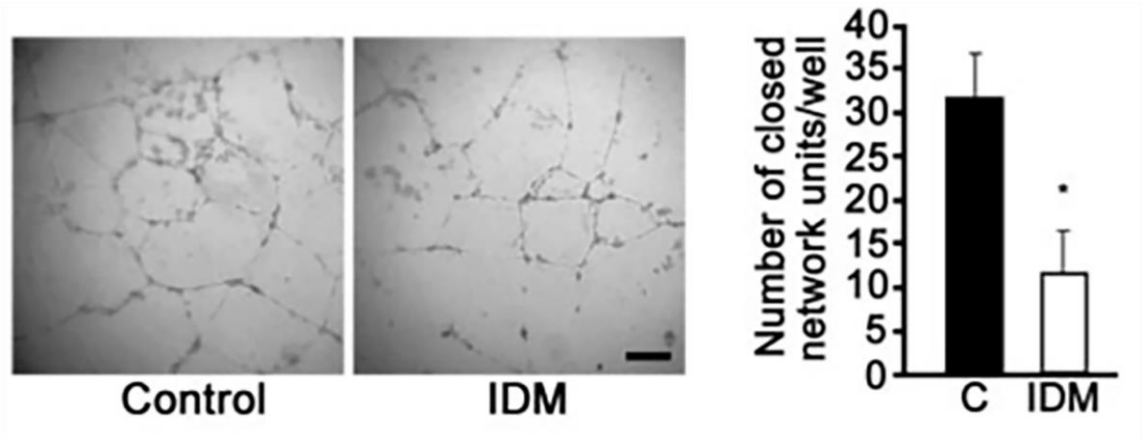

Representative photomicrographs of ECFCs derived from uncomplicated (C) and pre-gestational diabetic pregnancies (IDM) 24 hours after plating on Matrigel. Results are representative of three independent experiments. The scale bar represents 30μm. Quantitation of capillary vessel density 24 hours after plating on Matrigel. Data represent mean +/- SEM, n=4, *P<0.002 by Student‘s t test. *Figure adapted from Ingram et al., (2008)* [79].

Figure 5. Maternal Diabetes Mellitus Exposure Reduces Fetal, Cord Blood-derived ECFC Vessel Formation

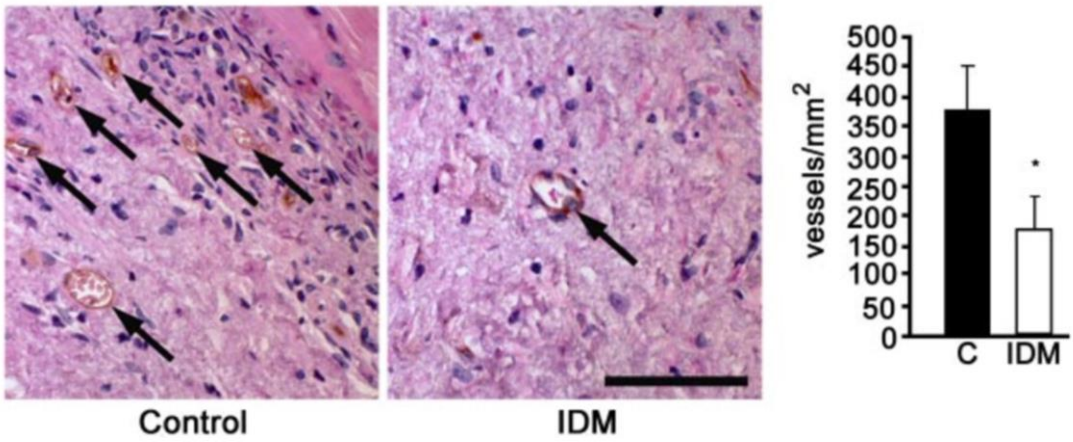

Representative photomicrographs (100x magnification) of cellularized grafts and surrounding murine tissue14 days after implantation into NOD/SCID mice stained with anti-human CD31 (brown) to identify human blood vessels. Grafts contained ECFCs from either uncomplicated (C) or pre-gestational diabetic pregnancies (IDM). Arrows indicate anti-human CD31+ vessels and capillaries in the ECFC grafts, which were perfused with murine erythrocytes. Results shown are representative of three independent experiments using cells from different donors. Quantitation of capillary density within cellularized grafts containing ECFCs from uncomplicated or diabetic pregnancies 14 days after implantation. Results represent the average number of capillaries containing murine erythrocytes/mm^2 of graft tissue +/- SE, n=3, *P<0.001 by Student‘s t test. *Figure adapted from Ingram et al., (2008)* [79].

Figure 6. Pathways for Maturity Onset Diabetes of the Young (MODY) and Notch Signaling

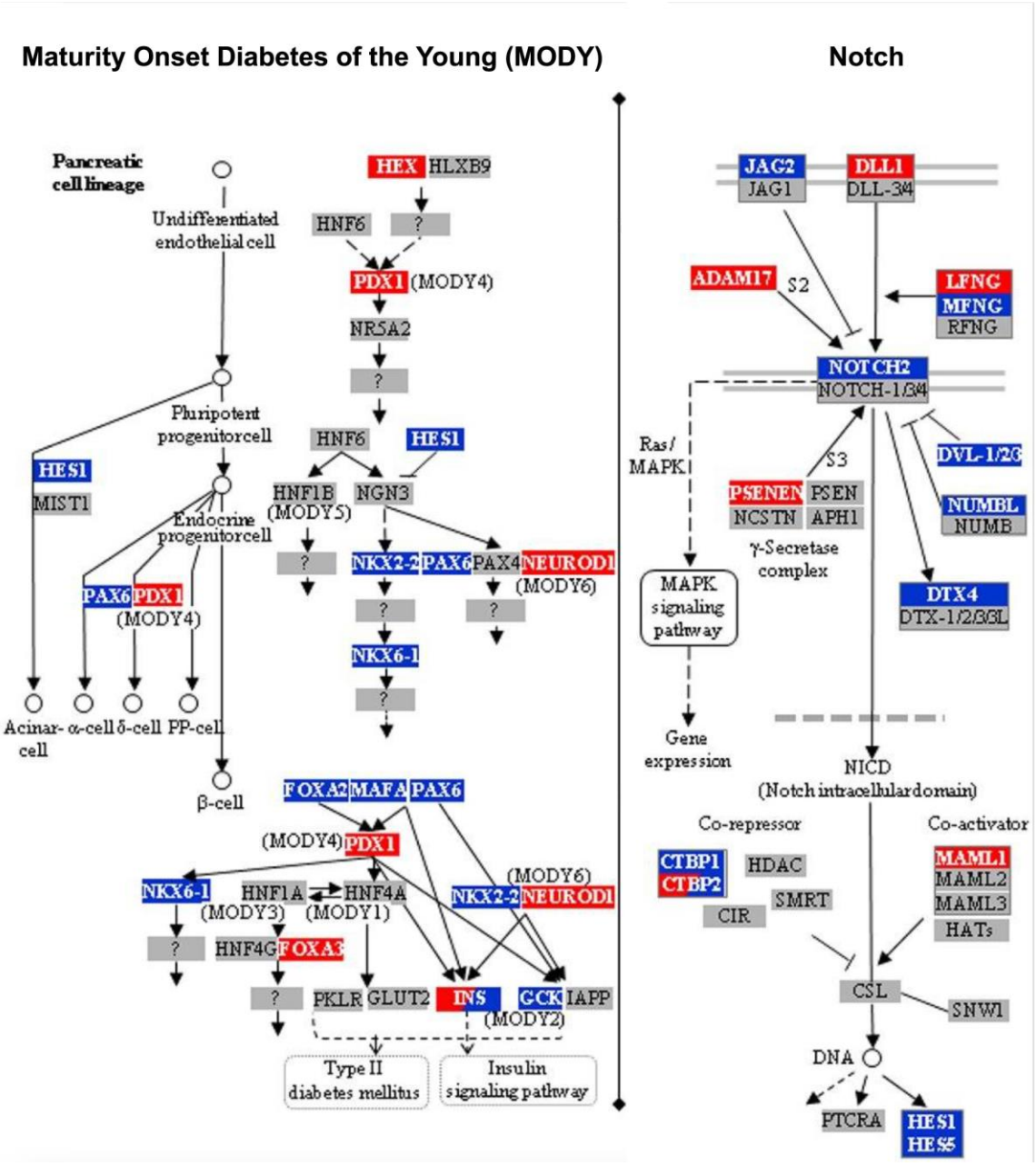

Maturity Onset Diabetes of the Young (hsa04950) and Notch signaling pathways (hsa04330); adapted from Kanehisa et al. [118]. Genes in the pathways which are hyper-methylated in ODM compared with ONDM are shown in red boxes, while hypo-methylated genes are shown in blue boxes. Genes that did not show differential methylation are in gray boxes. Boxes for INS and CTBP2 are marked with both red and blue indicating that two separate regions with different methylation status overlapped with the promoter of these two genes. *Figure adapted from del Rosario et al., (2014)* [85].

CHAPTER 2: MATERIALS AND METHODS

Umbilical Cord Blood Sample Acquisition

Umbilical cord blood samples were collected at the time of birth following written informed consent from the mothers. Samples were obtained from women with uncomplicated (UC) pregnancies and from women diagnosed with type 2 diabetes mellitus (T2DM) prior to pregnancy. All pregnancies were single gestation. Infants with known chromosomal abnormalities were excluded. Women with preeclampsia or hypertension, women with other illnesses known to affect glucose metabolism, and women taking medications known to affect glucose metabolism were excluded. Clinical data from women and infants are summarized in Tables 1 and 2, respectively. No significant differences were identified between the UC and T2DM groups for the following clinical values: maternal age, pre-pregnancy BMI, gestational age, infant weight, infant weight percentile, infant weight/length percentile, and ponderal index (all p-values >0.05).

ECFC Cell Culture

ECFCs were isolated from umbilical cord blood samples as previously described (Figure 7) [79,81]. Umbilical cord blood was diluted 1:1 with PBS and underlaid with Ficoll-Paque PLUS (GE Healthcare, Piscataway, NJ). The blood was centrifuged for 30 minutes at 740g. Mononuclear cells were isolated from the buffy coat and washed with Endothelial Growth Medium 2 (Lonza, Walkersville, MD) containing 10% Hyclone defined fetal bovine serum (FBS, ThermoFisher Waltham, MA), antibiotic-antimycotic solution (Corning, Manassas, VA), and MycoZap PR antibiotic (Lonza) (EGM2+10%FBS). Mononuclear cells were resuspended in EGM2+10%FBS and plated in six-well tissue culture plates pre-coated with type 1 collagen (Corning). Following 24 hours in culture, all wells were washed with EGM2+10%FBS to remove non-adherent cells, and medium was changed daily for 7 days and then on alternate days until first passage. ECFC colonies appeared between 5-8 days of culture. After reaching confluence, cells were detached with 0.25% trypsin-

EDTA (Invitrogen, Grand Island, NY) and frozen in 5% dimethyl sulfoxide (ThermoFisher) in FBS (Atlanta Biologicals, Flowery Branch, GA). ECFC aliquots were thawed, resuspended in EGM2+10%FBS, and plated on type 1 collagen coated flasks for culture. ECFCs used in these studies were passaged 2-5 times.

Workflow forAcquiring and Assaying Cord Blood-derived ECFCs

The overall approach in conducting these assays involved three stages (1-3) (Figure 7). First (1), in the Cell Sample Preparation stage, umbilical cord blood samples were collected at the time of birth and processed for derivation of ECFC colonies. This stage is described in detail in the Umbilical Cord Blood Acquisition and ECFC cell culture Method sections. The second stage (2) of the process primarily involved image acquisition. Several different imaging modalities were utilized to obtain photomicrographs for the newly developed assays including phase contrast microscopy, confocal microscopy, and conventional fluorescence microscopy. In the Kinetic Network Formation and Motility assays, phase contrast or fluorescence images were acquired every 10-15 minutes over the course of several hours, allowing for an in-depth assessment at network formation kinetics. Importantly, acquiring large numbers of images in stage 2 necessitated the third stage (3) of assay development, which was data analyses. In this stage, images were processed, and new software was developed to measure new phenotypes with the goal of identifying novel biologic phenomena.

Matrigel Assay Setup for KAV Experiments

ECFCs (passage 3-4) were plated at 400,000 cells per 100mm dish and incubated overnight. The following day, ECFCs were trypsinized (ThermoFisher), counted on a hemocytometer, and plated at equal densities in EGM2 supplemented with 10% FBS. ECFCs were plated on 10ul of Matrigel lot #4209014 (Corning) in 15 well µ-slides (Ibidi

USA, Inc.). The slide containing Matrigel was placed in the microscope stage-top incubator to maintain temperature, CO_2, and humidity, for overnight live cell imaging. Images of entire wells were collected using a cooled charge-coupled device (CCD) camera (Hamamatsu ORCA-ER) every 15 minutes for 15 hours for a total of 60 data points per ECFC sample in each experiment.

Microscopy Settings and Equipment for KAV Experiments

All imaging for KAV experimentation was performed on a fully automated Nikon TiE microscope equipped with a ProScan II motorized stage (Prior Scientific, Rockland, MA), xenon lamp source, Lambda LS, and Lambda 10-3 filter wheel controller (Sutter Instrument Company, Novato, CA), fitted with an ORCA-ER or ORCA-Flash 4.0 (Hamamatsu, Japan) controlled by Elements 4.20 (Nikon Instruments Inc., Melville, NY). Fluorescent filters were the Quad Sedat v89000 set (Chroma Technologies, Bellows Falls, VT). Experiments with phase contrast imaging used a CFI PlanFluor DLL 10X objective and those with fluorescence imaging for contrast used a CFI S Plan Fluor ELWD ADM 20x objective (Nikon Instruments Inc.). Multiple images and Z-positions were collected to cover the sample wells and stitched together with Elements as required. For live imaging the microscope was fitted with a stage top incubator with humidity (75-85%), temperature (37ºC) and CO_2 regulation (5%; OkoLab, Burlingame, CA).

Kinetic Analysis of Vasculogenesis (KAV)

Phase contrast images were compiled, processed, and analyzed using a custom FIJI plugin called Kinetic Analysis of Vasculogenesis (KAV) created by Seth Winfree in the Indiana Center for Biological Microscopy specifically for completion of this project. For image processing and analysis details see Appendices E and F on *Protocols for Automated Network Analysis in FIJI (Image J)*. KAV utilizes the Skeletonize 2D/3D and

Analyze Skeleton plugins in FIJI [119]. The software allowed for quantification of 8 distinct parameters of vasculogenesis over time including closed networks, network area, nodes, branches, the ratio of branches to nodes, branch length, nodes with 3 branch extensions, and nodes with 4 branch extensions. A closed network was defined in KAV as an enclosed area surrounded by cells. Network area is the size of the closed network openings. Definitions for nodes and branches were created to differentiate the structures in KAV. Nodes were defined as points within the network that have 3-4 branch extensions. Nodes with more than 4 branch extensions were not observed. A structure connected on at least one end by a node was defined as a branch. However, branches could be connected on both ends as indicated by the branches in Figure 9. KAV calculated the ratio of branches to nodes by dividing the total number of branches by the total number of nodes detected in a well. The values generated from the software analysis were graphed in Prism (Graphpad, San Diego, CA) and R (version 3.1.1) [120].

Matrigel Immunofluorescence Technique

Matrigel assays were conducted and analyzed at time points indicated using immunofluorescence staining [121]. Briefly, the samples were fixed with 4% paraformaldehyde five hours post-plating, permeabilized with 0.5% Triton X-100 in phosphate buffered saline (PBS), quenched with 100mM glycine, and blocked with 0.1% bovine serum albumin, 0.2% Triton X-100, 0.05% Tween-20, and 10% goat serum (Jackson ImmunoResearch Laboratories, Inc., West Grove, PA) in PBS. Samples were incubated with alpha-tubulin primary antibody at a 1:1000 dilution (#T6199, clone DM1A, Sigma-Aldrich, St. Louis, MO) overnight at room temperature. The following day, Alexa568-conjugated goat anti-mouse secondary antibody (#A11031, ThermoFisher Scientific) was added at 1:400 for 40 minutes at room temperature. Samples were imaged in PBS containing NucBlue Fixed Cell Stain Ready Probes reagent as recommended by

the manufacturer (#R37605, ThermoFisher Scientific) on the Nikon TiE inverted microscope with a xenon lamp source and fluorescent filters (Chroma Inc., Bellows Falls, VT). Negative controls lacking primary antibody did not show nonspecific secondary antibody staining. The alpha-tubulin antibody clone DM1A was selected because of its specificity as determined by Western blotting, which produces a single band at 50kDa in ECFCs (data not shown). Also, immunofluorescence staining for alpha-tubulin by DM1A yields identical staining to a separate clone that binds a different epitope on alpha-tubulin [122]. To ensure full coverage of the samples 6 z-planes were collected at 15 μm steps. The cells were imaged using a 20x objective on a Leica SP8 MP microscope.

Tissue Cytometry (TC) to Identify Mitotic Cells

Immunofluorescence images were processed and analyzed using the tissue cytometry (TC) software, Volumetric Tissue Exploration and Analysis (VTEA) [123]. For a detailed protocol see Appendix A: *Protocol for Analyzing Immunofluorescence Mitotic Index Images*. The software allows for single-cell quantification of both nuclear and cytoplasmic fluorescence intensities in three dimensions. A spatial measurement to assess the localization of cells within the network structures (i.e. branches and nodes) is accomplished using a combination of the original image volume and a scatter plot of cell associated signals. Populations of cells on the scatterplot were interrogated with a "gating" tool similar to flow cytometry, enabling quantitative analysis. Cells were identified by their nuclei following nuclear staining with NucBlue Fixed Cell Stain Ready Probes reagent (#R37605, ThermoFisher Scientific). The intensity of NucBlue staining was used to assess for mitotic cells. In some cases, a well-characterized antibody against phospho-Histone H3 was used to confirm accuracy of this approach [phospho-histone H3 staining (Ser10) conjugated to Alexa488 at a 1:50 dilution (#9708, Cell Signaling Technology) [124]. The accuracy of NucBlue intensity as an indicator of mitotic vs. non-mitotic cells,

and intensity thresholds for each experiment were assessed manually on a sub-region of one volume from each dataset. Between all experiments the specificity, precision, and accuracy were 96.8 ± 1.3%, 56 ± 5.2%, and 96.5 ± 1.2% respectively (mean ± SD). Branch and node thickness were determined with the Local Thickness tool in FIJI, which generated a distance map and hence thickness of a mask derived from microtubule staining of the network. This distance map was added as a channel to facilitate image analysis with VTEA.

Flow Cytometric Proliferation Analysis

Baseline ECFC proliferation was evaluated by flow cytometry on cells in standard culture conditions. Cells were washed with 2% FBS in PBS, re-suspended in cytofix/cytoperm buffer (BD Biosciences, San Jose, CA), and incubated for 20 minutes on ice. Cell suspensions were washed twice with perm/wash buffer (BD Biosciences), followed by incubation with phospho-histone H3 (Ser10) conjugated to Alexa488 (#9708, Cell Signaling Technology) for 45 minutes in the dark at 37°C. The suspensions were washed again with perm/wash buffer and re-suspended in 2%FBS in PBS for flow cytometric analysis. Samples were analyzed using an LSRII flow cytometer (Becton Dickinson, San Jose, CA) with at least 10,000 events collected per sample. FlowJo software (TreeStar, Inc., Ashland, OR) was used in analysis.

Stable Expression of GFP using Lentivirus for Single Cell Assay

The lentiviral vector plasmid (pUC2CL6IPwo), packaging accessory plasmid (pCD/NL2), and envelope plasmid (pVSVG) were generous gifts from Helmut Hanenberg (Heinrich Heine University School of Medicine, Düsseldorf, Germany) [125]. Lentiviral particles were produced by transfection of HEK293 cells with the pUC2CL6IPwo vector plasmid containing GFP (1.67 μg/ml), the pCD/NL2 packaging accessory plasmid (1.16 μg/ml) and

the VSVG envelope plasmid (1.16 μg/ml) using Fugene 6 (Roche Applied Science, Indianapolis, IN). Lentiviral supernatants were collected and filtered through a 0.45-μm asymmetric polyethersulfone filter unit (ThermoFisher). Supernatants were used immediately or stored at -80°C for future use.

Single Cell Assay

ECFCs were plated at 250,000 cells per dish in 100mm type 1 collagen-coated tissue culture dishes. The following day, lentiviral supernatant (GFP: described above) was added to each dish at dilutions of 1:2-1:10 and the cells were incubated overnight at 37°C. The media (EGM2+10%FBS) was changed 24h after transduction, and cells were incubated for a second overnight at 37°C. The second day after transduction, the ECFCs were removed from the dishes using Trypsin (ThermoFisher), washed, and resuspended in 2%FBS in PBS. GFP was used to select the brightest 15% of all transduced ECFCs, which were then sorted by FACS. One cell was sorted into each well of 96 well collagen-coated dishes containing 100μl of EGM2+10%FBS media, using a BD SORP Aria at the Flow Cytometry Research Facility in the IU Simon Cancer Center (Indianapolis, IN). Culture media was changed on day 7. On day 14 of culture wells were examined to quantitate the number of cells using a fluorescent microscope. Wells with endothelial cell counts of 2-50, 51-500, 501-2,000, and ≥ 2,001 were labeled as endothelial cell clusters (ECCs), low proliferative potential ECFCs (LPP), and high proliferative potential ECFCs (HPP) respectively and as previously described [17,32] (Figure 3). Results were graphed and statistical analysis was completed in Prism (GraphPad Software).

Baculoviral System for Nuclear GFP Expression

ECFCs (passage 3-4) were split and incubated using standard culture conditions overnight. The following day, Cell Light Nuclear-GFP BacMam2.0 (ThermoFisher Scientific) was added at a multiplicity of infection (MOI) of 30. The cells were incubated overnight, and then processed for Matrigel assays as described in the method for *Matrigel Assay Setup for KAV Experiments*.

TrackMate Motility Analysis

Images were processed in Elements (Nikon Instruments Inc.) and FIJI [126]. For a detailed description of image processing see Appendix B: *Protocol for Processing Fluorescence Images in FIJI (ImageJ) for Trackmate*. FIJI TrackMate was used to analyze cell motility parameters including displacement and speed. In TrackMate, the difference of Gaussian (DoG) detector was used with an estimated spot diameter of 25.0 pixels and a threshold of 2.0 for individual cell nuclei detection. The Simple LAP tracker with a linking max distance of 50 microns, a gap-closing max distance of 90 microns, and a 4 frame max gap-closing was used for tracking the cells through the time course images. Data from the TrackMate analysis were then analyzed using R, a programming language and software environment for statistical computing [120].

Quantitative Real-Time PCR

ECFCs were plated on collagen-coated cell culture dishes and lysed in Qiazol (Qiagen, Valencia, CA). RNA was obtained using the manufacturer's instructions and reverse transcribed using the Transcriptor Universal cDNA Master Kit (Roche Diagnostics, Risch-Rotkreuz Switzerland). Quantitative PCR was performed using Lightcycler 480 (Roche). Transgelin levels were normalized to hypoxanthine phosphoribosyltransferase (HPRT) using the $2^{-\Delta\Delta Ct}$ method. Detection of Transgelin 1 and hypoxanthine

phosphoribosyltransferase was performed on samples in duplicate using Lightcycler 480 SYBR Green I Master Mix (Roche) and the following primers: Transgelin 1 5'–GGCAGCAGTGCAGAGGAC-3'; 5'–TTATGCTCCTGCGCTTTCTT-3', MMP9 5'–GAACCAATCTCACCGACAGG-3'; 5'–GCCACCCGAGTGTAACCATA-3', and HPRT 5'-CCTTGGTCAGGCAGTATAATCCA-3'; 5'–GGTCCTTTTCACCAGCAAGCT-3'.

RNA Isolation on Matrigel

ECFCs (passage 3-4) were suspended in EGM2 (Lonza) and 34,000 cells were plated in a 24-well tissue culture plate (Corning) pre-coated with 160μl of Matrigel per well (lot #4209014, Corning). ECFCs were incubated at 37°C prior to RNA isolation using Qiazol (Qiagen). A Direct-zol RNA MicroPrep kit (R2060, Zymo Research, Irvine, CA) was used for RNA purification. RNA was reverse transcribed using the Transcriptor Universal cDNA Master Kit (Roche) and quantitative PCR was performed using Lightcycler 480 (Roche).

Western Blotting

Whole-cell ECFC lysates were collected using radio-immunoprecipitation assay (RIPA) buffer containing Complete Protease Inhibitor Cocktail (Roche Diagnostics). Equal amounts of protein were separated by sodium dodecyl sulfate polyacrylamide gel electrophoresis in 4-12% Bis-tris precast gels (Life Technologies, Grand Island, NY) run at 125 volts for 95 minutes. Protein was transferred onto nitrocellulose membrane at 24V for 16 hours at 4ºC. Immunoblotting was performed with antibodies to Transgelin 1 (ab14106, Abcam, Cambridge, MA), Vinculin (VIN-11-5, Sigma-Aldrich, St. Louis, MO), MYC-Tag 9B11 (#2276, BCell Signaling Technology, Danvers, MA), Phospho-Myosin Light Chain 2 (#3674 THr18/Ser19) (Cell Signaling Technology), and Anti-MYL12B (ab137063, Abcam). Secondary antibodies conjugated to horseradish peroxidase were obtained from BioRad (Hercules, CA), and blots were developed using Clarity Western

ECL Substrate (BioRad). Band intensity was quantified using Image J (NIH, Bethesda, MD).

siRNA Transfections of ECFCs

ECFCs were plated at 300,000 cells per 100mm tissue culture dish in EGM2 + 10% FBS the day of transfection. Lipofectamine (ThermoFisher Scientific, Waltham, MA) and short interfering RNA (siRNA) mixes were prepared in EBM2 (Lonza America, Inc., Allendale, NJ), and ECFCs were transfected with either TAGLN-specific (J-003714-08-0002, GE Dharmacon, Lafayette, CO) or a non-targeting control siRNA (D-001210-05-05, GE Dharmacon, Inc.). RNA samples and protein lysates were collected and analyzed, as described in the *Quantitative Real-Time PCR* and *Western Blotting* method sections respectively, to confirm knockdown for each transfection.

Generation of Lentivirus Encoding Transgelin cDNA Construct

The lentiviral vector plasmid (pUC2CL6IPwo), packaging accessory plasmid (pCD/NL2), and envelope plasmid (pVSVG) were generous gifts from Helmut Hanenberg (Heinrich Heine University School of Medicine, Düsseldorf, Germany) [125]. The TAGLN cDNA insert was amplified from ECFC-derived cDNA using the following primers: 5'–ATGGCCAACAAGGGTCCTTCC—3'; 3'—ACTGATGATCTGCCGAGGTCG—5'. The TAGLN insert was then cloned into the pUC2CL6IPwo vector plasmid using infusion cloning with the In-Fusion HD Cloning Kit (Takara Bio USA, Inc., Mountain View, CA) and the following primers: 5'—GCGGCCGCAACTCGAGATGGCCAACAAGGTCCT—3'; 3'—GCTGGAGCCGTCTAGTAGTCAATCCGATCGTAGCTTAAGA—5'. Lentiviral particles were produced by transfection of Lenti-X 293T cells with either the pUC2CL6IPwo lentiviral vector (empty vector control) (1.67 μg/ml), or the pUC2CL6IPwo lentiviral vector containing the TAGLN insert (1.67 μg/ml), in addition to the pCD/NL2 packaging accessory

plasmid (1.16 μg/ml) and the VSVG envelope plasmid (1.16 μg/ml) using Fugene 6 (Roche Applied Science, Indianapolis, IN). All lentiviral vectors contain a puromycin resistance cassette, which enabled a two-day selection of virally transduced ECFCs (described below). Lentiviral supernatants were collected and filtered through a 0.45-μm asymmetric polyethersulfone filter unit (ThermoFisher). Supernatants were used immediately, or stored at -80°C for future use.

Lentiviral Transduction of ECFCs for Expression of TAGLN

ECFCs were plated at 250,000 cells per 100mm tissue culture dish the day before transduction. Lentiviral vector supernatant was added to each plate in a 1:10 dilution for a final volume of 6 ml of EGM2 + 10% FBS and incubated overnight. The medium was changed and the cells were incubated for 48 hours. Transduced cells were selected in media containing 1 μg/ml puromycin (Life Technologies) for two days. Protein lysates were obtained as described, and Transgelin and MYC-tag expression levels were confirmed for each transduction by western blotting.

Matrigel Assay (General)

ECFCs (passage 3-4) were plated at 400,000 cells per 100mm dish in EGM2+10%FBS and incubated overnight at 37°C. The following day, ECFCs were removed from the dishes using Trypsin (ThermoFisher), counted on a hemocytometer, and plated at equal densities in EGM2. ECFCs were plated on 10ul of Matrigel lot #4209014 (Corning) in 15 well μ-slides (Ibidi USA, Inc.) and incubated at 37°C. Images of entire wells were then acquired using a Spot camera (Spot Imaging, Sterline Heights, MI) on an Axiovert 35 microscope (Zeiss, Thornwood, NY) at times indiciated in the figure legends. The number of closed networks per well was scored and averaged for each condition. A protocol for

Matrigel Assay image processing can be found in Appendix D: *Protocol for Merging Images in Photoshop*.

Trans-well Migration Assay

ECFCs were plated on collagen-coated transparent PET membranes (24 well, 8.0μm pore size) (Corning, Inc.) in EBM2 and incubated at 37ºC for 1-4 hours. The pro-migratory stimulus used was EGM2 + 10% FBS. Non-migratory cells were removed with cotton swabs, and cells were fixed with ice-cold methanol prior to staining with crystal violet. Eight different field images were obtained at 20X magnification for each sample and quantified. Images were obtained using a Spot camera (Spot Imaging Solutions) on an Axiovert 35 microscope (Zeiss). Refer to Appendix C: *Protocol for Overlapping Separate Images in Photoshop* for detailed protocol overviews.

Rho Kinase Inhibitor Assay

In trans-well assay set-up, cells were treated with 0.1μM rho kinase inhibitor Y27632 prior to plating in the assay. These cells were in rho kinase inhibitor for 4 hours during migration assay. For protein collection, cells in 6-well dishes plated the day before we treated with 0.1μM rho kinase inhibitor for 4 hours before being collected with RIPA.

Shear Stress Assay

ECFCs were plated in confluence on collagen-coated glass slides in EGM2+10%FBS. Cells were subjected to laminar flow for 7 hours as previously described [127,128]. Following exposure to flow, slides were fixed with 4% paraformaldehyde, quenched with 100mM glycine, blocked with 3% bovine serum albumin, and permeabilized with 0.5% Triton X-100 in 3% bovine serum albumin. Portions of the slide were incubated with

Transgelin 1 primary antibody at a 1:400 dilution (ab14106, Abcam, Cambridge, MA) for 1 hour at room temperature. AlexaFluor 568-conjugated goat anti-rabbit secondary antibody (1:400) (#A11011, Life Technologies) NucBlue Fixed Cell Stain Ready Probes reagent (#R37605, ThermoFisher Scientific), and ActinGreen 488 Ready Probes reagent (#R37110, ThermoFisher Scientific) were added for 30 minutes at room temperature. Slides were rinsed with phosphate buffered saline and mounted with Prolong Diamond Antifade mountant (P36970, ThermoFisher Scientific). Images were acquired using a Spot RT XE camera (Spot Imaging, Sterline Heights, MI) with a 40X objective on a Leica DM 4000B microscope (Leica Microsystems, Buffalo Grove, IL). Fluorescence images of F-actin were analyzed using the FIJI Directionality Plug-in [129,130]. All mean angle values produced by the Directionality Plug-in were used to generate the histograms and statistical analysis of angle means and variance.

Actin Centrifugation Assay

This protocol was adapted from the Gunst laboratory [131]. Briefly, ECFCs were homogenized in 200 µl of F-actin stabilization buffer **(**50 mm PIPES, pH 6.9, 50 mm NaCl, 5 mm MgCl2, 5 mm EGTA, 5% glycerol, 0.1% Triton X-100, 0.1% Nonidet P-40, 0.1% Tween-20, 0.1% β-mercaptoethanol, 0.001% antifoam, 1 mm ATP, 1 µg ml−1 pepstatin, 1 µg ml−1 leupeptin, 10 µg ml−1 benzamidine and 500 µg ml−1 tosyl arginine methyl ester). Supernatants of the protein extracts were collected after centrifugation (Beckman Coulter Optima MAX Ultracentrifuge, Danvers, MA, USA) at 150,000 g for 60 min at 37°C. The pellets were resuspended in 200 µl of ice-cold water containing 10 µm cytochalasin D and then incubated on ice for 1 h to depolymerize F-actin. The resuspended pellets were gently mixed every 15 min. Four microlitres of supernatant (G-actin) and pellet (F-actin) fractions were subjected to immunoblot analysis using anti-actin antibody (clone

AC-40; Sigma, St Louis, MO, USA). The ratios of F-actin to G-actin were determined using densitometry.

F-actin Assessment by Flow Cytometry

ECFCs were plated at 400,000 cells per 100mm dish in EGM2+10%FBS and incubated overnight at 37°C. The following day, the ECFCs were removed from the dishes using Trypsin (ThermoFisher) and cell counts were obtained manually using a hemocytometer. Cells (150,000) were aliquoted into to 5mL flow cytometry tubes (1 unstained control and 1 stained tube for each sample) and washed with 1 milliliter of PBS (ThermoFisher). The cell suspension was pelleted by centrifugation for 5 minutes at 1500rpm and the supernatant was aspirated. The cells were resuspended in 500µl of Cytofix/Cytoperm buffer (BD Biosciences) and incubated on ice for 20 minutes. Five milliliters of 1X Perm/Wash Buffer (BD Biosciences) was added to the cell suspension and mixed gently. The cell suspension was pelleted by centrifugation for 5 minutes at 1500rpm, and the wash was repeated a second time with an additional 5 milliliters of 1X Perm/Wash Buffer. The ActinGreen 488 Ready Probes reagent (#R37110, ThermoFisher Scientific) was diluted in Perm/Wash Buffer (BD Biosciences) by adding 2 drops of the probe per milliliter of buffer. 500µl of the diluted Ready Probes mix was added to gently resuspend the cell pellet, and the suspension was incubated in the dark for 20 minutes at room temperature. Cell suspensions were washed with 2 milliteres of 1X Perm/Wash Buffer and pelleted by centrifugation for 5 minutes at 1500rpm. The supernatant was aspirated and the pellets were resuspended in 300µl of 2%FBS in PBS. Samples were then analyzed by flow cytometry immediately on an LSR II.

Statistical Analysis

The kinetic network formation graphs for KAV data were created in Prism 6. The graphs represent the mean values ± SEM at each time point for the sample sizes indicated in the figure legends. To statistically analyze the differences between the entire kinetic curves, individual time point data were integrated to produce estimated mean difference curves and the corresponding 95% confidence intervals. These curves were generated using the spline smoothing technique, and the analysis was performed using the MGCV package in R, a programming language and software environment for statistical computing [120,132]. For histogram generation to analyze ECFC motility, the frequency of phenotype distribution was plotted such that x and y-axis ranges were kept constant for each variable between Phases 1 and 2. Data were binned based on fixed values described below, with bin sizes remaining consistent across phases. The bin sizes were as follows: Displacement 15, Mean Speed 0.005, and Max Speed 0.0015. Correlations of Displacement, Mean Speed and Max Speed were calculated using Phase 1 and Phase 2 motility data from both UC and T2DM samples. The Pearson product-moment correlation coefficient and the 95% confidence interval were computed in R. For models of kinetic and motility data correction, a multi-level model was built to test linear relationships between KAV and motility variables. The models incorporated Phase 1 motility data from all 20 ECFC samples (10 UC and 10 T2DM). Log transformations were applied to all three motility variables to normalize the distributions. Due to the sample size, simple linear regression models were utilized for analysis of kinetic data associations. P-values less than 0.05 were considered significant. One-way ANOVAs were performed on comparisons of more than two groups, as indicated in the figure legends. Paired t-tests were conducted when only two groups were compared in knockdown and over-expression studies and data were normally distributed. All basic graphing and statistics were carried out in Prism (GraphPad Software, La Jolla, CA) unless otherwise noted.

Code Availability

Codes for KAV and image processing can be found online at: https://github.com/icbm-iupui/kinetic-analysis-vasculogenesis [133].

Figure 7 and Tables (1-2)

Table 1. Clinical Data for Maternal Subjects

Sample	Maternal Age (y)	Medications	Maternal prepregnancy BMI	HbA1c
Uncomplicated 1	25	None	37.2	ND
Uncomplicated 2	32	None	27.4	ND
Uncomplicated 3	26	None	22.8	ND
Uncomplicated 4	27	None	27.6	ND
Uncomplicated 5	25	None	22.0	ND
Uncomplicated 6	37	None	33.5	ND
Uncomplicated 7	27	None	42.6	ND
Uncomplicated 8	27	None	31.7	ND
Uncomplicated 9	25	None	23.8	ND
Uncomplicated 10	42	None	34.6	5.6
T2DM 1	31	Insulin	25.6	6.8, 6.5
T2DM 2	25	Insulin, Lisinopril, Metformin	34.3	12.5, 13.5
T2DM 3	26	Insulin	30.5	15.2, 12.4, 11.7, 12, 11.9, 14.4
T2DM 4	38	Insulin	36.8	6.8, 5.8, 6.0
T2DM 5	35	Glyburide	32.9	6.5, 6.0, 5.5
T2DM 6	38	Insulin	38.7	9.2, 6.7, 5.9
T2DM 7	30	Metformin, Glyburide	29.1	5.5, 5.3
T2DM 8	30	Metformin, Insulin	48.4	6.1, 5.7
T2DM 9	31	Insulin	25.6	6.7, 5.8
T2DM 10	38	Insulin	29.9	ND

ND = Not Done, T2DM = Type 2 Diabetes Mellitus

Table 2. Clinical Data for Infant Subjects

Sample	Sex	Gestational age	Infant weight (kg)	Infant weight percentile (%)	Infant weight/length percentile (%)	Ponderal Index (kg/m^3)
Uncomplicated 1	Female	39	3.7	84.6%	55.2%	27.2
Uncomplicated 2	Female	37	3.6	79.4%	5.8%	23.6
Uncomplicated 3	Male	39	3.6	70.2%	31.9%	25.7
Uncomplicated 4	Female	40	2.9	24.2%	1.8%	22.3
Uncomplicated 5	Male	38	3.4	58.3%	38.6%	26.0
Uncomplicated 6	Male	40	3.6	68.1%	26.2%	25.3
Uncomplicated 7	Female	39	4.3	98.6%	74.4%	28.9
Uncomplicated 8	Female	41	3.3	55.2%	78.2%	28.8
Uncomplicated 9	Male	39	3.3	42.1%	83.1%	26.8
Uncomplicated 10	Female	38	2.9	23.3%	1.0%	21.9
T2DM 1	Male	37	4.5	98.6%	91.6%	30.4
T2DM 2	Female	39	3.4	61.8%	76.4%	28.7
T2DM 3	Male	38	3.7	81.1%	7.1%	23.9
T2DM 4	Female	39	3.6	80.0%	80.8%	29.0
T2DM 5	Female	38	3.2	50.0%	13.6%	24.3
T2DM 6	Male	38	3.3	45.2%	88.5%	29.7
T2DM 7	Male	39	3.9	84.6%	34.5%	26.0
T2DM 8	Female	37	2.7	11.9%	37.1%	26.2
T2DM 9	Male	36	3.1	32.6%	94.7%	31.1
T2DM 10	Female	39	3.7	84.6%	41.7%	26.5

ND = Not Done, T2DM = Type 2 Diabetes Mellitus

Figure 7. Workflow for Acquiring and Assaying Cord Blood-derived ECFCs

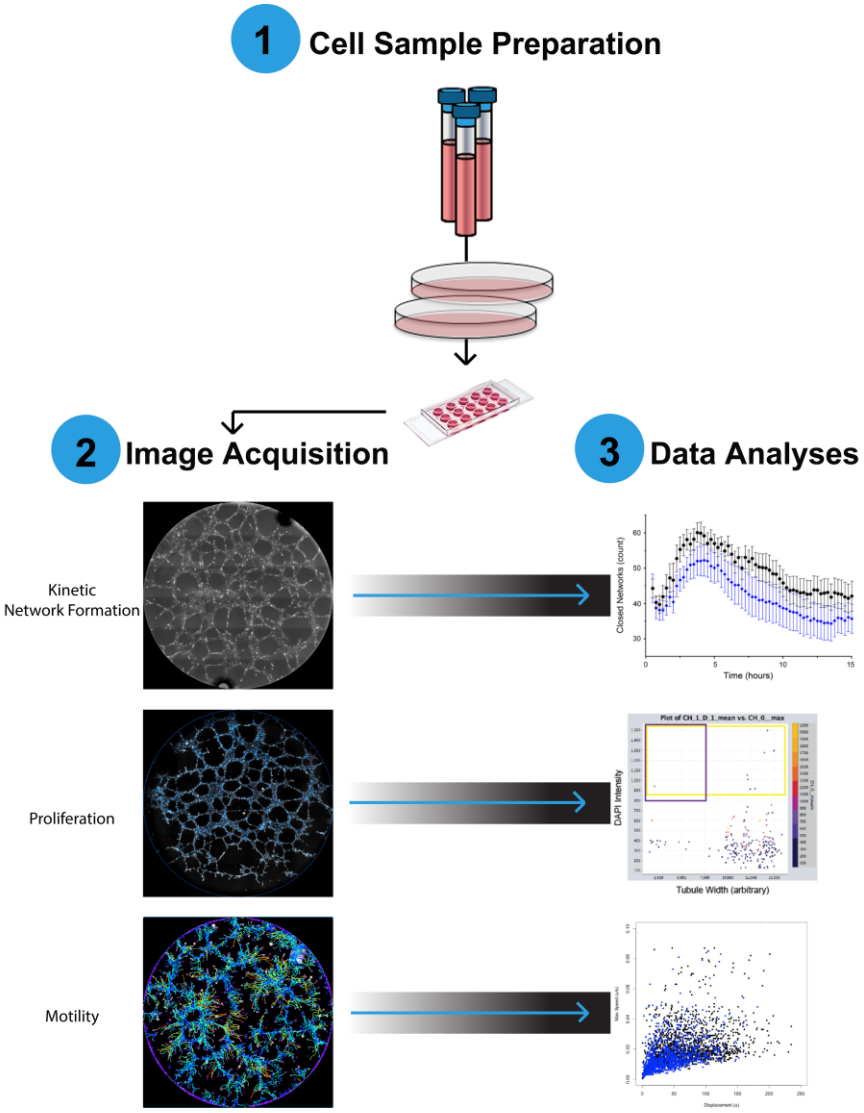

The first stage **(1)** of the workflow was cell sample preparation from human blood samples. Blood was isolated from the umbilical cord immediately following birth and processed for the derivation of mononuclear cells which were plated, as previously described, to isolate ECFCs [31]. ECFCs were cultured and passaged in tissue culture dishes containing EGM2+10% FBS. Prior to image acquisition, ECFCs were plated in µ-slide wells containing Matrigel, where they formed network structures. In the second stage **(2)**, images of the entire µ-slide wells were acquired. Time-lapse phase contrast images were captured and used in kinetic analysis of network formation. Static fluorescent images were acquired for assessment of proliferation on Matrigel. Additionally, fluorescent time-lapse images of ECFCs expressing nuclear GFP were captured to quantitate cellular motility. Once the images were acquired, the third stage **(3)** in the workflow involved the implementation of novel data analyses developed to assess ECFC function *in vitro*.

CHAPTER 3: RESULTS

Aim 1: To develop innovative methods to quantitatively assess the kinetics of ECFC vasculogenesis *in vitro*.

Dynamic Assessment of Neonatal ECFC Vasculogenesis

Current quantification methods of network formation are largely static, providing limited insight into potential mechanisms that contribute to functional deficits. To obtain a realistic depiction of the dynamic process of vasculogenesis, new assays were developed to measure the kinetics of umbilical cord-blood-derived ECFC network formation in real-time. ECFC samples derived from uncomplicated pregnancies were used to establish the new assays and perfect the analysis. In the Kinetic Network Formation assay, longitudinal data were analyzed from phase contrast images over 15 hours. To derive quantitative data, an analysis plug-in was created by myself and Seth Winfree for the FIJI image-processing package [126], which will be referred to as Kinetic Analysis of Vasculogenesis (KAV). KAV uses image segmentation followed by skeletonization to analyze network components from phase contrast images (Figure 8). The segmentation and skeletonization processes produce skeleton and mask renditions of the network structure, which are used to derive eight parameters (7 measured, 1 calculated) of network formation quantitated by KAV (Figures 8 and 9). Videos showing representative phase contrast, skeleton, and mask renditions from all time points analyzed are available online [133].

The seven parameters measured by KAV include: closed networks, network areas, nodes, branches, branch length, triple-branched nodes, and quad-branched nodes (Figure 9). These parameters were chosen to evaluate network structure and connectivity because of use in previous studies or their descriptive nature [115]. Using time-lapsed imaging of ECFC vasculogenesis coupled with KAV, several interesting observations were made. Closed networks increased for the first 4-5 hours and decreased thereafter (Figure 9),

suggesting that network formation occurs in two distinct phases. Concurrently, average network area initially decreased followed by increased network area (Figure 9). Total nodes and branches in the overall network structure steadily decreased in the first 10 hours and then stabilized. Quantitated KAV parameters provided a detailed summary of network components, however these measurements do not assess node connectivity. Given the observation of unstable or "broken" branch connections in some ECFC samples, KAV software was programmed to calculate a branch-to-node ratio, as an assessment of network connectivity. KAV identified that the branch-to-node ratio decreased in the first 5 hours as connectivity of the network increased, and then remained unchanged from 5-10 hours as the network structure became stable (Figure 9). After 10 hours, the ratio of branches to nodes increased slightly, indicative of node condensation and branch de-stabilization. In total, 5 hours post-plating was identified as a critical time point in network formation and represented the time of maximal network connectivity. By 5 hours, the essential components of the network were established with subsequent changes in structure being indicative of structure stability and/or remodeling. Identification of this critical time point guided later studies, such that the first 5 hours is referred to as Phase 1 and 5-10 hours is referred to as Phase 2.

Reproducibility of the Kinetic Network Formation assay was validated by evaluating a single ECFC sample on multiple days (Figure 10A-B). The mean ± standard deviation for sample values across three different days show assay variability (Figure 10A). The calculated coefficient of variation, or the ratio of the standard deviation to the mean, is another measure of data variability often used to analyze data sets with varying mean values. The coefficient of variation for the number of closed networks measured by KAV over three experimental days was between 8-15% across 15 hours of network formation, with the lowest values occurring near 5 hours post-plating (Figure 10B). To validate the

accuracy, a comparison was made between the traditional method of manual scoring and KAV (Figure 10C-E). Total networks and nodes identified by KAV were comparable to manual counts (Figure 10C-D). KAV detected slightly more branches than identified manually (Figure 10E). Given the difficulty in scoring >200 branches per well, this observation suggests that KAV may be more sensitive. Therefore, this novel, validated analytic method provides a longitudinal assessment of vasculogenic potential that is currently lacking in traditional, static quantification methods. Furthermore, this approach identified dynamic changes in network structure with a transition at 5 hours that may provide new mechanistic insights into vasculogenesis.

Tissue Cytometry Quantitates Dividing ECFC Frequency and Localization

Disrupted vasculogenic potential may be due to altered proliferation, survival, and/or migration, which are challenging phenotypes to assess *in situ* due to the semi-solid nature of the matrix used for *in vitro* studies. To address this technical obstacle, immunofluorescence methods were developed to evaluate ECFC proliferation and migration during network formation. Initially, to enhance visualization of key cellular components (i.e. cytoskeleton and nucleus), ECFC networks were fixed, permeabilized, and stained with anti-alpha tubulin and NucBlue for high-resolution imaging using confocal microscopy. Interestingly, dividing ECFCs were observed in both nodes and branches (Figure 11A). To achieve a comprehensive analysis of ECFC proliferation the immunofluorescence imaging technique was expanded to include the entire network, allowing for quantitation of the total number of dividing cells as well as their frequency and localization within the network structure (Figure 11B).

To quantitate the frequency and localization of dividing ECFCs, a tissue cytometry (TC) software was developed. The TC software was adapted from a broad Volumetric Tissue

Exploration and Analysis approach that was developed to quantitate cells associated with spatial parameters in 3D image volumes [123]. In the TC application, tubulin immunofluorescence generates a Euclidean distance map, which represents network structure width (Figure 12A). TC was programmed to recognize mitotic cells based on high NucBlue intensity. The distance map, in combination with NucBlue intensity, allows for identification of mitotic cells localized within a branch (thin <60 pixels) or node (thick >60 pixels, Figure 12A Insets 1 and 2). TC allows for 'gating' on specific cell populations within a sample based on localization and NucBlue fluorescence. Using this strategy, gates were applied to differentiate ECFCs located in both branch (Gate 1) and node regions of the network (Gate 2) (Figure 12A).

The TC methodology was validated across three days using multiple ECFC samples (Figure 12B). Imaging the entire structure enabled quantitation of all cells comprising the structure, not just those undergoing mitosis. Whole-well analysis confirmed visual observation that approximately 75% of all network cells are in the nodes. Additionally, around 75% of dividing cells are also localized to nodes (Figure 12B). Thus, both nodes and branches have an equal propensity for cell division since total cell number is predictive of cell division. Although the overall percentages observed in this analysis were not surprising, the high consistency across samples and experimental days was unexpected for this type of cell organization measure. Importantly, these analyses were conducted on entire wells, enabling simultaneous, large-scale quantitation of thousands of cells *in situ* across the whole network.

FIJI TrackMate Assesses ECFC Motility at the Single Cell Level

To assess ECFC motility kinetics, a time-lapse imaging approach was established to track cell movement during *in vitro* vasculogenesis. A baculoviral delivery system labeled

ECFC nuclei with green fluorescent protein (GFP) to allow for immunofluorescence image capture (Figure 13A). Fluorescence imaging of punctate GFP signal enabled FIJI TrackMate to more easily identify and track individual cells (Figure 13B-C) [126]. Using this approach, three parameters of motility were assessed: including displacement, mean speed, and maximum speed. Cumulative cell movement over the time-course is summarized as tracks representing individual cell displacement or speed (Figure 13D-F). To determine whether observed phenomenon was the result of differences in cell plating numbers, cell counts were generated using TrackMate. Importantly, cell numbers were equivalent in Phase 1 ($p=0.75$) and Phase 2 ($p=0.28$). Equal cell numbers at the first time point in Phase 1 confirms similar plating. Equivalent cell numbers at the beginning of Phase 2 (5h) suggests that proliferation and apoptosis are unlikely contributing to alterations in total cell number after five hours of formation.

Qualitatively, individual cells assemble into primitive network structures in Phase 1, while more coordinated cell movements are observed in Phase 2. Coordinated movement in Phase 2 is speculated to be the result of increased ECFC proximity, as cells are already comprising larger network structures during the second phase of formation. In Phase 1, ECFCs exhibit increased displacement and speed compared to ECFCs in Phase 2 ($p=0.0001$ and $p=0.0002$, respectively), suggesting that greater cell movement occurs in early network formation. Linear models were generated to determine if mean ECFC motility in Phase 1 is maintained in Phase 2. Assessments using linear models indicate that the amount of displacement, mean speed, and maximum speed are all positively correlated between Phase 1 and Phase 2 (Table 3). These analyses confirm that samples with greater displacement and speed in Phase 1 continue to exhibit higher displacement and speed in Phase 2. Overall, all parameters of motility, including speed and displacement, positively correlates with the other parameters (Table 4; all p-values

<0.05). Positive correlations between displacement and speed demonstrate that faster moving ECFCs also move farther. This observation further suggests that ECFC movement is coordinated during network formation.

Data Integration to Enhance Mechanistic Insights of Vasculogenesis

KAV, TC, and motility assays assess ECFC function within the same context of network formation. The power of this approach is the identification of correlated phenotypes that promote disrupted ECFC vasculogenic function and the potential discovery of mechanisms involved. Correlating TC data (Figure 12) with KAV data (Figure 9) revealed that ECFC samples with increased cell division in branches formed fewer closed networks ($r= -0.50$, $p=0.048$). KAV also determined that some ECFC samples achieved maximal network number quickly while other samples displayed delayed maximal network formation. Therefore, to assess whether localized cell division impacted the rate of network formation the time to maximum networks was analyzed. ECFCs with increased branch division reached maximal networks more quickly than samples with lower branch division ($r= -0.51$, $p=0.044$). These data suggest that increased branch division and faster network formation result in an overall reduction in total network number. In addition, associations were discovered between KAV and motility data. Decreased ECFC displacement and mean speed in Phase 1 were associated with a higher branch to node ratio ($r= -0.85$, $p=0.039$ and $r= -0.64$, $p=0.035$, respectively). Similarly, ECFCs with reduced displacement in Phase 2 also had a higher ratio of branches to nodes, though not statistically significant ($r= -0.27$, $p=0.11$). Importantly, these results indicate that ECFCs that move a shorter distance or at a slower speed have higher ratios of branches to nodes, which is indicative of reduced network connectivity. Overall, these observations guided subsequent studies outlined in the second aim to determine how intrauterine exposure to maternal T2DM alters ECFC vasculogenesis.

Figures (8-13) and Table 3

Figure 8. Kinetic Analysis of Vasculogenesis Produces Skeleton and Mask Renditions from Phase Contrast Images

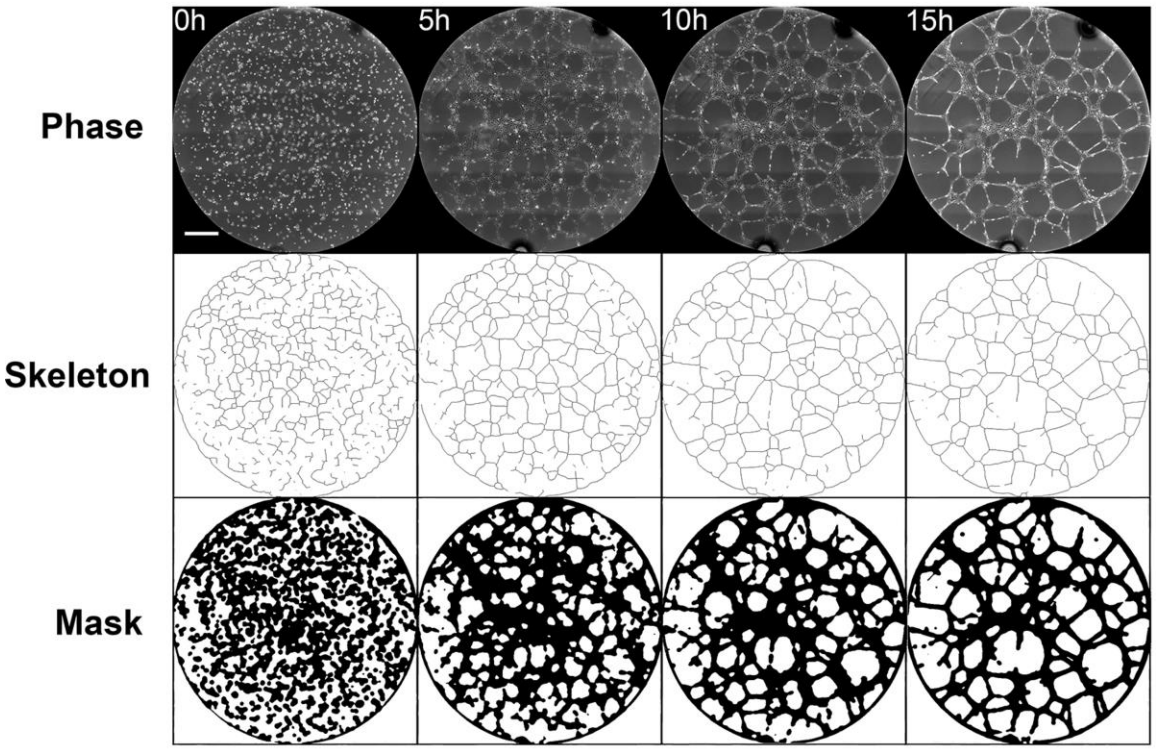

Images of ECFC network formation were captured every 15 minutes for 15 hours by phase contrast microscopy. Representative phase contrast images at 5-hour increments, starting at the time of plating (0h), are shown. The phase contrast images were analyzed using KAV to produce both “skeleton” and “mask” renditions of the network structure. The scale bar represents 500 μm. Videos showing the phase, skeleton, and mask renditions from all time points analyzed can be found at the following website http://ajpcell.physiology.org/content/312/4/C446.figures-only [133].

Figure 9. KAV Quantitates Network Metrics

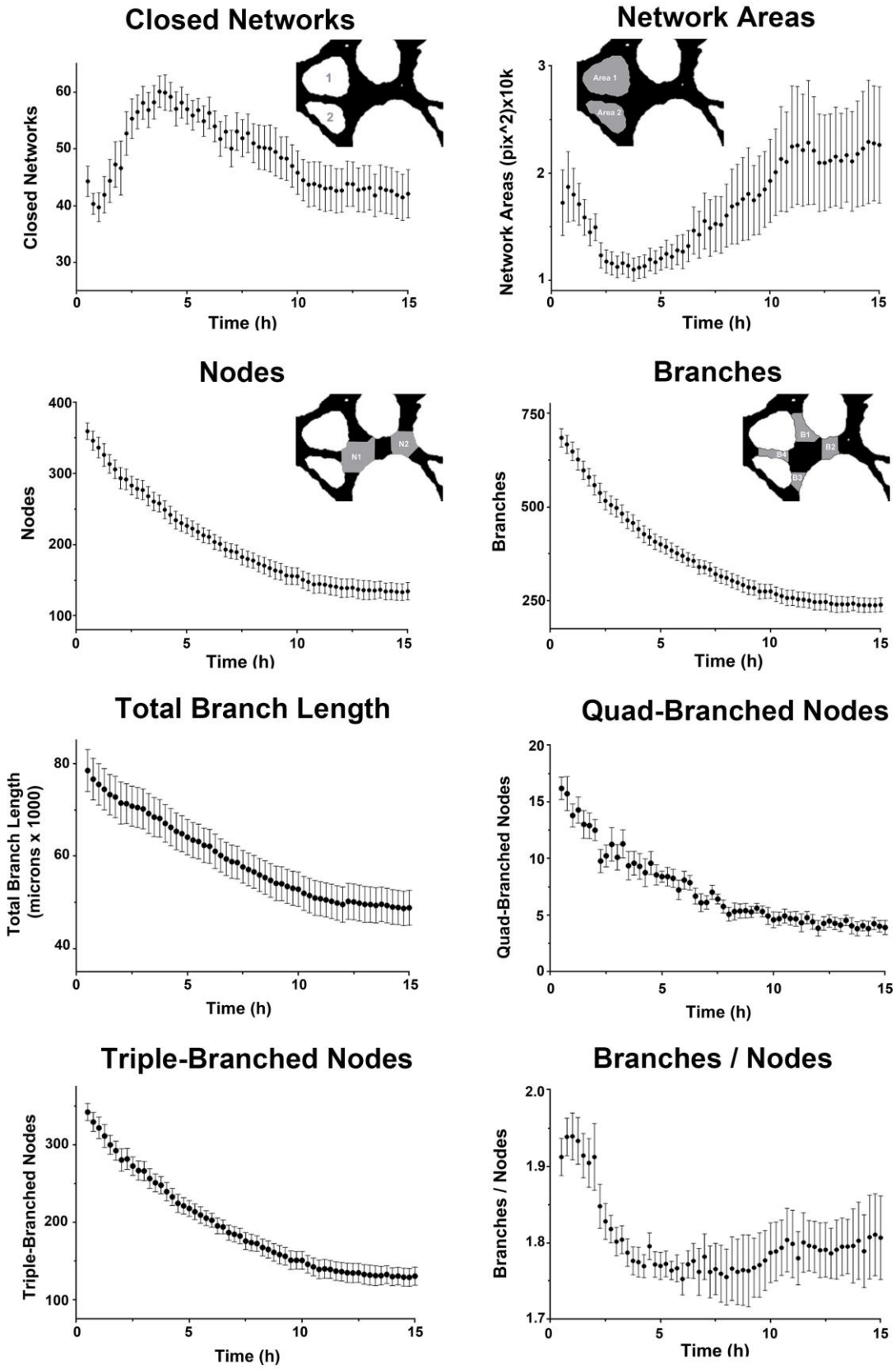

Figure 9 continued:

Mean data of 8 parameters of network structure are illustrated for 10 ECFC samples from uncomplicated pregnancies. Data were quantitated using the newly developed KAV FIJI plugin over a 15 hour period. Magnified regions of "mask" are depicted for the top four graphs. The parameter analyzed in the corresponding line graphs below is highlighted in gray. Line graphs for the following measured parameters are shown: closed networks, network area, nodes, branches, total branch length, triple-branched nodes, and quad-branches nodes. The ratio of branches to nodes, a calculated parameter, is also shown. The line graphs represent the mean data (± SEM) for 10 separate patient samples from uncomplicated (UC) pregnancies.

Figure 10. Validation of KAV Quantification

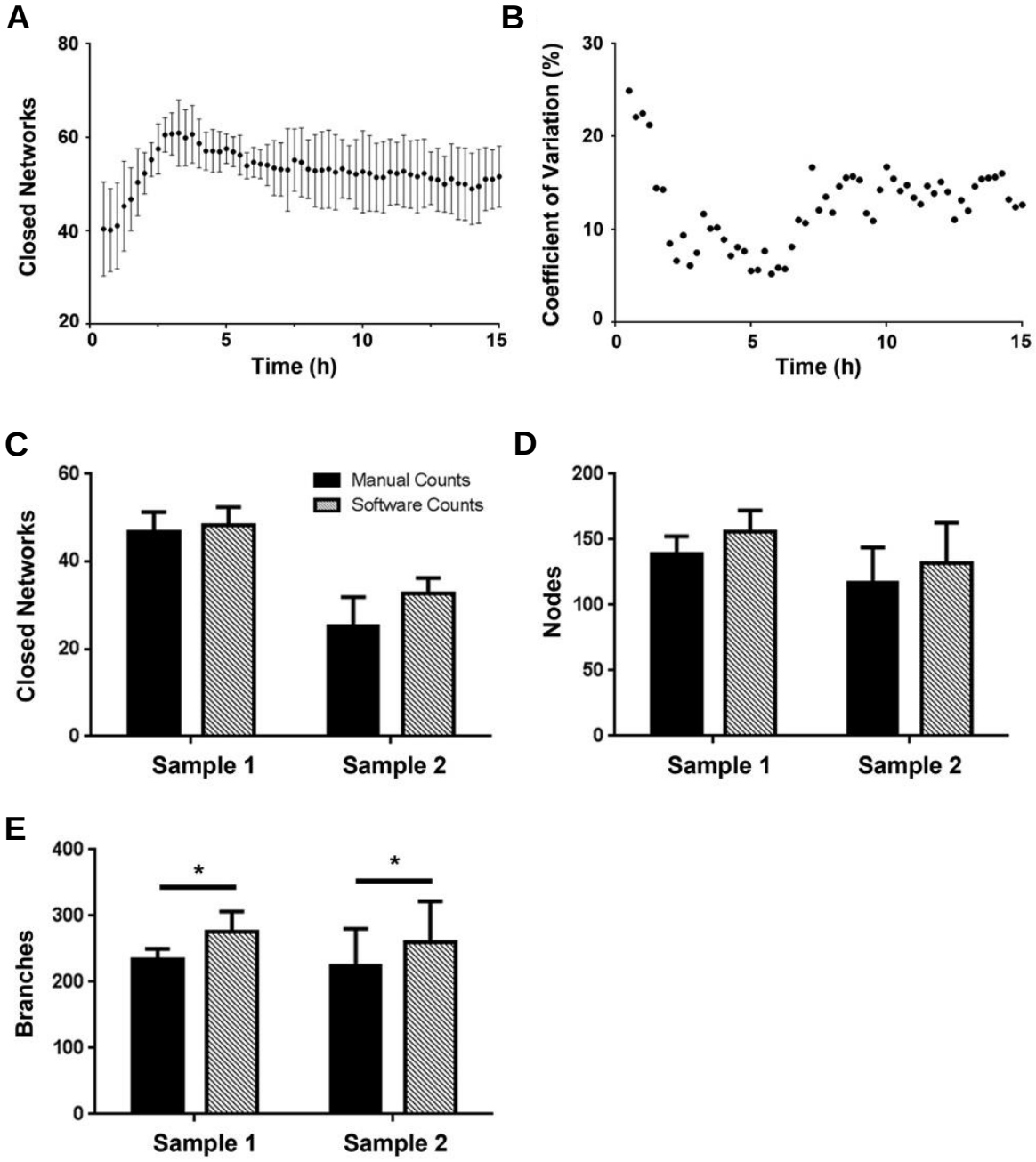

A) To determine day-to-day variation of the assay design, KAV analysis was run for a single ECFC sample on 3 different days. Data shown represent mean ± SD. **B)** Coefficient of variation (%) is shown for the data in Panel A. **C-E)** To validate the KAV software, manual scoring of network formation was compared with data generated by KAV for two individual ECFC samples on 4 different experimental days. **C-D)** The number of Closed Networks and Nodes was no different between KAV and manual scoring. **E)** The number of branches detected was significantly increased when using KAV compared to manual counting for both samples (*$p<0.05$). Data are shown as mean ± SD.

Figure 11. ECFCs Undergo Proliferation During Network Formation.

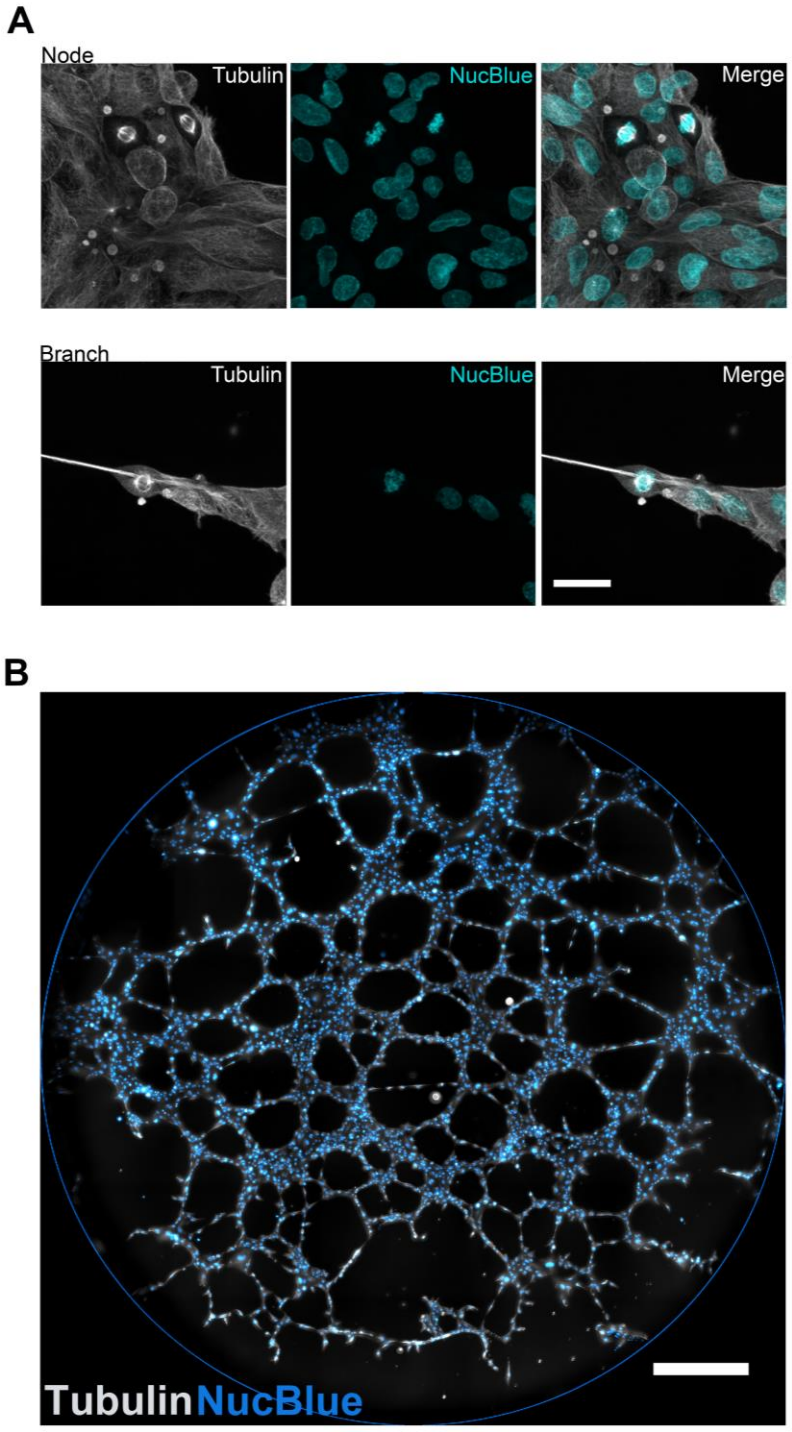

A) ECFCs were plated on Matrigel for 5 hours, then fixed and stained for α-tubulin (gray) and NucBlue (cyan). Representative photomicrographs of dividing cells in a node and branch are shown. The scale bar represents 30 µm. **B)** The immunofluorescence staining and imaging protocols were scaled-up to include entire µ-wells. The scale bar represents 500µm).

Figure 12. Tissue Cytometry Quantifies the Frequency and Localization of Proliferating ECFCs on Matrigel

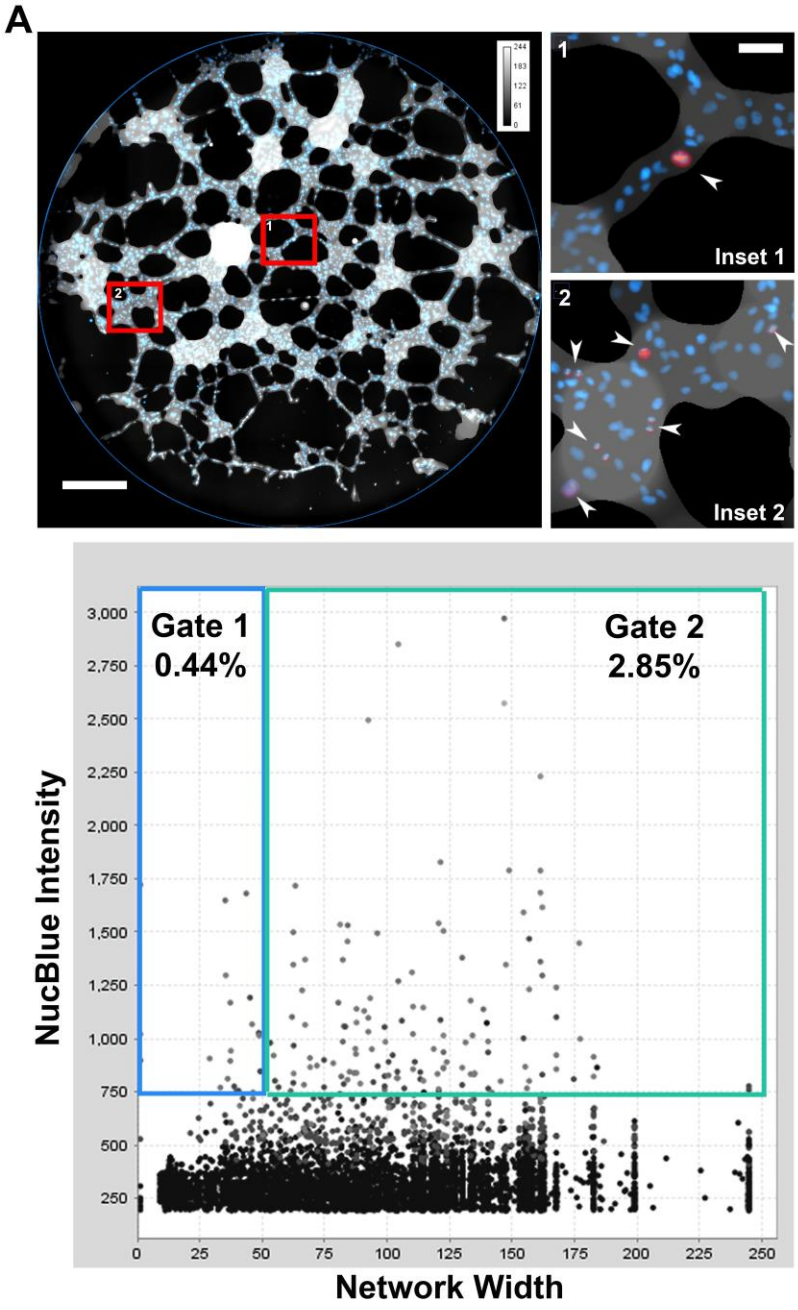

Figure 12 continued:

A) Tissue cytometry (TC) analysis generated an overlay based on alpha-tubulin immunofluorescence, which was used to quantitate network width and discriminate between node and branch structures. Mitotic cells, highlighted in red, were in branches (Inset 1) and nodes (Inset 2). TC integrated network width and NucBlue fluorescence intensity to generate scatter plots that included all cells detected in the network (n=4733 cells). Gating identified mitotic cells within branches (Gate 1) and nodes (Gate 2). Scale bars represent 500µm (left and middle panels) and 50µm (Inset 1). **B)** Percent of total ECFCs (left graph) and percent of mitotic ECFCs (right graph) located in nodes or branches was determined by TC for 3 independent ECFC samples on 3 days (S1 = sample 1, S2 = sample 2, S3 = sample 3). Individual points represent data from different days. Mean ± SD is shown.

Figure 13. Assessment of ECFC Motility During Network Formation Using FIJI TrackMate

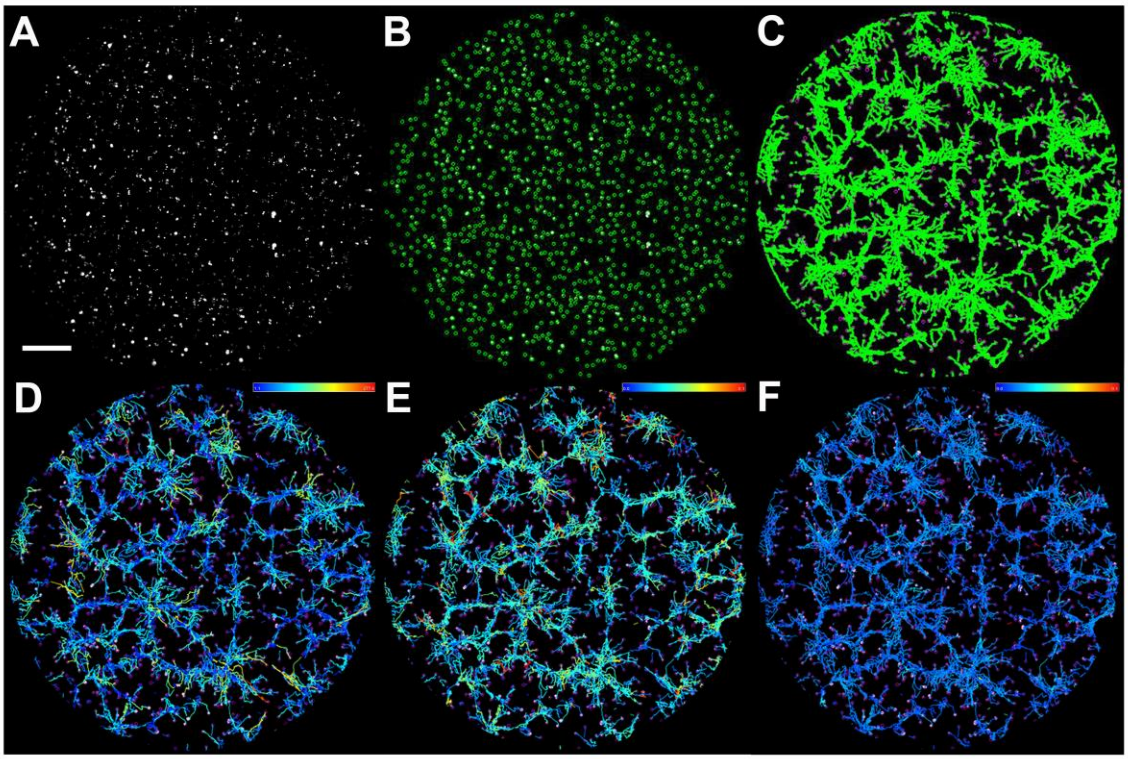

A) Representative photomicrograph of nuclear GFP labelled ECFCs immediately following plating on Matrigel. GFP fluorescence is shown in gray. **B)** GFP signal was used to segment individual ECFCs in TrackMate. ECFCs identified by the system are highlighted in green circles. **C)** The series of fluorescence images acquired over time were analyzed as stacks using FIJI TrackMate. TrackMate produces paths, shown in green, representative of total cell movement over the imaging interval (10 hours shown). **D-F)** Individual ECFC paths are color-coded by the software based on variables such as **(D)** displacement, **(E)** maximum speed, and **(F)** mean speed. The color scales indicate the displacement or speed ranges, with high values depicted by orange/red, and low values represented by blue. The scale bar represents 500µm. Videos showing ECFC displacement at all time points analyzed can be found at the following website http://ajpcell.physiology.org/content/312/4/C446.figures-only [133].

Table 3. Phase 1 and 2 Motility Parameters

Phase 1	Phase 2	Slope	Standard Error	p-value
Displacement	Displacement	0.4747	0.1279	0.0026
Mean Speed	Displacement	4326.2	1506.3	0.0131
Mean Speed	Mean Speed	0.5741	0.2312	0.0275
Mean Speed	Max Speed	1.5891	0.6615	0.0319
Max Speed	Displacement	1772.7	785.03	0.0418
Max Speed	Mean Speed	0.3745	0.0863	0.0008
Max Speed	Max Speed	1.0939	0.2326	0.0004

Aim 2: To identify novel phenotypic differences in ECFC vasculogenesis following exposure to intrauterine diabetes.

ECFCs from Diabetic Pregnancies Exhibit Altered Network Formation Kinetics

After establishing that KAV enabled advanced assessments of ECFC function, KAV was applied to ECFCs exposed to maternal T2DM *in utero* to further elucidate potential functional deficits [79]. KAV demonstrated that the complexity of network structures is qualitatively and quantitatively different between ECFCs from uncomplicated (UC) and T2DM pregnancies (Figure 14). Qualitatively, ECFCs from T2DM pregnancies form fewer closed networks and have larger network areas compared to ECFCs from uncomplicated pregnancies (Figure 14). Although gross qualitative differences in network structure are visible around 10 hours post-plating, KAV analysis was performed to achieve a more accurate and quantitative measure of differences in network formation. Qualitative observations were confirmed by quantitative KAV analyses (Figure 15). In addition to confirming differences in closed network number and network area, reductions in more subtle phenotypes, such as total nodes and total branches, were also identified by KAV for T2DM-exposed ECFCs (Figure 15). Additionally, despite evidence of qualitative differences at 10 hours post-plating, KAV analysis elucidated that significant differences in many of the structural phenotypes occur much earlier than 10 hours post-plating. For example, T2DM-exposed ECFCs don't form the same number of closed networks initially, as indicated by a lower peak in the closed network graph (Figure 15). Therefore, differences in network structure are attributable, at least in part, to impairment in the early stages of formation.

Decreased network stability, or increased "broken" branch connections, was also observed in T2DM-exposed ECFC networks during Phase 2. Quantitation by KAV

confirmed that the ratio of branches to nodes, a connectivity measure, is increased in T2DM-exposed ECFCs, with the greatest differences occurring in Phase 2. This observation suggests that not only do ECFCs from T2DM pregnancies form fewer networks in Phase 1, but that the network connections formed are not maintained. For example, UC ECFC samples exhibited the highest branch to node ratio in Phase 1, just prior to maximal network formation. Conversely, ECFCs from T2DM pregnancies achieved maximal branch to node ratio more frequently in Phase 2 ($p=0.005$), suggesting a higher frequency of broken connections and condensing networks.

Despite differences in several structural phenotypes, ECFCs from T2DM pregnancies still exhibit a bi-phasic pattern of network formation. Like ECFCs from UC pregnancies, T2DM ECFCs undergo two phases of formation with a change occurring around 5 hours post-plating. Although the bi-phasic pattern of formation is maintained, KAV analysis identified clear differences in sample variability of individual ECFC samples from uncomplicated and T2DM pregnancies. ECFCs from uncomplicated pregnancies exhibit smaller variability across time (Figure 15 black lines). However, greater variation was detected in ECFCs from T2DM samples (Figure 15 gray lines). Importantly, increased variability in T2DM ECFC function has been observed in numerous other assays as well and is likely attributable to increased patient heterogeneity [79].

To rigorously evaluate alterations in network formation for T2DM samples, estimated differences between time-lapse data were calculated (Figure 15). Statistically significant differences exist between uncomplicated and T2DM groups when the estimated difference (± the 95% confidence limit, CI) does not cross the reference line ($y=0$). These analyses indicate that for most of the 15-hour time course, significant differences were detected between uncomplicated and T2DM data in all KAV parameters. Similar to qualitative

observations, the greatest difference between the curves (furthest point from reference line) for network area and branch to node ratio occurs in Phase 2. Total closed networks, nodes, and branches initially peak near 5 hours and then level off, suggesting that differences in KAV parameters are phase-specific. Together these results confirm that T2DM-exposed ECFCs form fewer closed networks, nodes, and branches, but develop larger network areas and an increased branch to node ratio compared to ECFCs from uncomplicated pregnancies.

Diabetes Exposure Does Not Alter ECFC Proliferation During Network Formation

To begin to identify underlying mechanisms contributing to the dramatic differences in network structure between ECFC samples from uncomplicated and T2DM pregnancies, proliferation was assessed. First, ECFC proliferation was evaluated in the context of network formation. After establishing the TC method to assess the frequency and localization of dividing cells on Matrigel, proliferation of ECFCs from T2DM pregnancies was assessed. A 5-hour time point was chosen based on KAV results indicating the time for maximal closed networks (Figure 15). TC analysis revealed that most ECFCs (~75% of all cells), including dividing and non-dividing, were localized in nodes in both experimental groups (Figure 16). ECFCs from uncomplicated and T2DM pregnancies divided at similar rates overall (UC 4.1% ± 2.4, and T2DM 4.5% ± 2.8%, n=9 UC and n=7 T2DM). Additionally, dividing ECFCs in both groups were primarily located within nodes (75%) compared to branches (25%), indicating an equal propensity to divide irrespective of network location. Unlike KAV analysis, sample variability was similar in both the UC and T2DM groups in this assay. One outlier was observed in the number of dividing cells in the T2DM group. Overall, however, there were no differences between the two sample groups.

ECFC proliferation was also assessed prior to plating on Matrigel using flow cytometric approaches. Overall, approximately 2-2.5% of ECFCs were undergoing division on collagen prior to plating (Figure 17). Similar to TC data, ECFC proliferation was not different between T2DM and uncomplicated samples as determined by flow cytometry (n=9 UC, n=9 T2DM, p=0.35). Thus, neither ECFC localization nor intrauterine T2DM exposure alters the likelihood of ECFCs to divide on collagen or after 5 hours on Matrigel. These measures of proliferation are acute in nature, capturing only a brief period of time. Therefore, to assess ECFC clonogenic potential, single cell assays were conducted on cells from uncomplicated and T2DM pregnancies.

ECFCs from T2DM Pregnancies have Altered Clonogenicity

Single cell assays, where ECFCs are FACS sorted and cultured for two weeks prior to colony size quantification, were conducted to assess ECFC clonogenicity. Colony size is indicative of the ability of a single cell to proliferate and differentiate into additional cells, and is, therefore, a direct measure of clonogenic potential [31]. Similar to the well-established hierarchies of hematopoietic progenitor cells, ECFCs can be distinguished by clonogenic and growth characteristics [134]. High proliferative potential ECFCs (HPP-ECFCs) have high clonogenic capacity and proliferative potential, and can give rise to colonies with over 2000 cells after two weeks in culture. Importantly, HPP-ECFCs form secondary and tertiary colonies upon re-plating and give rise to all cell types in the hierarchy, including other HPP-ECFCs [31]. Next in the hierarchy are low-proliferative potential ECFCs (LPP-ECFCs). LPP-ECFCs form colonies containing 50-2000 cells after two weeks in culture, however, upon re-plating are unable to form secondary LPP-ECFC colonies. Third in the hierarchy are cells that give rise to endothelial cell clusters, which are colonies containing 2-50 cells. Cells comprising endothelial cell clusters are not able

to be re-plated into additional colonies, and are, therefore, considered to be more mature, differentiated cells.

In the single cell assay, ECFCs from T2DM pregnancies form no HPP-ECFC colonies and significantly fewer LPP-ECFC colonies compared to ECFCs from uncomplicated pregnancies (Figure 18). Conversely, a higher percentage of T2DM-exposed ECFCs maintain individual, or single cell colonies after two weeks in culture. Previously, this phenotype was described as representing a differentiated endothelial cell. Therefore, ECFCs from T2DM pregnancies have reduced clonogenic potential compared to uncomplicated controls. Future studies aimed at identifying markers of ECFC clonogenic potential would provide an opportunity to determine if and how clonogenicity impacts ECFC vasculogenesis.

ECFC Motility is Not Altered Following Maternal T2DM Exposure in utero

Based on video microscopy and KAV analysis, it is evident that ECFC network formation is a highly dynamic process involving numerous cellular processes. One process that stood out from the video analyses was cell movement as the ECFCs migrated to form network structures. Therefore, ECFC movement was assessed in ECFCs from uncomplicated and T2DM pregnancies to determine if alterations in migratory ability contributed to differences in network structure identified by KAV (Figure 19). ECFC movement during Phase 1 and Phase 2 was assessed using FIJI TrackMate as described in Figure 13. ECFC samples from uncomplicated and T2DM pregnancies were analyzed to determine if alterations in displacement, mean speed, or maximum speed could be underlying observed differences in network formation kinetics. TrackMate identified and analyzed a similar number of tracks for both the uncomplicated and T2DM groups in Phase 1 and Phase 2 ($p=0.79$ and $p=0.23$ respectively). An equal number of ECFCs identified

in Phase 1 confirms equal plating densities between sample groups. Equivalent track numbers in Phase 2 also suggests similar proliferation, as was observed in Figure 16, as well as survival between experimental groups. Moreover, the number of individual ECFCs analyzed between the uncomplicated and T2DM groups were comparable. Of the three parameters evaluated, including displacement, mean speed, and maximum speed, each parameter positively correlated with the other two parameters in the uncomplicated as well as T2DM-exposed ECFCs (Figure 19 and Table 3; all p-values <0.05). The positive associations between the motility parameters was also consistent between Phase 1 and Phase 2 for both groups. Interestingly, the correlation coefficients (r) were consistent across sample groups and phases, suggesting that displacement, mean speed, and maximum speed have similar associations in all scenarios evaluated. These observations confirm that ECFCs that move faster also move farther on average compared to ECFCs with slower mean and maximum speed. In addition, intrauterine exposure to T2DM does not alter the positive correlations between the three motility variables tested, suggesting that coordinated cell movements are maintained in ECFCs from T2DM pregnancies.

Overall, ECFC motility in the uncomplicated and T2DM groups was heterogeneous. Some ECFCs exhibited decreased motility, as indicated by reduced displacement (Figure 20A). However, this phenotype was not consistently representative of a single clinical group. Following statistical analysis, no differences were detected in displacement, mean speed, or max speed between the uncomplicated and T2DM groups in Phase 1 or Phase 2 as indicated by nearly complete overlap of the histograms (Figure 20B). Therefore, alterations in ECFC motility are not responsible for the observed structural differences in ECFC network formation resulting from intrauterine T2DM exposure.

Clinical Data Provide Unique Translational Insights

The combination of using the primary human patient samples and having access to clinical measurements provides a unique opportunity for translational insight. Both maternal and infant clinical data were assessed with an emphasis on values that may reflect the severity of diabetes during gestation, such as maternal hemoglobin A1c. Two T2DM ECFC samples (T2DM 2 and T2DM 3) were obtained from pregnancies with highly elevated hemoglobin A1c (> 11), indicating poor glucose control compared to normal levels which are less than 5 (Table 1). These two ECFC samples, especially T2DM 3, had exacerbated KAV phenotypes, including a reduced number of closed networks and an increased ratio of branches to nodes, compared to the T2DM average of all 10 samples (Figure 21A). Additionally, motility analyses showed that T2DM 3 had reduced displacement in both Phase 1 and Phase 2 compared to a representative UC sample, as indicated by shortened tracks from FIJI TrackMate analysis (Figure 21B). Together, these observations suggest that poor glycemic control induces change at the cellular level, which can be studied *in vitro* using analyses such as KAV. Thus, KAV measurements may correlate with the severity of T2DM exposure *in utero*. Testing additional samples, including those representing a wide range of diabetes severity, would further support this initial observation.

Modeling Differences in Uncomplicated and T2DM Network Formation

After performing several assessments of ECFC network formation, a few phenotypes were identified that appear to represent the primary differences between sample groups. The ratio of branches to nodes, a novel phenotype representing network connectivity, is the most dramatically different ECFC phenotype discovered as a result of T2DM exposure (Figure 15). Importantly, unlike many of the other phenotypes analyzed using KAV, the ratio of branches to nodes is not a measured value, but a calculated value derived from

two measurements. Therefore, to clearly model this phenotype, a method to measure network connectivity was developed, and is depicted in Figure 22. When a network structure is highly interconnected, the number of branches and nodes produce a smaller ratio, such that for 26 branches and 13 nodes the ratio is 2 (Figure 22A). Two phenomena can occur to increase this ratio, as observed in the T2DM ECFC samples (Figure 15). First, a condensation of the nodes could occur, such that total nodes, or the denominator, is reduced, resulting in a higher ratio. Alternatively, the number of branches could increase due to breaking apart of previously stable network connections (Figure 22B). Although it is possible that both phenomena are occurring in T2DM networks, based on qualitative observation and KAV analysis, it appears that T2DM network structures are largely breaking apart in Phase 2. Breaking branch connections results in an increased branch to node ratio, as the number of branches (numerator) increases (Figure 22B-C). Qualitatively, it is clear how the number of closed networks would decrease along with an increase in the average area of the closed networks due to broken branch connections. These three structural phenotypes combine to produce an overall working model of ECFC network formation (Figure 22C). In Phase 1, ECFCs from T2DM pregnancies form fewer closed networks initially as well as fewer nodes and branches. Concurrent with reduced closed network numbers, the area network areas are larger on average. The initial impairments incurred in Phase 1 are followed by reduced stability in Phase 2. Reduced network stability results in fewer maintained connections and a higher ratio of branches to nodes. This working model of kinetic network formation can now serve as a baseline for understanding mechanisms contributing to alterations in network formation. Subsequent perturbations to the system can be compared to these observations to determine mechanisms underlying ECFC vasculogenesis.

Figures (14-22) and Table 4

Figure 14. ECFCs from T2DM Pregnancies Exhibit Impaired Network Formation

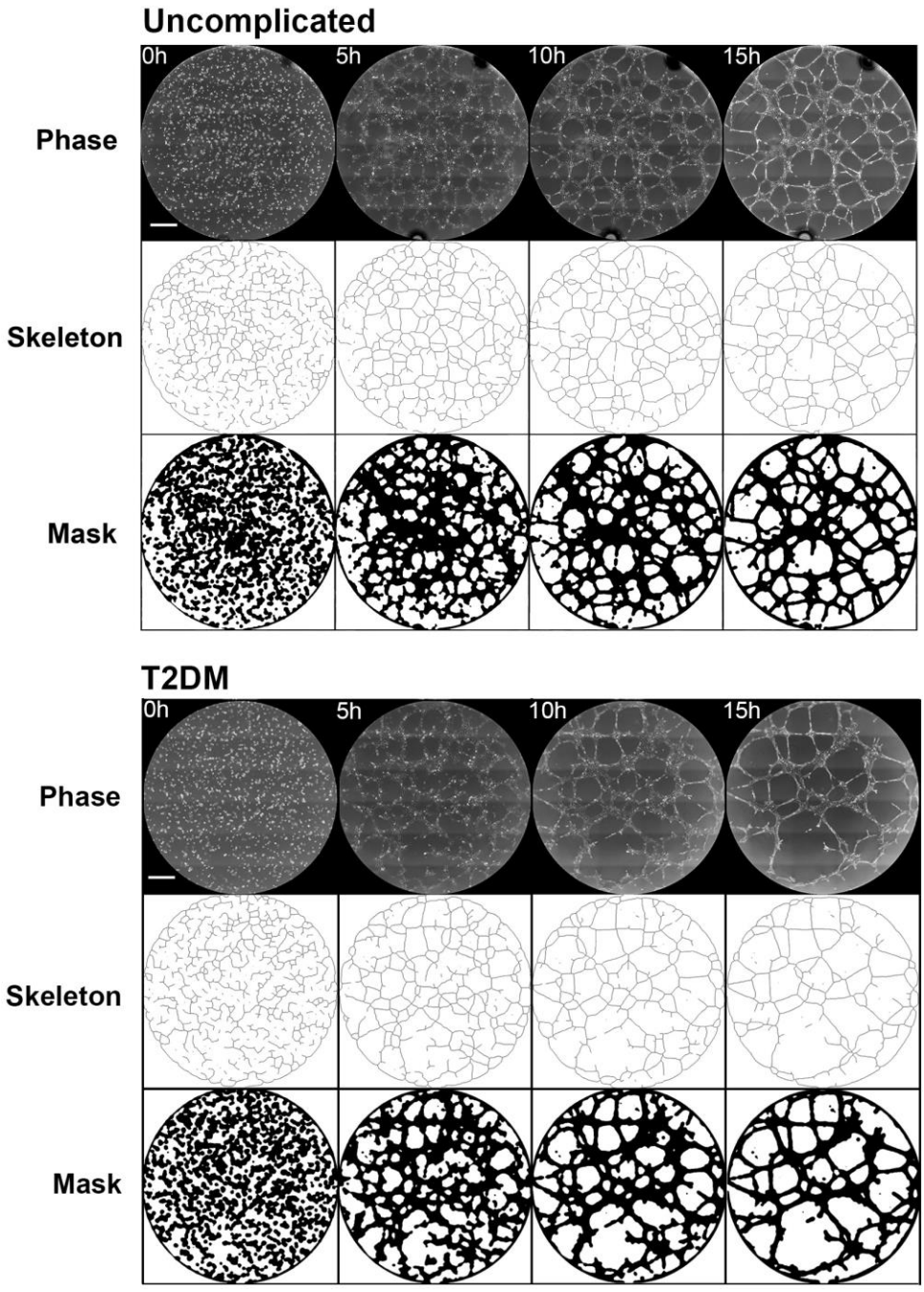

Representative phase contrast, skeleton, and mask images of ECFCs plated on Matrigel at 5 hour increments, starting at the time of plating (t=0), are shown. ECFCs were obtained from uncomplicated pregnancies (UC) and pregnancies complicated by T2DM. The scale bars represent 500 µm.

Figure 15. ECFCs from T2DM Pregnancies Exhibit Altered Network Formation Kinetics

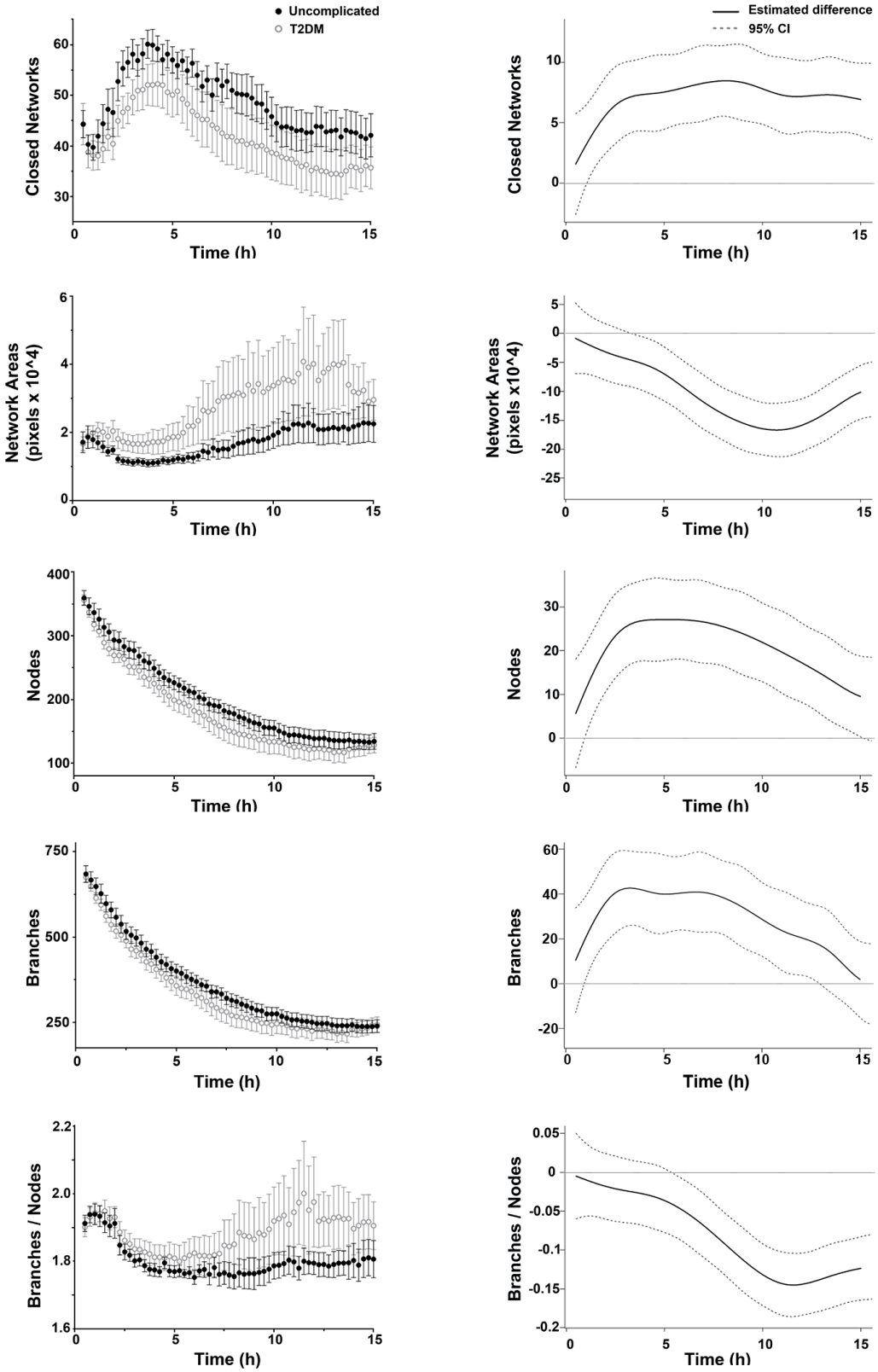

Figure 15 continued:

Kinetic analysis of vasculogenesis (KAV) software quantitated closed networks, network areas, nodes, branches, and the ratio of total branches divided by total nodes for both UC (closed circles) and T2DM pregnancies (open circles). The data illustrated represent the mean ± SEM of 10 separate ECFC samples from each experimental group. Differences between the mean kinetic curves of the two experimental groups for each parameter are shown as solid black lines with the 95% confidence interval (CI) represented by dotted lines. A significant difference between the curves for a specific time point is detected if the CI of the difference curve does not cross the reference line (y=0) at that time point.

Figure 16. Exposure to T2DM Does Not Alter ECFC Proliferation Five Hours into Network Formation

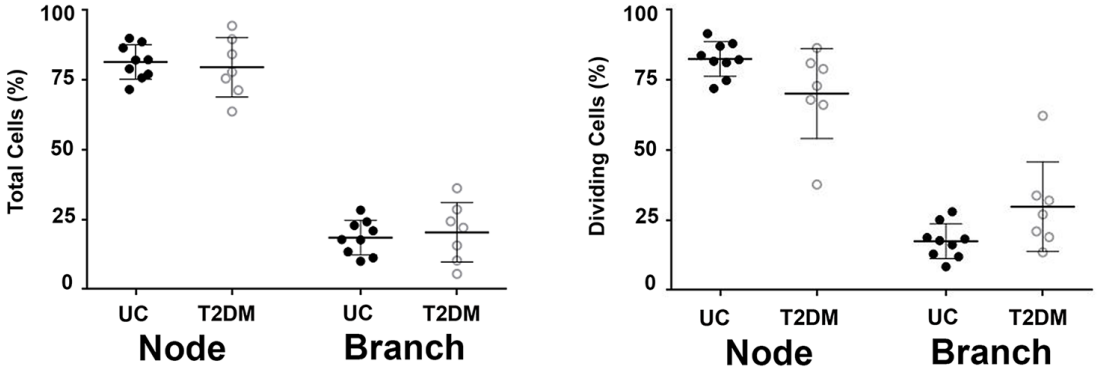

Percent of total ECFCs (left graph) and percent of mitotic ECFCs (right graph) located in nodes or branches was determined for UC and T2DM experimental groups. Graphs represent mean ± SD (individual points represent a unique ECFC sample).

Figure 17. ECFC Proliferation in UC and T2DM Samples is Equivalent by Flow cytometry

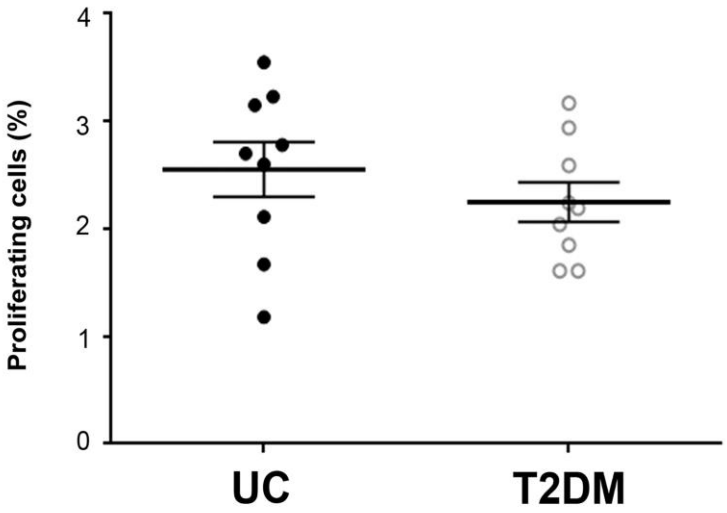

The percentage of ECFCs undergoing proliferation (± SEM) was determined by flow cytometry using phosphorylated histone H3 staining. Approximately 2-3% of cells were undergoing division and there was no statistical difference between cells from uncomplicated and T2DM pregnancies (UC n=9, T2DM n=9, p=0.35).

Figure 18. ECFCs from T2DM pregnanices Form Fewer LPP and HPP Colonies

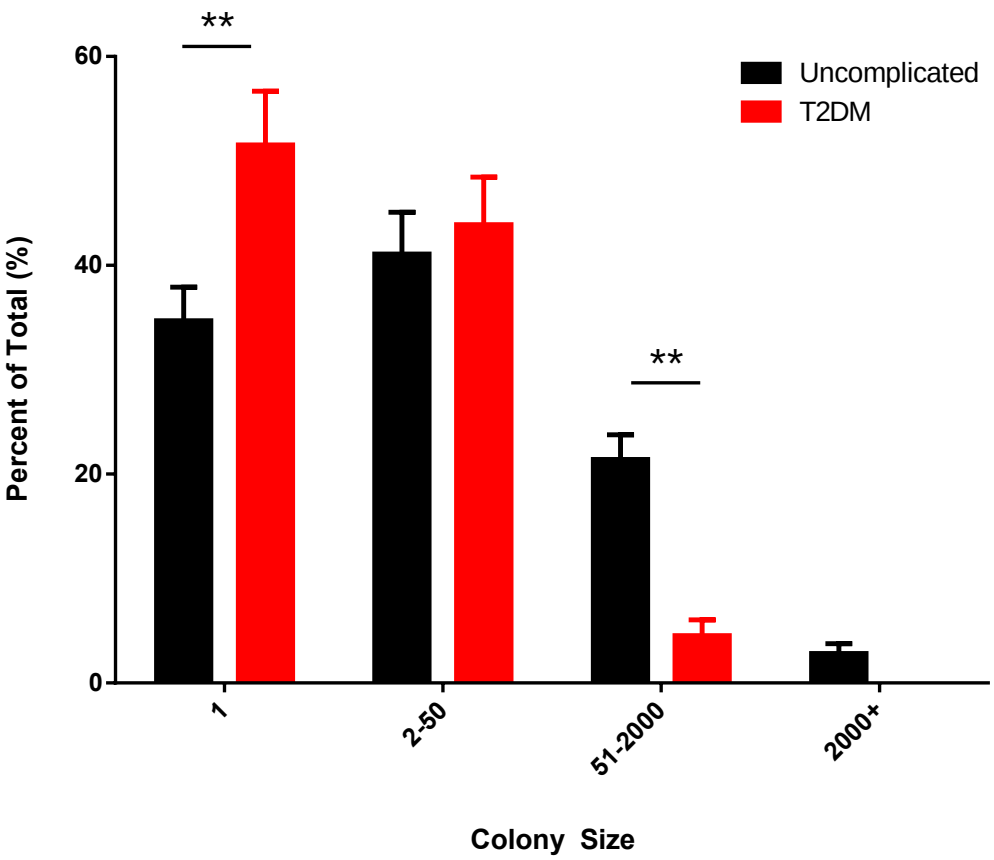

ECFCs from uncomplicated and T2DM pregnancies were plated in single cell assays and colony sizes were scored after 14 days in culture. Colony sizes are reported as previously described [31,135] with a single cell (1) representing a differentiated endothelial cell, 2-50 cells indicative of endothelial cell clusters, 51-2000 cell colonies representing low-proliferative potential (LPP) ECFCs, and 2000+ cells indicative of high-proliferative potential (HPP) ECFCs. ECFCs from T2DM pregnancies have a higher percentage of ECFCs that are differentiated and remain as single cells in culture. T2DM ECFCs also form fewer LPP colonies compared to uncomplicated controls. (n=6 for each group, **$p \leq 0.01$).

Figure 19. Speed and Displacement are Correlated in Phases 1 and 2 of Network Formation in Uncomplicated and T2DM ECFCs

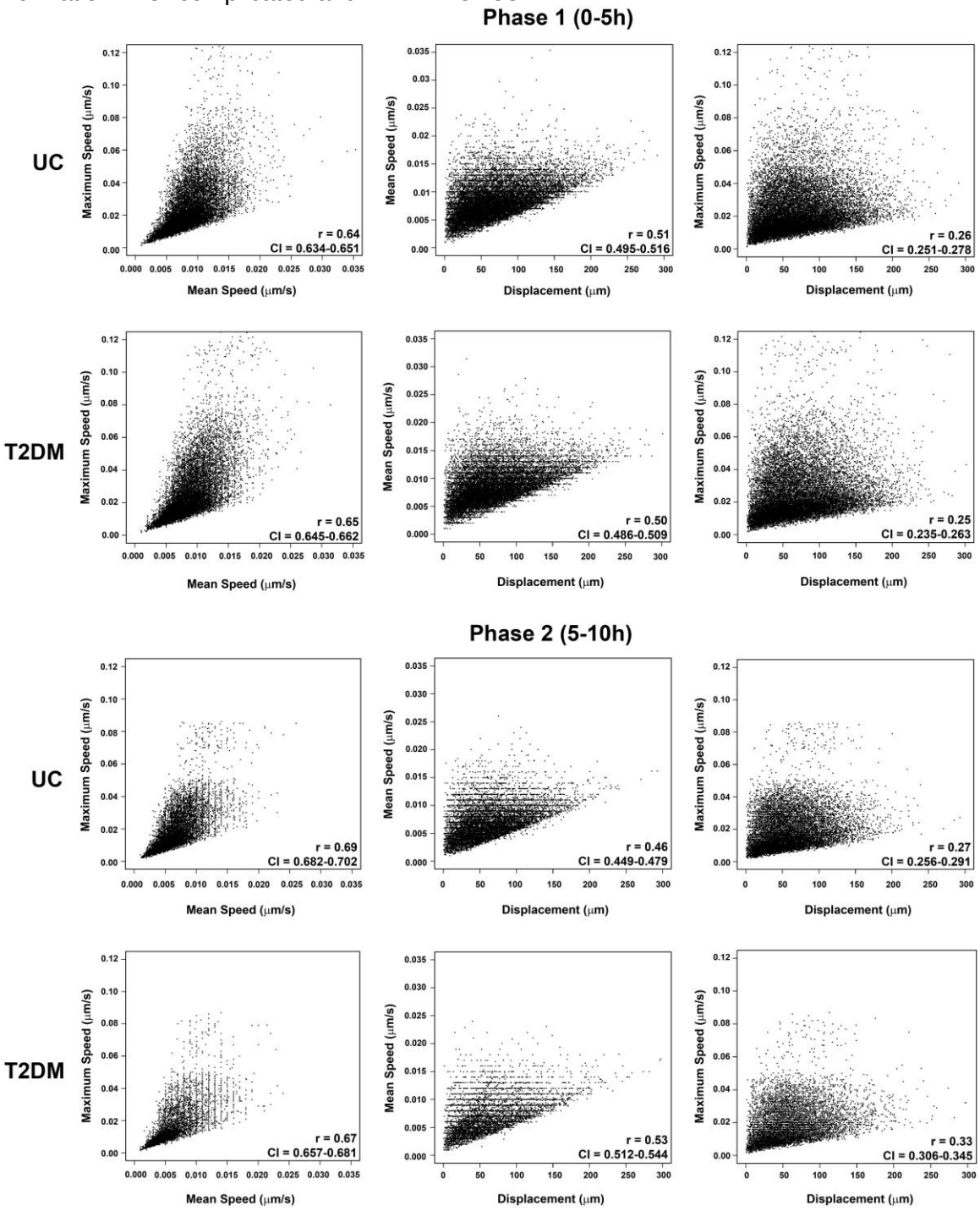

ECFC motility was assessed at the single cell level in Phases 1 and 2 for uncomplicated (UC) and T2DM samples. Associations between the three motility variables assessed (Mean Speed, Max Speed, and Displacement) for both phases and sample groups are represented as dot plots. Each dot represents an individual cell. The correlation value (r) and confidence intervals (CI) are shown in the bottom right corner of each graph. All parameters display positive associations.

Table 4. Motility Parameter Correlations

Phase 1	UC	T2DM
Mean Speed vs. Max Speed	0.64 (0.634-0.6510	0.65 (0.645-0.662)
Displacement vs. Mean Speed	0.51 (0.495-0.516)	0.50 (0.486-0.509)
Displacement vs. Max Speed	0.26 (0.251-0.278)	0.25 (0.235-0.263)
Phase 2	**UC**	**T2DM**
Mean Speed vs. Max Speed	0.69 (0.682-0.702)	0.67 (0.657-0.681)
Displacement vs. Mean Speed	0.46 (0.449-0.479)	0.53 (0.512-0.544)
Displacement vs. Max Speed	0.27 (0.256-0.291)	0.33 (0.306-0.345)

values: Correlation Value, r (Confidence Interval, CI)

Figure 20. ECFCs Exhibit a Wide Range of Motility

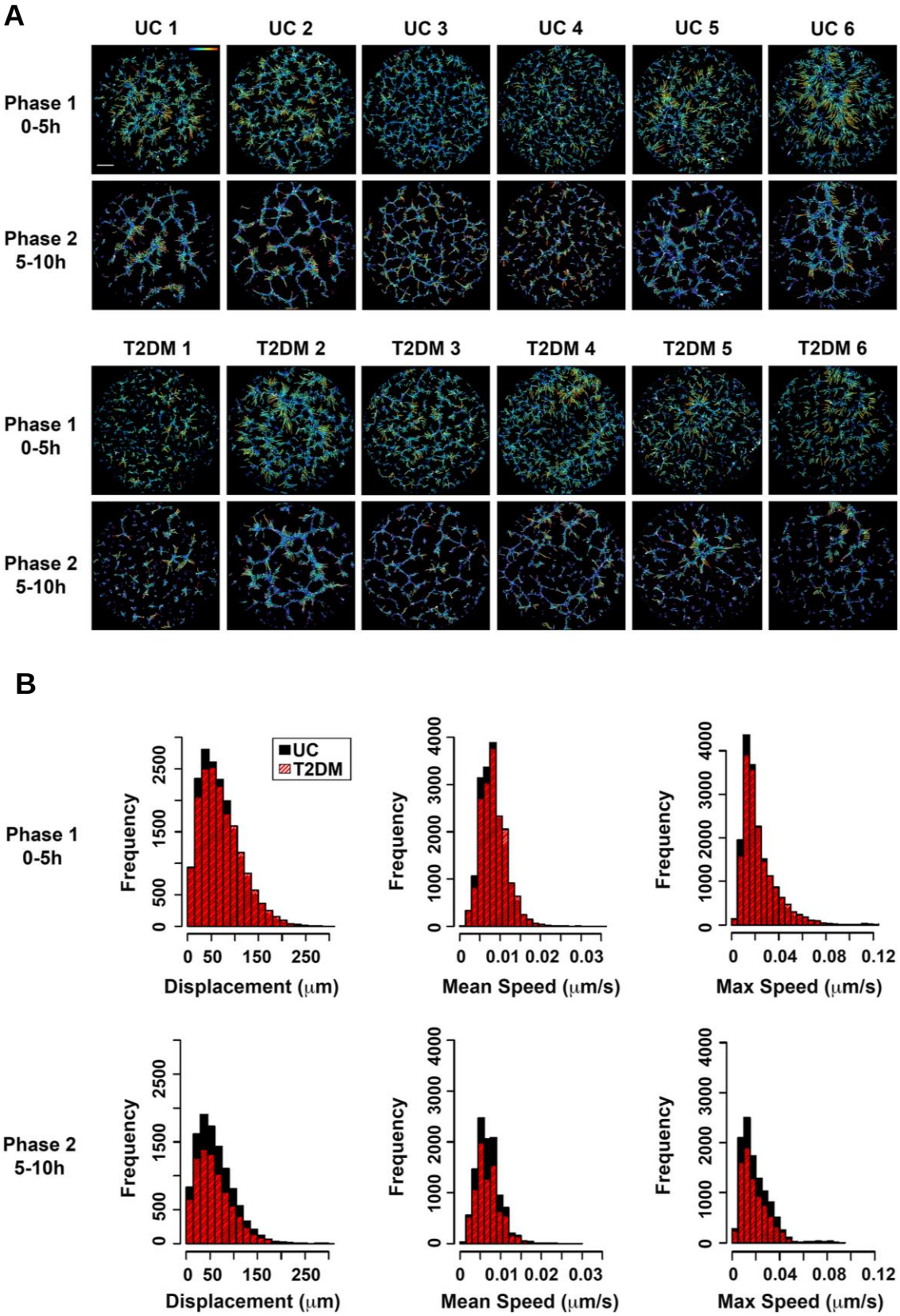

Figure 20 continued:

A) Time-lapse images of network formation were captured over 10 hours. ECFC displacement was assessed separately for Phase 1 (0-5 hours) and Phase 2 (5-10 hours). Data from 6 UC and 6 T2DM-exposed ECFC samples are shown. A colored path represents total displacement, with greater displacement indicated by orange/red and less displacement indicated in blue. A color scale is depicted in the upper right corner of the Phase 1 UC Sample 1 (UC 1) photomicrograph. The scale bar represents 500µm. **B)** Histograms represent the frequency of ECFC displacement, mean speed, and maximum speed in Phases 1 and 2 for UC (black) and T2DM (red) samples. Approximately 35,000 individual ECFCs were analyzed for Phase 1 (n=20 samples, 10 UC and 10 T2DM), and 20,000 individual ECFCs were analyzed for Phase 2 (n=15, 8 UC and 7 T2DM).

Figure 21. Maternal Patients with High Hemoglobin A1c Have Exacerbated Phenotypes

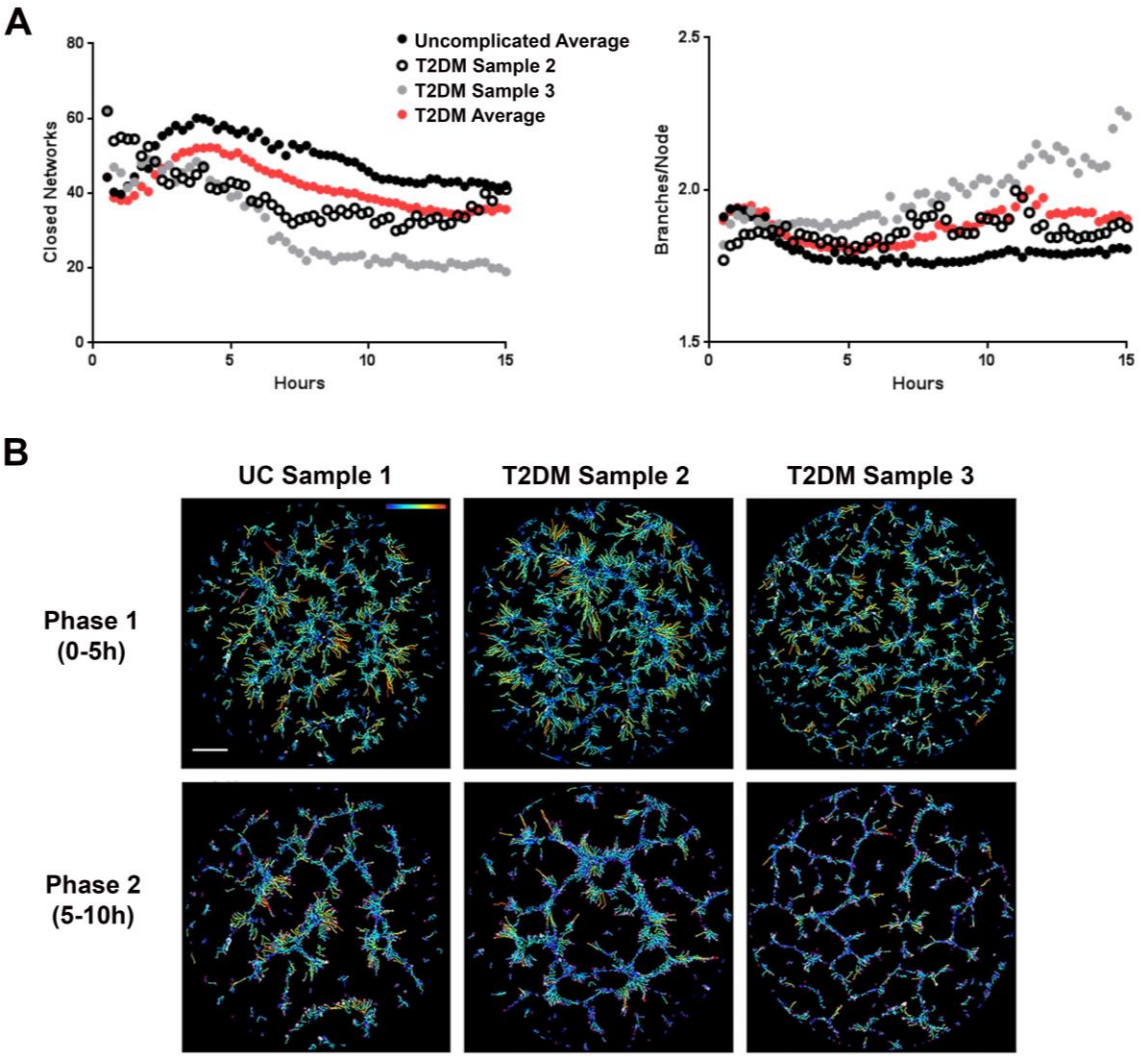

A) KAV analysis was performed on ECFC samples from uncomplicated and T2DM pregnancies over 15 hours of network formation. Kinetic graphs representing the number of Closed Networks and the ratio of Branches to Nodes are shown. The average from 10 uncomplicated ECFC samples (black) and the average from 10 T2DM ECFC samples is shown (red). Individual T2DM ECFC samples (2 and 3) are represented by the open black circle and gray circle, respectively. These samples are from mothers with high hemoglobin A1C levels (>11), indicating poor glucose control during gestation (Table 1). **B**) The total displacement of individual ECFCS from UC Sample 1 and T2DM ECFC Samples 2 and 3 are shown for Phase 1 (0-5h) and Phase 2 (5-10h). The scale bar represents 500µm.

Figure 22. Schematic of Network Connectivity Models T2DM ECFC Phenotypes

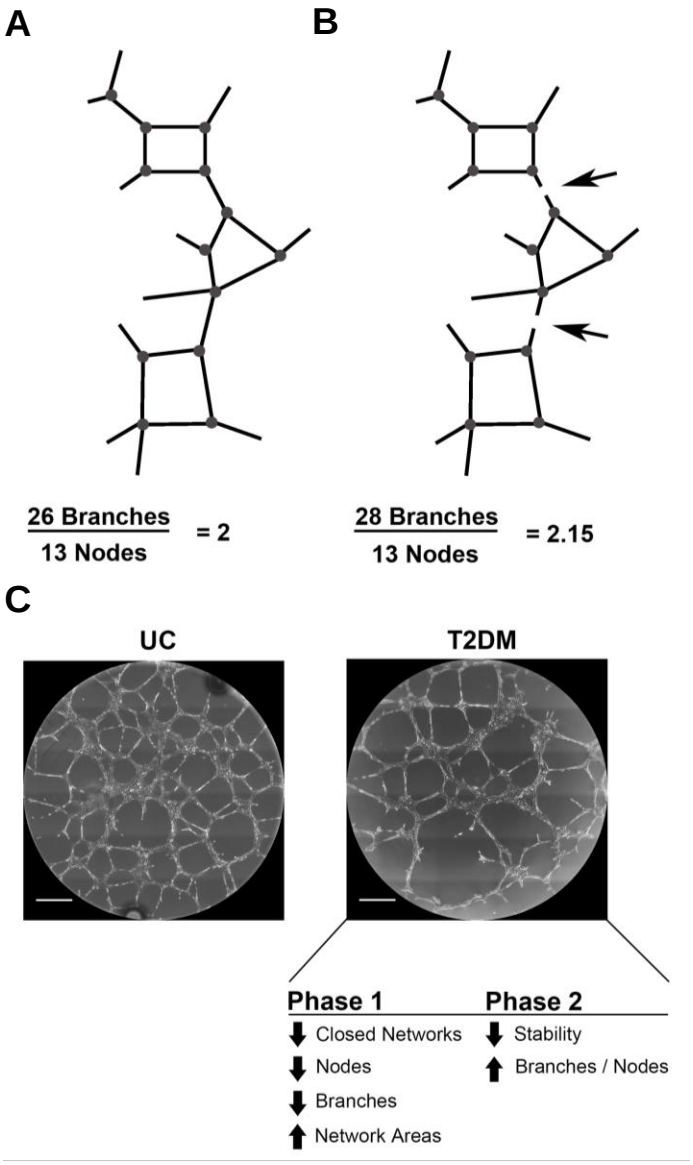

A) A model network structure comprised of 26 branches and 13 nodes is completely connected to create one continuous structure. Due to structure continuity, even though each node has 3-4 branches, the ratio of branches to nodes equals 2. **B)** The same network structure is shown, but with breaks in two branches (arrows). No longer a continuous structure, the number of branches identified by KAV increases by 2, resulting in an increase in the branch to node ratio to 2.15. Decreased network connectivity results in discontinuous structures, which increases the ratio of branches to nodes. Network structures not to scale. **C)** Representative phase contrast images from UC and T2DM experimental groups are shown. In summary, our data support a model whereby in Phase 1 T2DM samples exhibit decreased closed networks, nodes, and branches resulting in increased network areas. These changes in early network formation contribute to an overall decrease in network stability leading to an increase in the branch to node ratio in Phase 2; changes indicative of decreased network connectivity. Scale bars represent 500µm.

Aim 3: To determine if increased Transgelin 1 expression in ECFCs from gestational diabetic pregnancies impairs vasculogenesis.

GDM Exposure Increases Transgelin 1 Expression in ECFCs

Previously, Dr. Haneline's laboratory conducted a microarray analysis on ECFC samples from uncomplicated pregnancies and those complicated by GDM to identify alterations in fetal gene expression following exposure to GDM [83]. One gene significantly upregulated in GDM-exposed ECFCs was Transgelin 1 (TAGLN). To confirm that TAGLN expression is increased in ECFCs from GDM pregnancies, qRT-PCR and Western blotting analyses were conducted (Figure 23A-B). GDM pregnancies were separated into two groups based on treatment strategy, including conservative management with diet and exercise or pharmacologic management with insulin therapy. While some heterogeneity in TAGLN levels was evident in GDM-exposed samples, TAGLN was consistently higher in the insulin-treated group, but not in the conservatively managed patients (Figure 23A-B). Therefore, ECFC samples from the insulin-treated group were used in subsequent functional assays.

Reducing TAGLN in GDM-exposed ECFCs Enhances Vasculogenic Functions

ECFCs from GDM pregnancies exhibit impaired network formation *in vitro*, forming fewer closed networks in Matrigel assays [79,81]. During network formation, the ability of cells to move in response to pro-migratory stimuli is critical. Therefore, ECFC migration was assessed in samples from GDM pregnancies to determine if altered migration contributes to differences in network formation. Despite heterogeneity in the migration of ECFCs from GDM pregnancies, the average number of migrating ECFCs was comparable to samples from uncomplicated pregnancies two and four hours post-plating (Figure 24). Since heterogeneity was observed in both TAGLN expression and ECFC migratory abilities,

correlative analyses were conducted on untreated ECFC samples to determine if TAGLN expression was associated with ECFC migration *in vitro*. Correlation analyses detected no associations between TAGLN expression and ECFC migration (UC n=9, GDM n=7, p=0.86).

TAGLN is an actin binding protein that has been implicated in regulating cell migration, a critical step in establishing vascular networks [108,111,112]. Previously, we showed that ECFCs from GDM pregnancies exhibit impaired network formation [81]. Therefore, we hypothesized that elevated TAGLN expression in GDM-exposed ECFCs induces impaired network formation. To test this hypothesis, TAGLN was reduced in ECFCs from GDM pregnancies using siRNA techniques. Representative data of repeated analyses demonstrated TAGLN reductions of over 90% at the RNA and protein levels (Figure 25A-B). Importantly, TAGLN protein levels following knockdown were similar to protein levels observed in ECFC samples from uncomplicated pregnancies (Figure 25B). SiRNA-mediated reduction in TAGLN expression increased the number of closed networks formed by GDM-exposed ECFCs and enhanced cell migration (Figure 25C-D). Together, these results suggest that reducing TAGLN in GDM-exposed ECFCs improves vasculogenic and migratory abilities.

Surprisingly, though ECFCs from GDM pregnancies did not exhibit reduced migration compared to ECFCs from uncomplicated pregnancies, TAGLN reduction in GDM-exposed ECFCs enhanced migration. Therefore, additional siRNA knockdown experiments were conducted with ECFCs from uncomplicated pregnancies, despite low TAGLN expression, to evaluate for improved function. Reducing TAGLN in ECFCs from uncomplicated pregnancies did not alter network formation (Figure 26A). However, decreasing TAGLN did increase ECFC migration in trans-well assays (Figure 26B). Since TAGLN is less

abundant in ECFCs from uncomplicated pregnancies, it was not surprising that differences in network formation were not observed. However, it was surprising that ECFC migration was significantly enhanced following TAGLN knockdown. Consistent enhancement of migration in both sample groups following TAGLN knockdown suggests that TAGLN inhibits ECFC migration. Discrepancy between migration and network formation results likely reflect differences in the functions measured by the Matrigel and trans-well assays. For example, the assays require different extracellular matrices, such that network formation is assessed on Matrigel while migration is assessed on type 1 collagen. Additionally, network formation involves coordinated cell movement in multiple directions, while the trans-well assay involves primarily unidirectional movement toward a pro-migratory stimulus. Therefore, future studies aimed at evaluating the impact of TAGLN on ECFC function using different extracellular matrices and pro-migratory stimuli would provide additional insight into TAGLN regulation of vasculogenesis.

To obtain a detailed, kinetic readout of ECFC network formation following reduced TAGLN expression, KAV methods developed in Aim 1 were applied. Skeleton and mask renditions of representative network structures enable qualitative comparisons (Figure 27A). Qualitative differences were not obvious at the early time point (4 hours), however 8 hours after plating, differences in network structure were apparent. Both untreated GDM (UT) and siControl-treated GDM ECFCs exhibit a clear reduction in the number of closed networks compared to siTAGLN (Figure 27A). This qualitative observation was confirmed quantitatively as the number of closed networks in the siTAGLN group peaks close to 80 networks, while the UT and siControl groups peak around 60 networks (Figure 27B). Importantly, the number of closed networks in the siTAGLN group remains higher throughout the time course compared to the other two groups. These results confirm the initial Matrigel studies at a single time point in which the numbers of closed networks were

quantified manually (Figure 25). A discriminating phenotype identified in Aim 2 studies was the ratio of branches to nodes (Figure 15), which was indicative of decreased connectivity in Phase 2 of network formation. Similar to ECFCs from T2DM pregnancies, ECFCs from GDM pregnancies (UT and siControl) have an increased ratio of branches to nodes that occurs between 5 and 10 hours of formation (Figure 27B). In contrast, the ratio of branches to nodes in the siTAGLN group was constant during Phase 2 suggesting network stability. Another interesting observation was decreased variability in the ratio of branches to nodes in the siTAGLN group. The variability in the GDM UT and siControl groups was much larger, which was also previously observed in ECFC samples from T2DM pregnancies (Figure 15). Overall, KAV analysis confirmed previous results from static assays that were counted manually as well as provided a more detailed readout of network formation kinetics following TAGLN reduction in GDM-exposed ECFCs.

Increasing TAGLN in ECFCs from Uncomplicated Pregnancies Impairs Migration and Network Formation

To determine whether increased TAGLN expression was sufficient to reduce vasculogenic function, a lentiviral-mediated approach was used to overexpress TAGLN in ECFCs from uncomplicated pregnancies. TAGLN overexpression was confirmed by Western blotting (Figure 28A). Importantly, TAGLN overexpression in ECFCs from uncomplicated pregnancies was comparable to endogenous TAGLN levels observed in GDM-exposed ECFCs (Figure 28A). Following TAGLN overexpression, trans-well and Matrigel assays were performed to test ECFC migratory and network-forming abilities. Increasing TAGLN expression significantly reduced the number of closed networks formed by ECFCs in Matrigel assays (Figure 28B). Additionally, higher levels of TAGLN reduced ECFC migration in trans-well migration assays (Figure 28C). Complimentary to the results

obtained in the siRNA knockdown experiments, increasing TAGLN in ECFCs from uncomplicated pregnancies reduced ECFC migration and network formation *in vitro*.

Previous expression analyses were conducted with ECFCs plated on type 1 collagen, the primary matrix used for plating and passaging. On collagen, ECFCs proliferate to form monolayers, producing a cobblestone-like morphology. However, Matrigel elicits a different response. As discussed in Aims 1 and 2, ECFCs plated on Matrigel organize to form networks instead of monolayers [133]. Therefore, to determine if *TAGLN* expression is altered on different extracellular matrices, a novel approach was developed to isolate RNA from ECFCs on Matrigel to assess TAGLN expression by qRT-PCR. Using this new method (described in *RNA Isolation on Matrigel*, Materials and Methods), it was determined that endogenous *TAGLN* expression decreased over time on Matrigel, compared to the baseline measurement on type 1 collagen prior to plating (Figure 29A). Additionally, *TAGLN* expression was consistently reduced in ECFCs plated for equal durations (10 hours) on Matrigel compared to type 1 collagen (Figure 29B). Importantly, reductions in *TAGLN* were observed in ECFCs from uncomplicated pregnancies as well as those from T2DM and GDM pregnancies. Together, these observations suggest that endogenous *TAGLN* expression is reduced in ECFCs during network formation. However, despite reductions in *TAGLN* expression on Matrigel, these preliminary studies suggest that GDM-exposed ECFCs maintain higher TAGLN expression compared to an uncomplicated control.

To obtain a comprehensive view of ECFC network formation following TAGLN overexpression, KAV analysis was performed. Qualitative observations of the networks using the skeleton and mask renditions demonstrated differences in network structure (Figure 30A). However, in contrast to siRNA studies, differences in network structure were

evident at the 4-hour time point (Figure 27A). These qualitative observations were confirmed quantitatively by KAV (Figure 30B). ECFCs from uncomplicated pregnancies [untreated (UT) and empty vector (EV) control] formed equivalent numbers of closed networks. Upon overexpression of TAGLN (TAGLN OE), the number of closed networks peaked at a much lower number compared to controls, with reductions maintained over time. As an indication of reduced connectivity, the ratio of branches to nodes increased in Phase 2 in the TAGLN OE group as well (Figure 30B). Conversely, the ratio remained relatively constant in the uncomplicated UT and EV control groups.

TAGLN Mediates Migration via Myosin Light Chain Phosphorylation in ECFCs

We identified that TAGLN overexpression reduces ECFC migration and network formation, however the specific mechanism involved is unknown. In 2006, TAGLN was identified as a novel regulator of matrix metalloproteinase 9 (MMP9) expression [112]. Specifically, TAGLN repressed MMP9 expression by reducing AP-1-dependent trans-activation of the MMP9 gene through compromised ERK activation [112]. Reduced MMP9 transcript was confirmed in cells overexpressing TAGLN, and conversely, increased MMP9 transcript and protein were confirmed following TAGLN knockdown [112]. MMP9 is a type IV collagenase that cleaves extracellular matrix components, including elastin and type III, IV, and V collagen, to enable cell migration [136]. In addition to TAGLN regulation of MMP9 expression, Transgelin 2 (TAGLN2) was identified as a negative regulator of myosin light chain (MLC) phosphorylation via reduction of Rho GTPase activity [111]. MLC phosphorylation is involved in actin-myosin interactions which are required for actin cytoskeletal rearrangement in cell migration [137]. Although TAGLN2 was implicated in MLC phosphorylation, this mechanism was also evaluated in ECFCs since TAGLN and TAGLN2 have high genomic sequence conservation, increasing the likelihood for similar functions. Additionally, the previous studies outlined above were

conducted in different cell types. Specifically, MMP9 data were generated in HT1080 (human fibrosarcoma) and WI-38 (lung fibroblast) cells, while the myosin light chain data were obtained in human umbilical vein endothelial cells (HUVECs). Therefore, MMP9 expression and phosphorylation of myosin light chain were assessed in GDM-exposed ECFCs to determine if TAGLN regulates cell migration through a conserved mechanism previously identified in other cell types.

At the transcript level, *MMP9* expression was not detectable in ECFC samples from GDM or uncomplicated pregnancies, suggesting that either decreased *MMP9* is not likely the primary mechanism by which TAGLN reduces ECFC migration, or the sensitivity of the assay was not sufficient to draw conclusions (UC n=6, GDM n=8). However, at baseline, ECFC samples from GDM pregnancies exhibited nearly three fold more MLC phosphorylation compared to uncomplicated controls (Figure 31A). To evaluate whether increased TAGLN promotes myosin light chain phosphorylation, TAGLN was overexpressed in ECFCs from uncomplicated pregnancies to similar levels as GDM-exposed ECFCs (Figure 28A). ECFCs from uncomplicated pregnancies overexpressing TAGLN had approximately 1.5-fold increase in basal phosphorylation of MLC compared to control (Figure 31B), with no differences in total MLC protein observed between groups. We speculate that the difference in the magnitude of increased MLC phosphorylation between GDM-exposed ECFCs and ECFCs overexpressing TAGLN may be attributable to additional alterations in mechanisms that regulate MLC phosphorylation as a result of intrauterine GDM exposure.

Converse to TAGLN overexpression, siRNA-mediated TAGLN reduction in GDM-exposed ECFCs did not alter MLC phosphorylation (Figure 32). This result was surprising since increased MLC phosphorylation was observed in ECFCs overexpressing TAGLN. One

possibility is that the timing of analysis is not appropriate and alterations in MLC phosphorylation were missed. Therefore, additional time course studies could evaluate the effect of knockdown duration on MLC phosphorylation. Additionally, it is quite possible that siRNA-mediated reductions in TAGLN are not complete (100%), such that residual TAGLN is sufficient to maintain MLC phosphorylation. In previous studies, phenotypic differences in GDM-exposed ECFCs were enhanced under conditions of stress, such as serum starvation or exposure to hyperglycemia [81]. Therefore, it is possible that stress conditions, such as ionomycin treatment which increases MLC phosphorylation, could enhance differences in MLC phosphorylation following TAGLN knockdown. Future studies that evaluate the effects of timing and stress conditions on MLC phosphorylation following TAGLN knockdown would help to confirm the initial observations presented in this work. However, since increases in MLC phosphorylation were observed in both GDM and TAGLN-overexpressing ECFCs, additional functional studies were conducted to determine if MLC regulation was involved in TAGLN-mediated dysfunction.

Myosin light chain kinase (MLCK) directly phosphorylates myosin light chain (Figure 33) [138,139]. Conversely, a myosin light chain phosphatase complex (MLPC), comprised of three subunits, de-phosphorylates myosin light chain. The MLPC is inactivated by Rho kinase, which phosphorylates one of the MLPC subunits [138,139]. Compound Y27632 inhibits Rho kinase, resulting in reduced MLPC phosphorylation, increased MLPC activity, and decreased MLC phosphorylation (Figure 33). To evaluate whether decreased MLC phosphorylation induces increased ECFC migration, an approach using the Rho kinase inhibitor Y27632 to reduce MLC phosphorylation was developed (Figure 33). ECFCs treated with Y27632 had reduced MLC phosphorylation (Figure 34). Guided by previous studies in the literature, Y27532 inhibitor treatment conditions were optimized for both timing and dose [140,141]. Following optimization, a concentration of 0.1μM Y27632 was

added to cell suspensions just prior to plating in trans-wells to reduce, but not totally deplete, MLC phosphorylation in GDM-exposed ECFC. To determine if reducing MLC phosphorylation improved ECFC function, migration assays were performed following inhibitor treatment. Although differences were not observed in ECFCs from uncomplicated pregnancies, GDM-exposed ECFCs treated with the Rho kinase inhibitor demonstrated increased migration (Figure 35). This observation was expected, since ECFCs from GDM pregnancies have elevated MLC phosphorylation compared to uncomplicated controls. Similarly, Y27632-mediated Rho kinase inhibition rescued migration of ECFCs overexpressing TAGLN (Figure 35). Thus, reducing the TAGLN-mediated increase in MLC phosphorylation was sufficient to rescue impairments in ECFC migration. Based on these data, additional studies are warranted to evaluate the effect of reducing TAGLN-mediated MLC phosphorylation on ECFC vasculogenesis.

TAGLN Does Not Alter Total Filamentous Actin Levels

In response to laminar flow, endothelial cells rearrange their cytoskeleton to align in the direction of the flow [110]. This well-characterized phenomenon is indicative of the ability of endothelial cells to respond successfully to environmental cues. One primary mechanism involved in endothelial cell alignment to shear stress is actin cytoskeletal rearrangement. TAGLN is an actin binding protein that contributes to the formation and stabilization of filamentous actin (F-actin) bundles or stress fibers [106–109]. Therefore, to determine whether TAGLN overexpression increases total F-actin, relative amounts of globular (G-actin) and F-actin were measured in ECFCs following TAGLN overexpression using two different approaches. First, G-actin and F-actin protein levels were quantified using a centrifugation technique followed by western blotting (Figure 36). Using this approach, differences in total F-actin protein were not observed in TAGLN overexpressing cells compared to empty vector controls (EV control). This observation suggests that

TAGLN does not increase the amount of F-actin in the cell. Additionally, an intracellular, flow cytometric technique was used to evaluate TAGLN overexpression and quantify F-actin in ECFCs. To determine the sensitivity of the assay and the range of detection, initial studies using Cytochalasin D were performed. Cytochalasin D was chosen as it inhibits actin polymerization as well as induces de-polymerization of actin filaments [142]. ECFC treatment with Cytochalasin D significantly reduced the amount of F-actin detected by flow cytometry (Figure 37A). Importantly, while optimizing the experimental approach, an inverse relationship was identified between the number of cells stained and the amount of F-actin and TAGLN probes detected (Figure 37B). Taking this data into account, subsequent studies were conducted using stringent cell counting techniques. Several EV control samples were used to test assay variability and reproducibility. Consistent intracellular TAGLN and F-actin levels were observed across EV control samples (Figure 37C). Finally, upon comparison of EV control and TAGLN OE samples, TAGLN was increased, however no differences in F-actin were observed between sample groups (Figure 37D). These results are consistent with data from the centrifugation assay (Figure 36). TAGLN overexpression did not alter total F-actin in ECFCs from uncomplicated pregnancies. Although the total amount of F-actin is unchanged following TAGLN overexpression, it is still unclear whether TAGLN expression alters organization of F-actin, such as F-actin bundling into stress fibers. Therefore, future studies to assess the amount of F-actin bundling may clarify the mechanism by which TAGLN expression alters ECFC migration.

TAGLN Regulates ECFC Response to Laminar Flow

Previous studies reported co-localization of TAGLN and F-actin using immunofluorescence techniques [106,107]. Therefore, confocal microscopy was used to confirm localization of TAGLN and F-actin in ECFCs. Using confocal microscopy, it was

evident that TAGLN and F-actin primarily co-localize within the cell (Figure 38). This observation is not surprising as TAGLN has a conserved actin binding domain. However, co-localization in ECFCs had not been previously reported. Following confirmation of co-localization, shear assays were conducted to determine if TAGLN impacts the ability of ECFCs to align in response to flow, a conserved endothelial cell phenotype [110].

To determine whether ECFCs overexpressing TAGLN align in the direction of laminar flow, ECFCs were transduced with either empty vector control (EV control) or TAGLN-containing (TAGLN OE) lentivirus. Following transduction, ECFCs were either maintained in static culture, or subjected to seven hours of flow as previously described [127,128]. Glass slides from static culture and the flow chamber were fixed and stained for TAGLN, F-actin, and NucBlue. Fluorescence images were captured from eight field-matched locations on the slide, and the ImageJ Directionality Plug-in was used to analyze ECFC alignment based on the F-actin immunofluorescence images (Figure 39) [130]. Based on the direction of the flow, proper cell alignment should result in a mean angle slightly greater than zero (*arrows Figure 39A). Qualitatively, ECFCs transduced with EV control lentivirus under static culture conditions exhibited slight alignment at baseline (Figure 39A). However, following exposure to seven hours of laminar flow, alignment of EV control cells increased as evidenced by near complete unidirectional F-actin filament alignment (Figure 39A). Upon overexpression of TAGLN, ECFCs did not have coordinated alignment at baseline, but appeared random and disjoined in relation to neighboring cells (Figure 39A). Following exposure to laminar flow, TAGLN OE ECFC attempt at alignment was evident, but often the angle of alignment was not clearly in the direction of the flow (Figure 39A). Quantitation of cell alignment using the ImageJ Directionality Plug-in supported qualitative observations. Blue histograms generated by the Plug-in represent the distribution of the angles detected within the corresponding F-actin fluorescence images in Panel A (Figure

39B). A Gaussian distribution, like in the EV control +Flow histogram, indicates consistent cell alignment. Alternatively, flat histograms indicate randomized cell alignment. Individual image data for each condition were combined to produce single graphics of overlaid, individual histograms (Figure 39C). This analytic approach enabled visualization of mean angle variation and distribution. Interestingly, ECFCs transduced with empty vector control lentivirus (EV control) exhibited partial alignment even in the absence of flow, as indicated by overlapping histograms (Figure 39C). Following seven hours of laminar flow, ECFCs transduced with EV control lentivirus aligned in the direction of the flow as indicated by greater histogram overlap with histogram peaks at angles slightly greater than zero (Figure 39C). Conversely, TAGLN overexpressing cells (TAGLN OE) displayed greater variability in cell alignment at baseline, indicated by non-overlapping histograms with random peaks indicative of varying alignment angles (Figure 39C). This finding was surprising because initial speculation was that differences in cell alignment would be enhanced and identified under conditions of shear stress, or flow. However, qualitative observations of TAGLN immunofluorescence images suggest that increased baseline heterogeneity could reflect heterogeneity in TAGLE overexpression across the cell population analyzed. Following exposure to seven hours of laminar flow, ECFCs overexpressing TAGLN attempted to align, but were unable to align to the same extent as the ECFCs transduced with EV control. Partial alignment is indicated by flattened histograms located at angles slightly greater than zero as well as histograms with peaks at angles less than zero (Figure 39C). Overall, the angle variance, or spread in mean angle distribution, was low in EV control samples which consistently align in the direction of the flow (Figure 39D). ECFCs overexpressing TAGLN attempt to align, but don't achieve an arrangement as uniform as EV control samples, which results in a lower mean angle and greater angle variance (Figure 39D). Analysis by Two-way ANOVA confirmed that the mean angle of cell alignment is impacted by TAGLN expression under basal and

flow conditions (p=0.0037). Additionally, flow significantly impacts angle variance, with a 466-unit (se=120) reduction in the variance of mean angles following flow (p=0.0002). However, angle variance is also significantly associated with TAGLN expression, such that the variance is increased 416-units (se=120) in the TAGLN OE group compared to the EV control group (p=0.0009). Thus, ECFCs effectively respond to shear stress by aligning to the direction of the flow. However, TAGLN overexpression alters basal and flow-mediated cell alignment.

ECFCs from Uncomplicated and GDM Pregnancies Align to Laminar Flow

Given that GDM-exposed ECFCs exhibit increased TAGLN expression and ECFCs overexpressing TAGLN exhibit a decreased response to laminar flow, I hypothesized that ECFCs from GDM pregnancies would have a decreased response to laminar flow. Therefore, additional assays were conducted to evaluate for differences between ECFC samples from uncomplicated and GDM pregnancies. Representative photomicrographs of ECFCs from uncomplicated (UC) and GDM pregnancies indicate basal and flow-induced cell alignment (Figure 40A). Qualitatively, ECFCs from UC pregnancies exhibited random, uncoordinated alignment under static culture conditions (Figure 40A). Following exposure to seven hours of laminar flow, ECFCs from UC pregnancies conformed to unidirectional alignment in the direction of the flow (Figure 40A). GDM-exposed ECFCs also exhibited non-coordinated alignment under static culture conditions. Similar to ECFCs from UC pregnancies, exposure to laminar flow prompted GDM-exposed ECFC alignment (Figure 40A). Qualitative observations were confirmed quantitatively using the ImageJ Directionality Plug-In. Single graphics depicting histograms representing data from nine individual image fields are shown for three UC and GDM samples (Figure 40B). Non-uniform alignment of ECFCs from UC pregnancies under static culture conditions resulted in decreased histogram overlap with mismatched peaks. Different patterns of cell

alignment were evident in the individual samples tested (Figure 40B). However, following exposure to laminar flow, all three UC samples displayed unidirectional alignment as indicated by increased histogram overlap with peaks occurring near the angle of the flow direction. ECFCs from GDM pregnancies also exhibited multi-directional alignment under static culture conditions as indicated by histogram misalignment (Figure 40B). Exposure to seven hours of laminar flow resulted in an increase in GDM-exposed ECFC alignment compared to static culture controls. However, upon comparison to ECFCs from UC pregnancies under flow, GDM-exposed ECFCs did not appear to align to the same extent, as indicated by reduced histogram overlap (Figure 40B, statistical analysis performed below). This observation suggests that GDM-exposed ECFCs attempted to align in response to shear stress, but were not as proficient as samples from UC pregnancies, resulting in greater variability. Statistical analysis was conducted on the data generated by the Directionality Plug-in to quantitatively compare ECFC response to shear stress. Under static culture conditions, both UC and GDM groups exhibited similar mean angle values, although GDM-exposed ECFCs displayed greater mean angle heterogeneity indicated by larger deviation (Figure 40C). Larger deviation in angle variance was also evident in GDM-exposed samples (Figure 40C). Statistical modeling confirmed that cell alignment, indicated by the mean angle, was influenced by exposure to laminar flow, irrespective of the sample group ($n=6$, $p=0.034$). Similarly, angle variance was impacted by laminar flow exposure ($n=6$, $p=4.0e-08$). Contrary to the original hypothesis, intrauterine GDM exposure did not impact angle variance (UC $n=3$, GDM $n=3$, $p=0.08$). Additionally, analysis by two-way ANOVA indicated no interaction between intrauterine GDM exposure and laminar flow in relation to ECFC alignment (UC $n=3$, GDM $n=3$, $p=0.07$). Although statistical differences between UC and GDM samples were not identified in this study, low sample size may be limiting the ability to detect differences. Previous functional assessments of GDM-exposed ECFCs required high sample

numbers, likely due to disease heterogeneity and duration. Therefore, additional studies with higher sample numbers are needed to formulate conclusions.

Figures (23-40)

Figure 23. TAGLN is Elevated in ECFCs from GDM Pregnancies

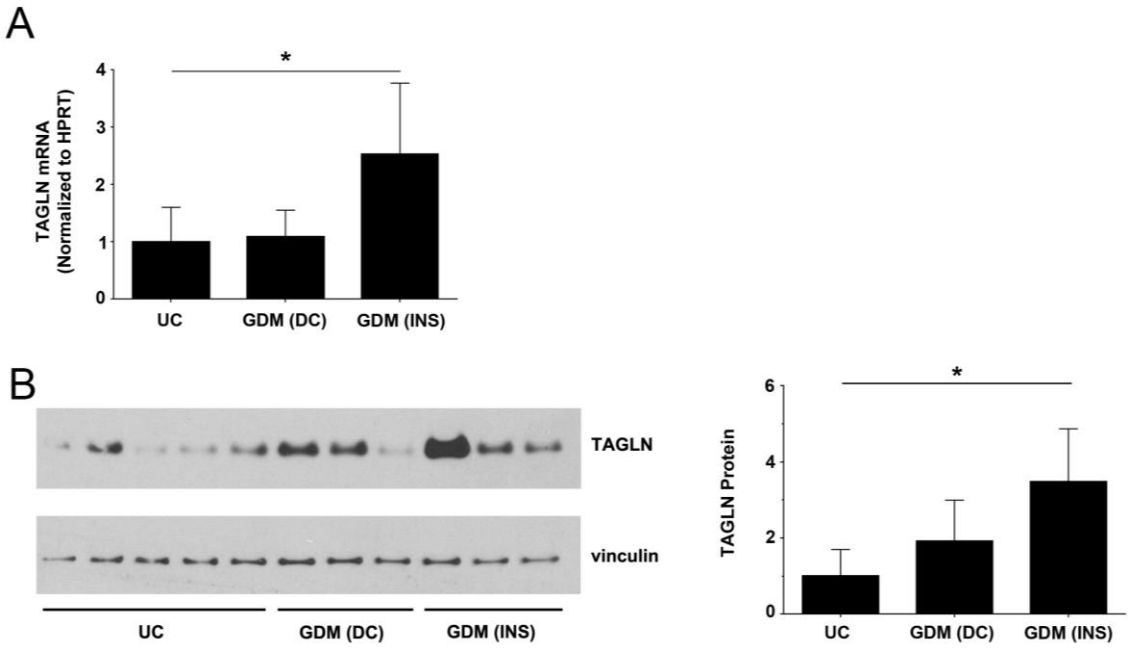

A) RNA was isolated from ECFCs obtained from uncomplicated, GDM-diet, and GDM-insulin controlled pregnancies. Using qRT-PCR, relative amounts of Transgelin mRNA were quantified and normalized to HPRT. ECFCs from GDM-insulin pregnancies had significantly higher levels of Transgelin mRNA compared to samples from uncomplicated control pregnancies (UC n=8, GDM-diet controlled (DC) and GDM-insulin controlled (INS) n= 4, p=0.017). **B)** A representative Western blot of repeated analyses depicting whole-cell ECFC protein lysates from uncomplicated, GDM-DC, and GDM-INS pregnancies. The membrane was probed with antibodies against Transgelin 1 (TAGLN) and vinculin. Western blot densitometry confirmed that ECFC samples from GDM pregnancies have more TAGLN protein compared to uncomplicated controls (UC n=5, GDM-DC and GDM-INS n=3, p=0.014).

Figure 24. Intrauterine GDM Exposure Does Not Alter ECFC Migration

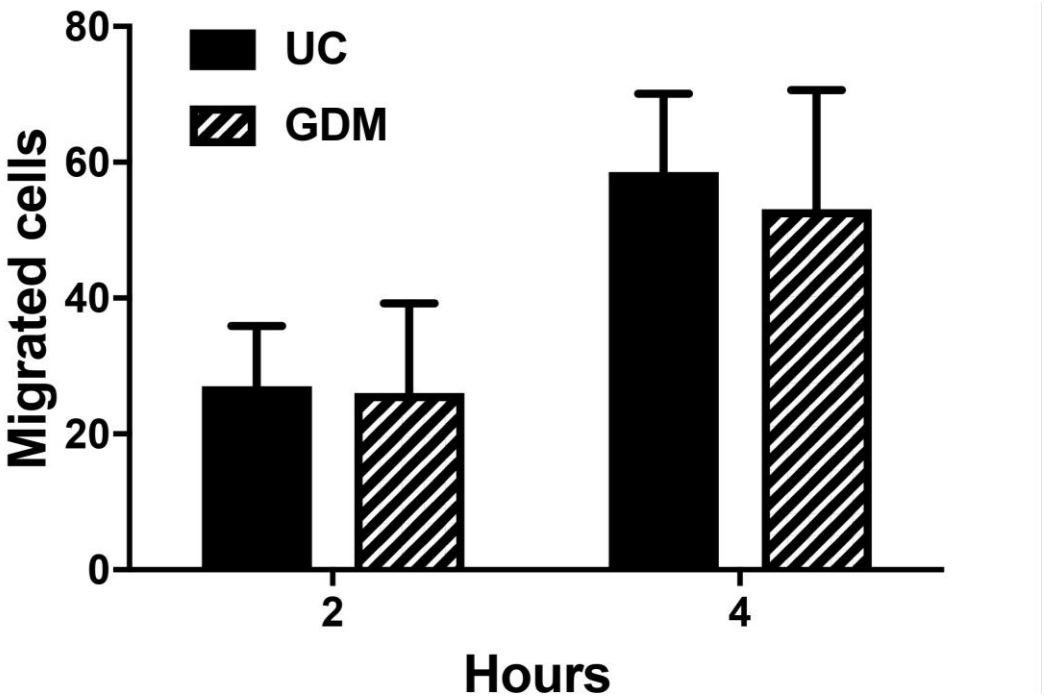

Trans-well migration assays were performed with ECFCs from uncomplicated (UC, black bars) pregnancies and pregnancies complicated with gestational diabetes mellitus (GDM, patterned bars). The number of migrated cells was quantified at two and four hours post-plating. Results were analyzed by two-way ANOVA. Time impacted the number of migrated cells ($p<0.0001$), but GDM did not ($p=0.61$). There was no interaction between time and GDM by two-way ANOVA analysis ($p=0.62$). (UC n=6, GDM n=6)

Figure 25. Elevated TAGLN in GDM-exposed ECFCs is Sufficient to Impair Function

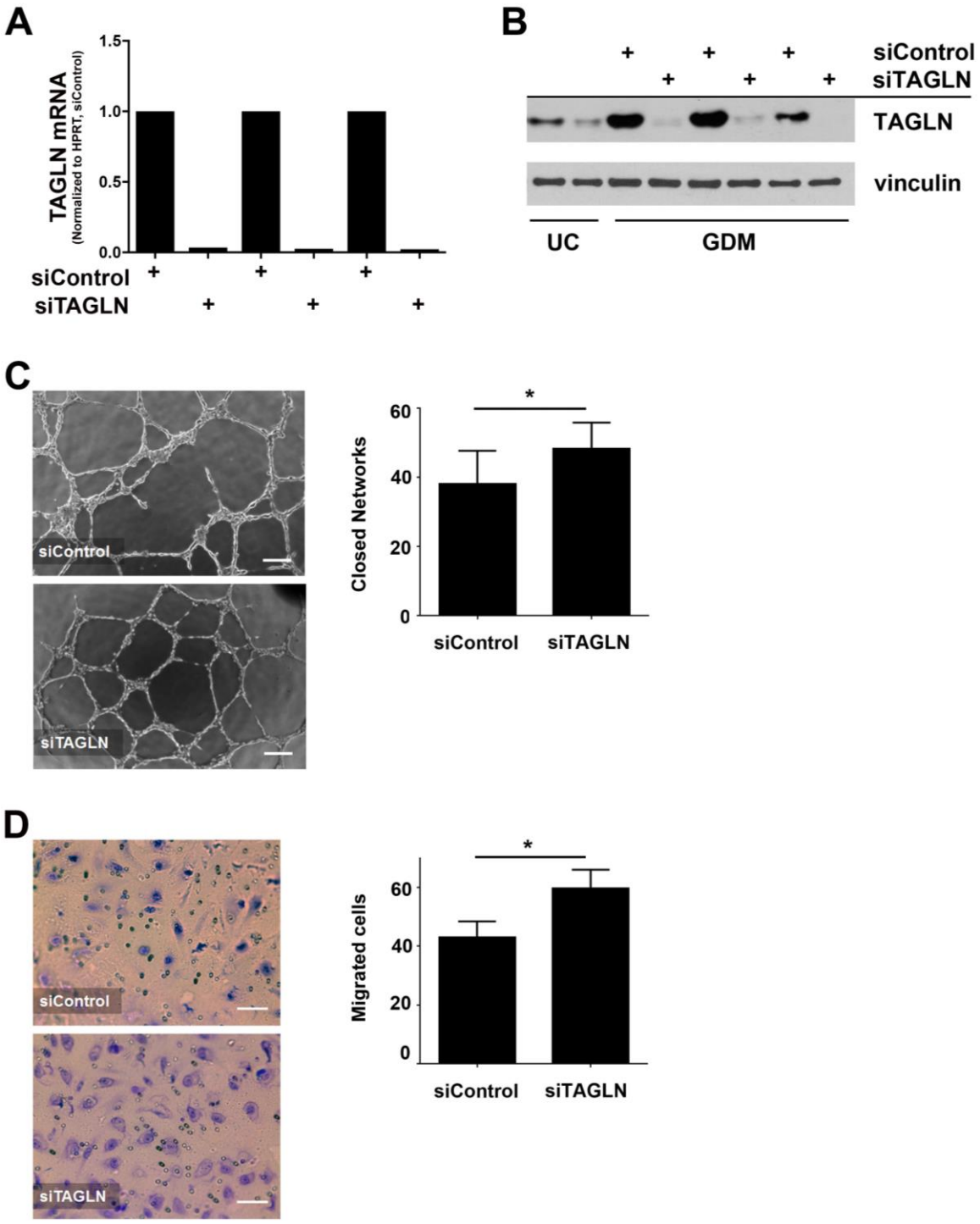

A) *TAGLN* transcript levels were measured 48 hours post-transfection in three different ECFC samples treated with siControl or siTAGLN. All *TAGLN* levels were normalized to HPRT. siTAGLN values were then normalized to their corresponding siControl sample

Figure 25 continued:

values. (n=3) **B)** A western blot depicting whole-cell protein lysates from untreated ECFCs from uncomplicated pregnancies (UC) and ECFCs from GDM pregnancies treated with non-specific siRNA (siControl) or TAGLN-specific siRNA (siTAGLN). Membranes were probed for TAGLN and Vinculin. **C)** Phase contrast images of ECFC network formation on Matrigel 10 hours post-plating following siControl or siTAGLN treatments. The numbers of closed networks formed were quantified and graphed (n=8 transfections, *p=0.019). **D)** Trans-well migration assays were performed with ECFCs transfected with siControl or siTAGLN. Photomicrographs depict migrated ECFCs stained with crystal violet. The numbers of migrating cells after four hours were quantified and graphed (n=10 transfections, *p=0.028).

Figure 26. Reducing TAGLN in ECFCs from Uncomplicated Pregnancies Alters Migration but Not Network Formation

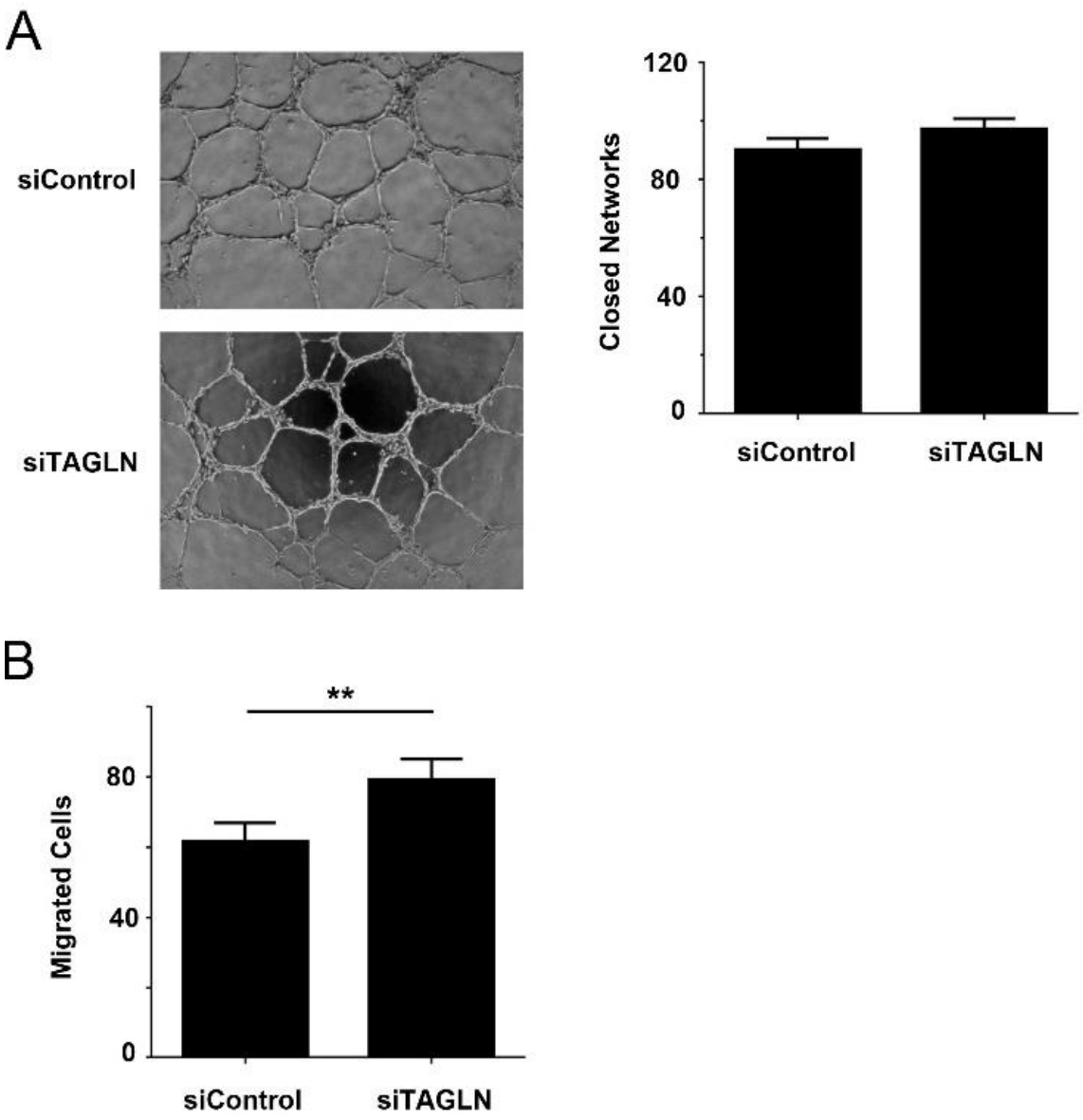

A) Phase contrast images of ECFC network formation on Matrigel 10 hours post-plating following treatment with non-specific siRNA (siControl) or TAGLN-specific siRNA (siTAGLN). The numbers of closed networks were quantified and graphed with no differences observed between treatment groups (n=4 transfections, p=0.12). **B)** Trans-well migration assays were performed following treatment with non-specific siRNA (siControl) or TAGLN-specific siRNA (siTAGLN). The numbers of migrating cells after four hours were quantified and graphed (n=5 transfections, **p=0.005).

Figure 27. KAV Analysis Confirms siRNA-mediated Knockdown of TAGLN in GDM-exposed ECFCs Rescues Network Formation

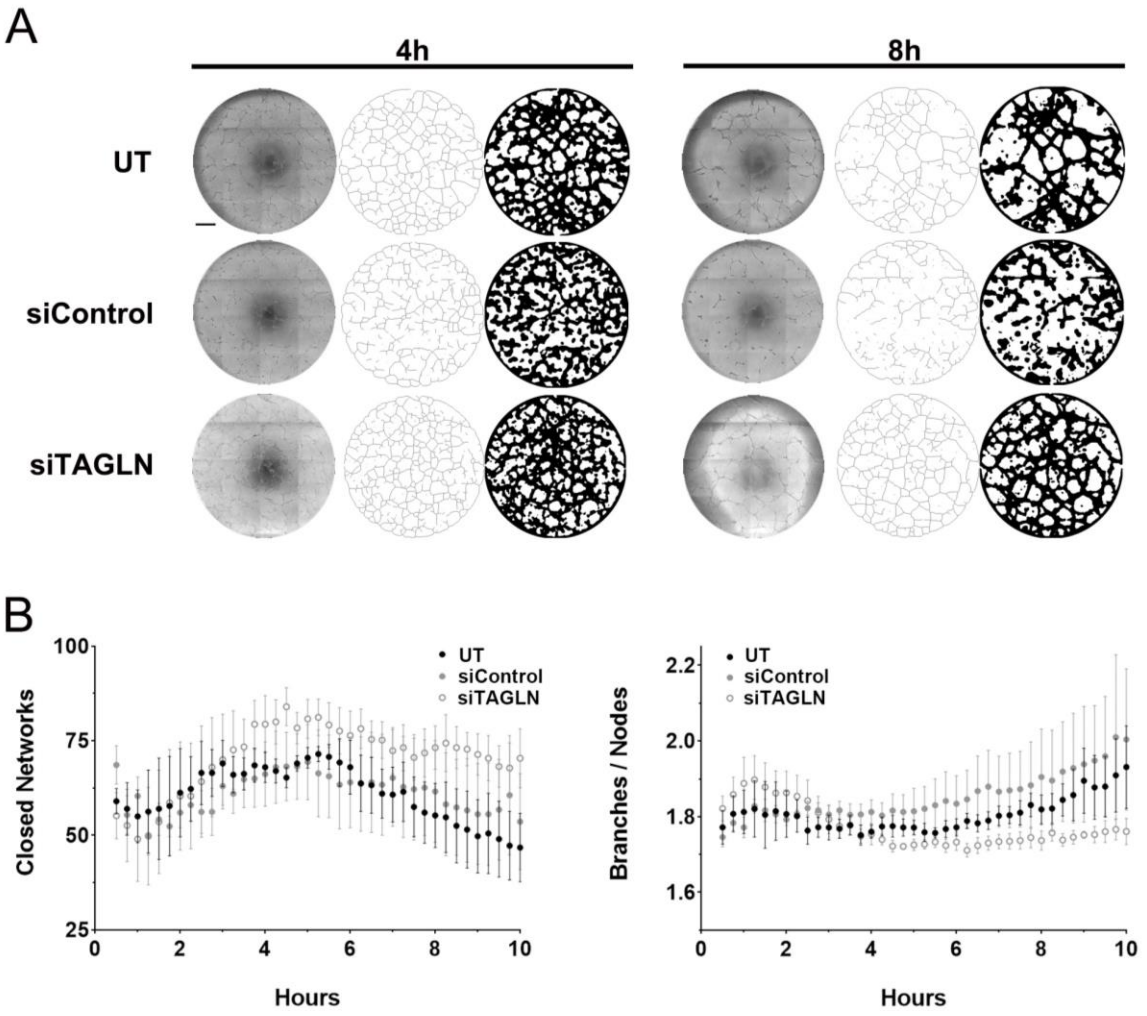

A) Representative phase contrast, skeleton, and mask images of ECFC network formation on Matrigel at 4 and 8 hours post-plating. ECFCs were obtained from GDM pregnancies and were untreated (UT) or treated with non-specific siRNA (siControl) or TAGLN-specific siRNA (siTAGLN). The scale bar represents 500 µm. **B)** Kinetic analysis of vasculogenesis (KAV) software quantitated closed networks and the ratio of total branches divided by total nodes for UT (black), siControl (gray), and siTAGLN (white) samples. The data illustrated represent the mean ± SEM of 3 separate experiments for each group.

Figure 28: Increasing TAGLN in Low-expressing ECFCs is Sufficient to Impair Function

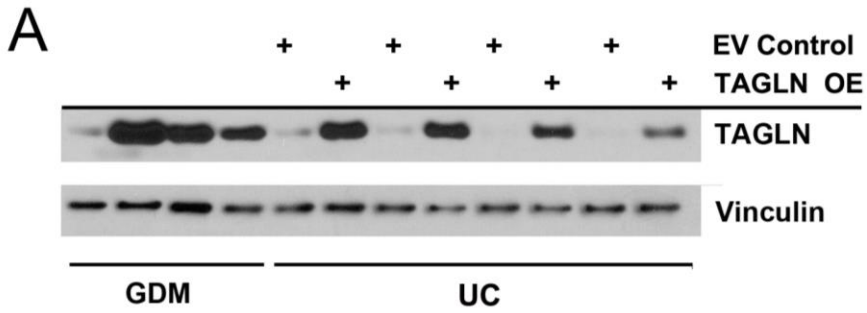

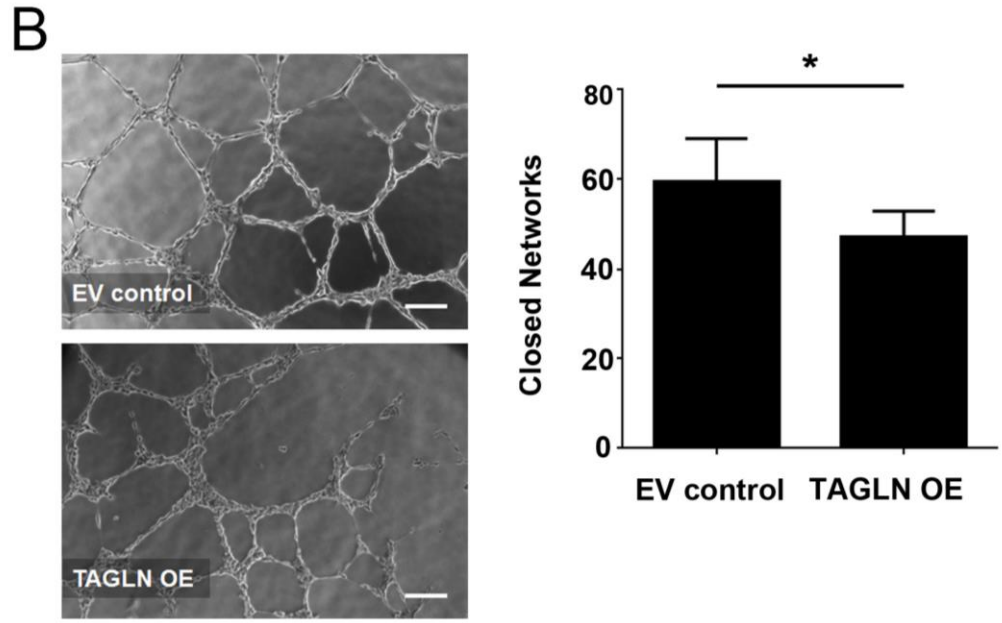

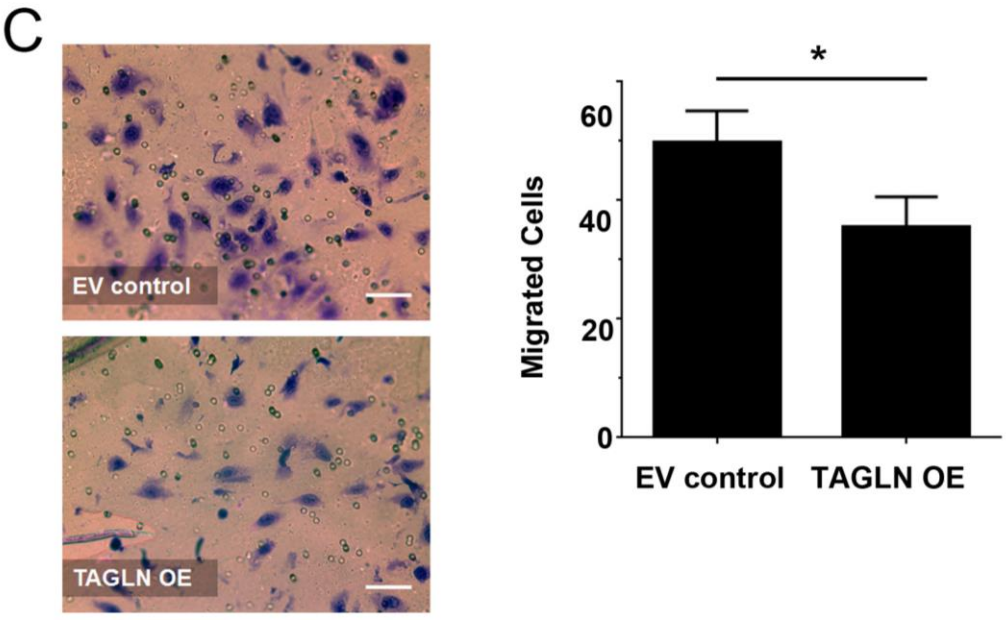

Figure 28 continued:

A) A western blot depicting whole-cell protein lysates collected on type 1 collagen from untreated GDM-exposed ECFCs and ECFCs from uncomplicated pregnancies transduced with a control lentivirus (EV control) or a TAGLN-expressing lentivirus (TAGLN OE). Membranes were probed for TAGLN and Vinculin. **B)** Phase contrast images of ECFC network formation on Matrigel following transduction with either EV control or TAGLN OE lentivirus. The numbers of closed networks were quantified 10 hours post-plating and graphed (n=9 transductions, p=0.047). **C)** Trans-well migration assays were performed with ECFCs transduced with EV control or TAGLN OE lentivirus. Photomicrographs depict migrated ECFCs stained with crystal violet 4 hours after plating. The numbers of migrating cells after four hours were quantified and graphed (n=11 transductions, p=0.015).

Figure 29. *TAGLN* Transcript Levels are Decreased on Matrigel

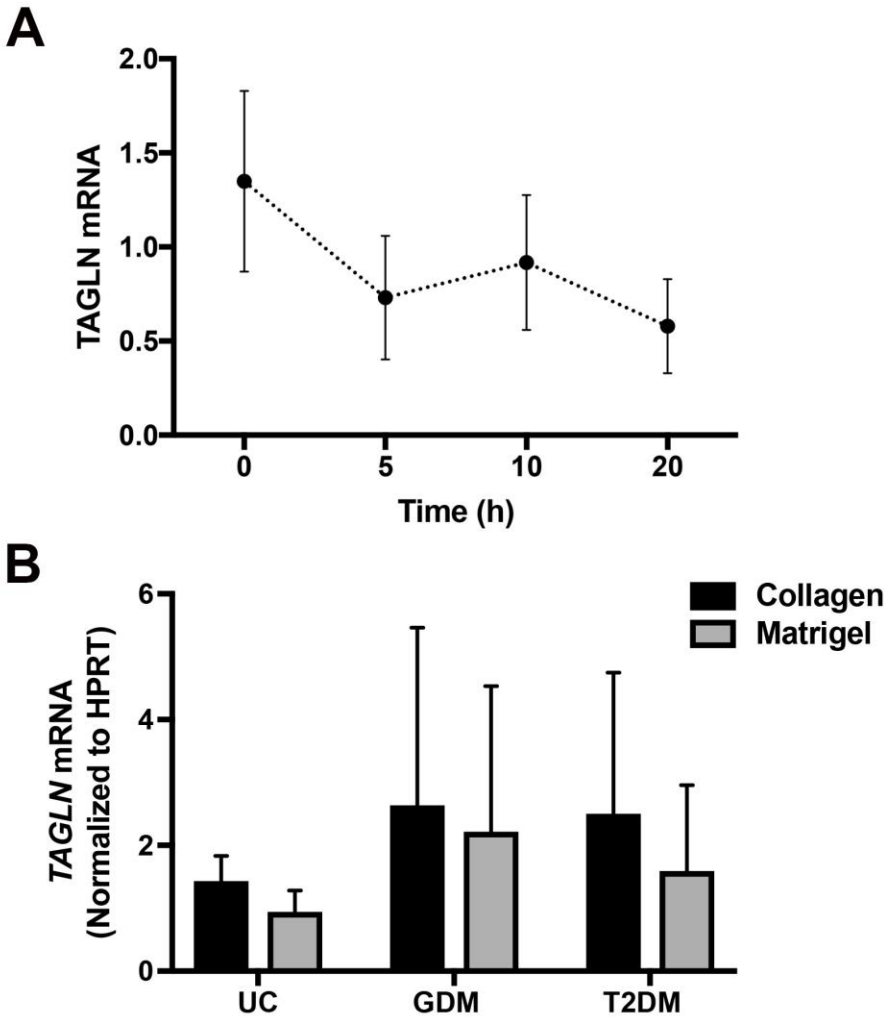

A) *TAGLN* mRNA was measured in three different ECFC samples at baseline (0h) on type 1 collagen, and at 5, 10, and 20 hours on Matrigel (UC n=2, T2DM n=1). *TAGLN* mRNA levels were normalized to HPRT. Analysis by one-way ANOVA identified a difference in *TAGLN* transcript at the different time points (n=3, *p=0.0479). **B)** RNA was collected from ECFC samples plated on type 1 collagen (black) or Matrigel matrix (gray) for 10 hours. *TAGLN* transcript levels were normalized to HPRT (mean ± SD). Results were analyzed by a Two-way ANOVA (UC n=3, GDM n=6, T2DM n=3). *TAGLN* expression is reduced on Matrigel compared to type 1 collagen (p=0.008).

Figure 30. KAV Analysis Confirms Impaired ECFC Vasculogenesis following TAGLN Overexpression

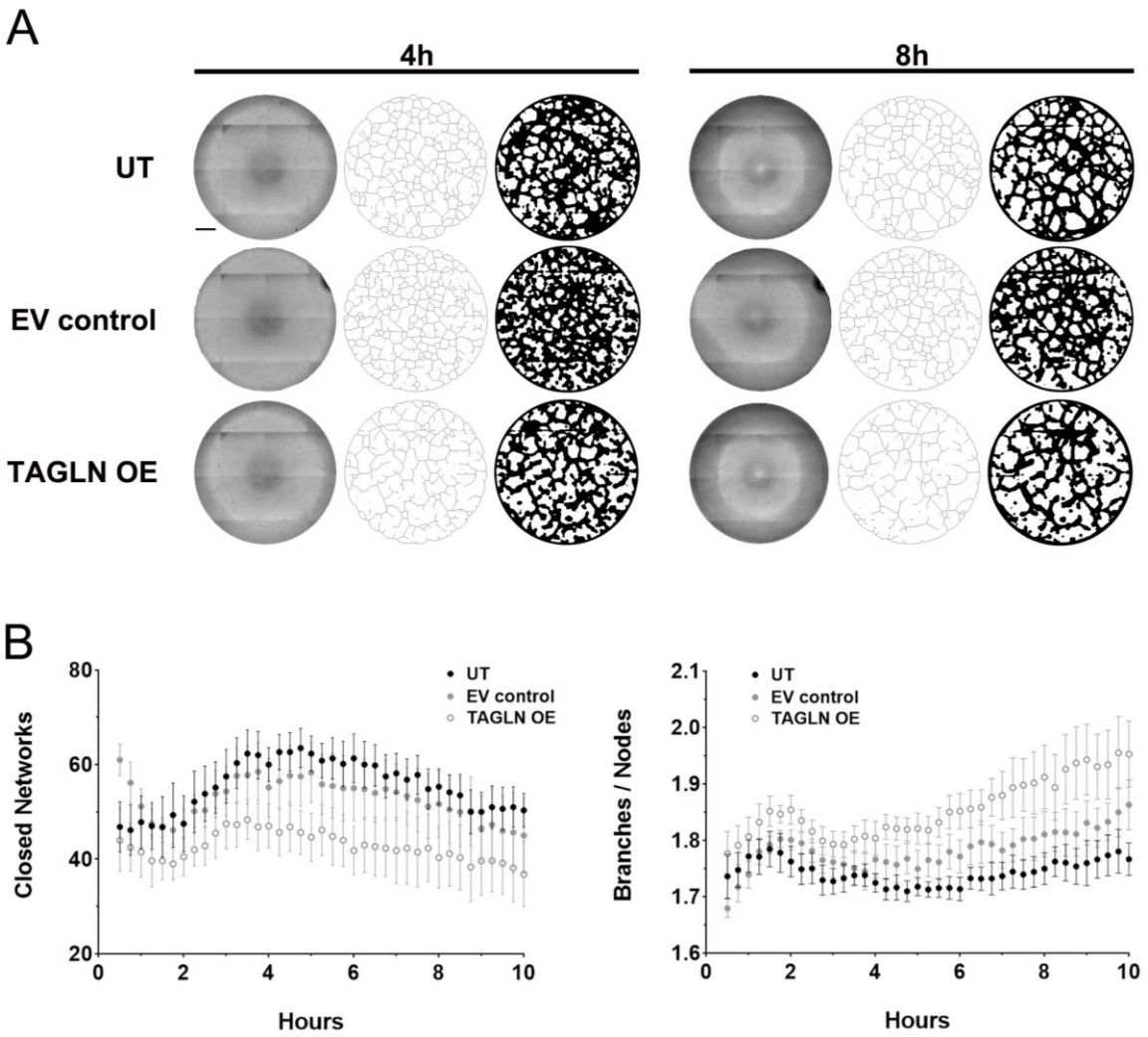

A) Representative phase contrast, skeleton, and mask images of ECFC network formation on Matrigel at 4 and 8 hours post-plating. ECFCs were obtained from uncomplicated pregnancies and were untreated (UT) or treated with a control lentivirus (EV control) or TAGLN-containing lentivirus (TAGLN OE). The scale bar represents 500 µm. **B)** Kinetic analysis of vasculogenesis (KAV) software quantitated closed networks and the ratio of total branches divided by total nodes for UT (black), EV control (gray), and TAGLN OE (white) samples. The data illustrated represent the mean ± SEM of 3 separate experiments for each group.

Figure 31: Myosin Light Chain Phosphorylation is Increased in ECFCs with Elevated TAGLN

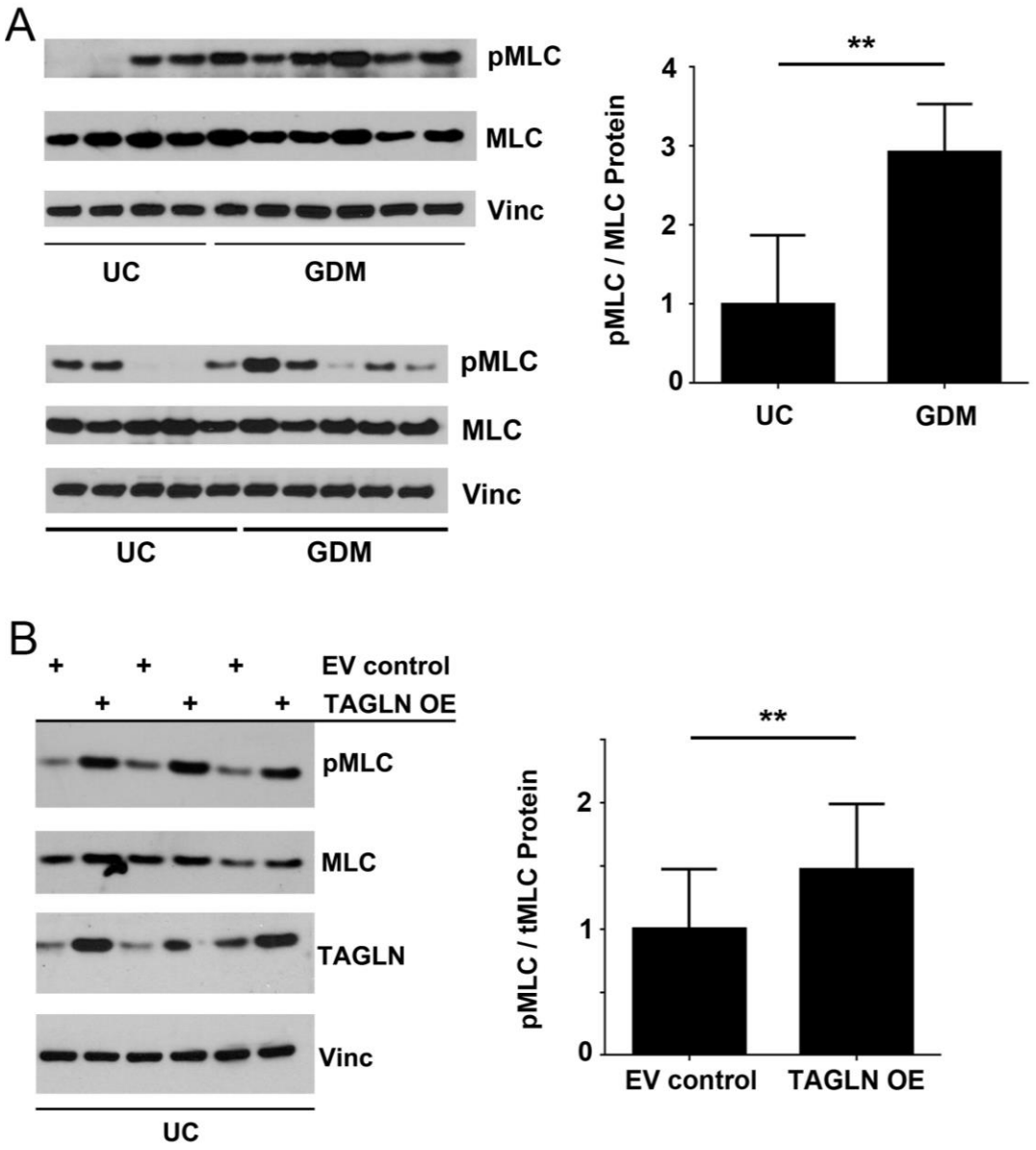

A) Two western blots depicting whole-cell protein lysates from ECFCs isolated from uncomplicated (UC) or GDM pregnancies. Membranes were probed with antibodies against phospho-myosin light chain (p-MLC), total myosin light chain (MLC), and vinculin (Vinc). Western blot quantification confirmed increased levels of pMLC relative to total myosin light chain in samples from GDM pregnancies (UC n=4, GDM n=6, **p=0.003). **B)** A western blot depicting whole-cell protein lysates from ECFCs from uncomplicated pregnancies treated with control lentivirus (EV control) or lentivirus containing TAGLN (TAGLN OE). The membrane was probed with antibodies against phospho-myosin light chain (p-MLC), total myosin light chain (MLC), Transgelin (TAGLN), and vinculin (Vinc). Western blot quantitation confirmed increased levels of pMLC relative to total myosin light chain (n= 7 transductions, **p=0.002).

Figure. 32. Reducing TAGLN in GDM-exposed ECFCs Does Not Alter Myosin Light Chain Phosphorylation

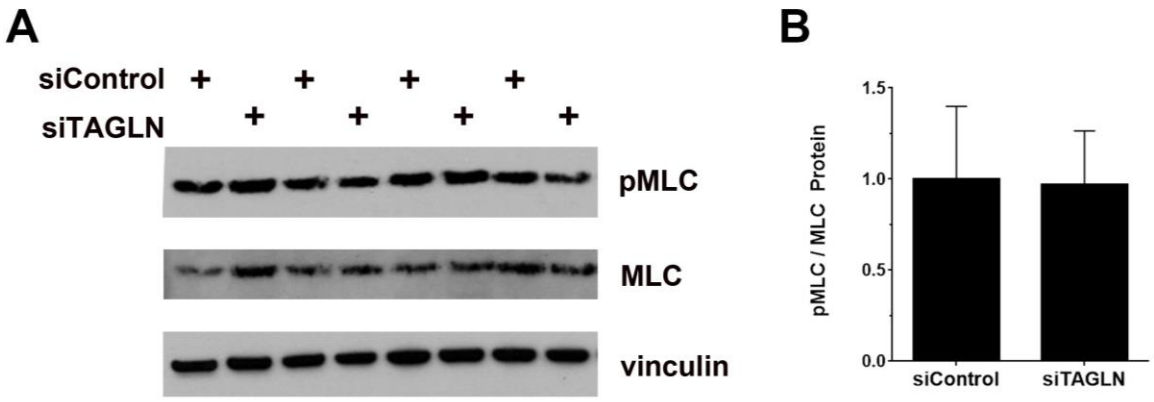

A) A representative western blot depicting whole-cell protein lysates from ECFCs from GDM pregnancies treated with non-specific siRNA (siControl) or TAGLN-specific siRNA (siTAGLN). Membranes were probed for phosphorylated myosin light chain (pMLC), total myosin light chain (MLC), and Vinculin. **B)** Western blot densitometry confirmed no difference in myosin light chain phosphorylation following TAGLN knockdown in GDM-exposed ECFCs (n=7, p=0.86).

Figure 33. Schematic Depicting Strategy to Regulate Myosin Light Chain Phosphorylation

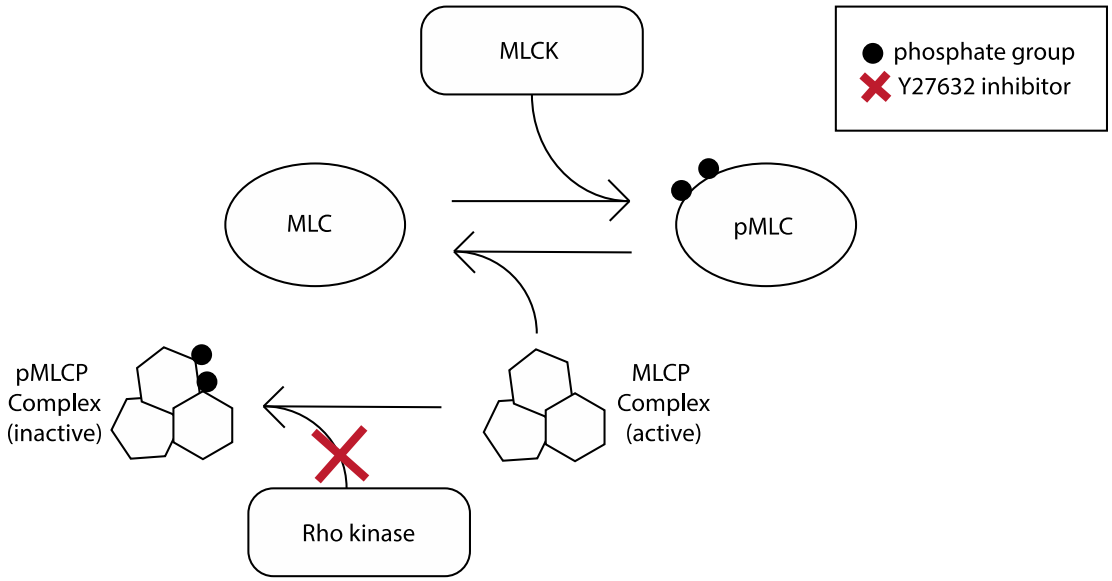

Myosin light chain (MLC) phosphorylation is regulated by two primary mechanisms. First, myosin light chain kinase (MLCK) directly phosphorylates (black circle) MLC. Second, a three-subunit myosin light chain phosphatase complex (MLPC), de-phosphorylates MLC when in the active (de-phosphorylated) state. The MLPC is regulated by Rho kinase, which phosphorylates one of the subunits in the complex, rendering the complex inactive. The Y27632 inhibitor (red X) blocks Rho kinase activity, such that it is unable to render MLPC inactive through phosphorylation. *Schematic is adapted from Ramachandran et al. (2011)* [139].

Figure 34. Optimization of Rho kinase Inhibitor (Y27632) Treatment

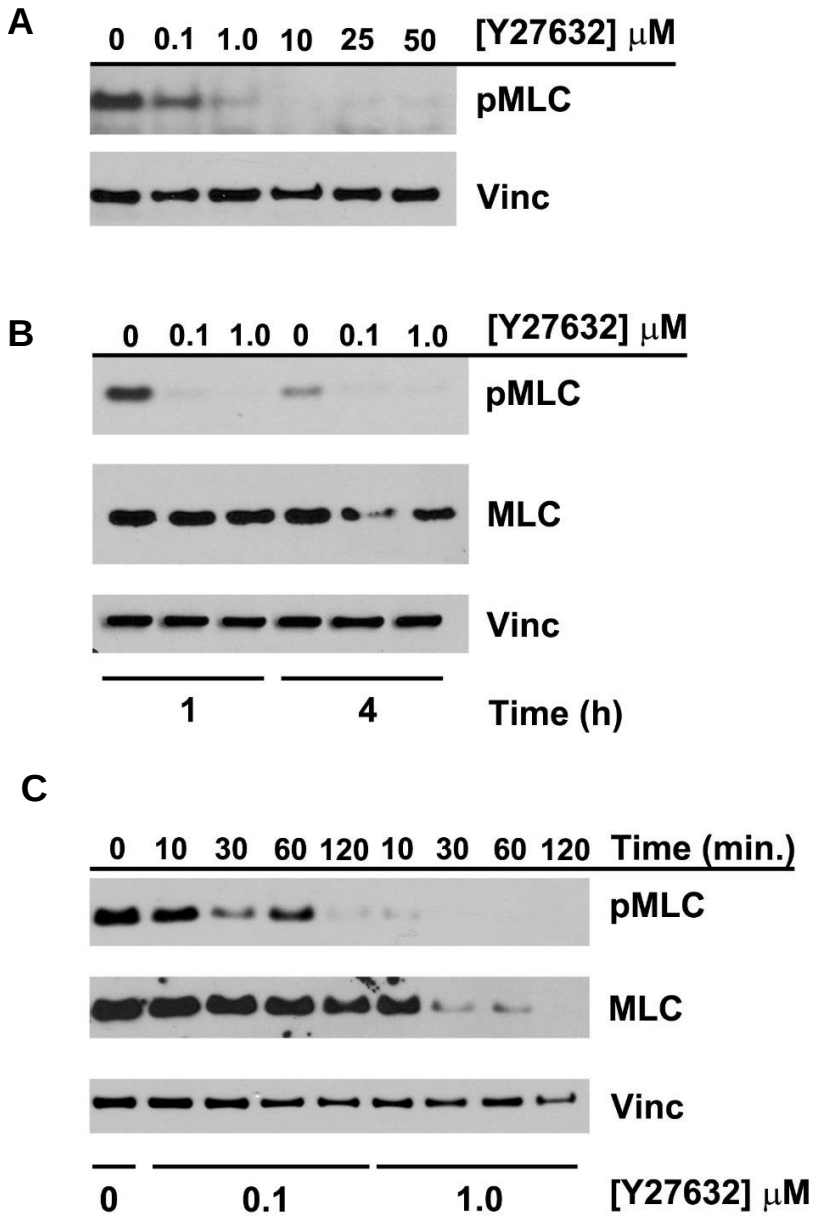

A) ECFCs from GDM pregnancies were treated with different concentrations (0-50μm) of a Rho kinase inhibitor (Y27632) for one hour prior to lysate collection. A western blot depicts phosphorylated myosin light chain (pMLC) and vinculin (Vinc). **B)** ECFCs from GDM pregnancies were treated with either 0, 0.1, or 1.0 μM of Y27632 for one or four hours as shown. A western blot depicts phosphorylated myosin light chain (pMLC), total myosin light chain (MLC), and vinculin (Vinc). **C)** ECFCs from GDM pregnancies were treated with 0, 0.1, or 1.0 μM of Y27632 inhibitor in a time-course assay with treatments ranging from 0-120 minutes as shown. A western blot depicts phosphorylated myosin light chain (pMLC), total myosin light chain (MLC), and vinculin (Vinc).

Figure 35. Reducing Myosin Light Chain Phosphorylation Rescues ECFC Migration

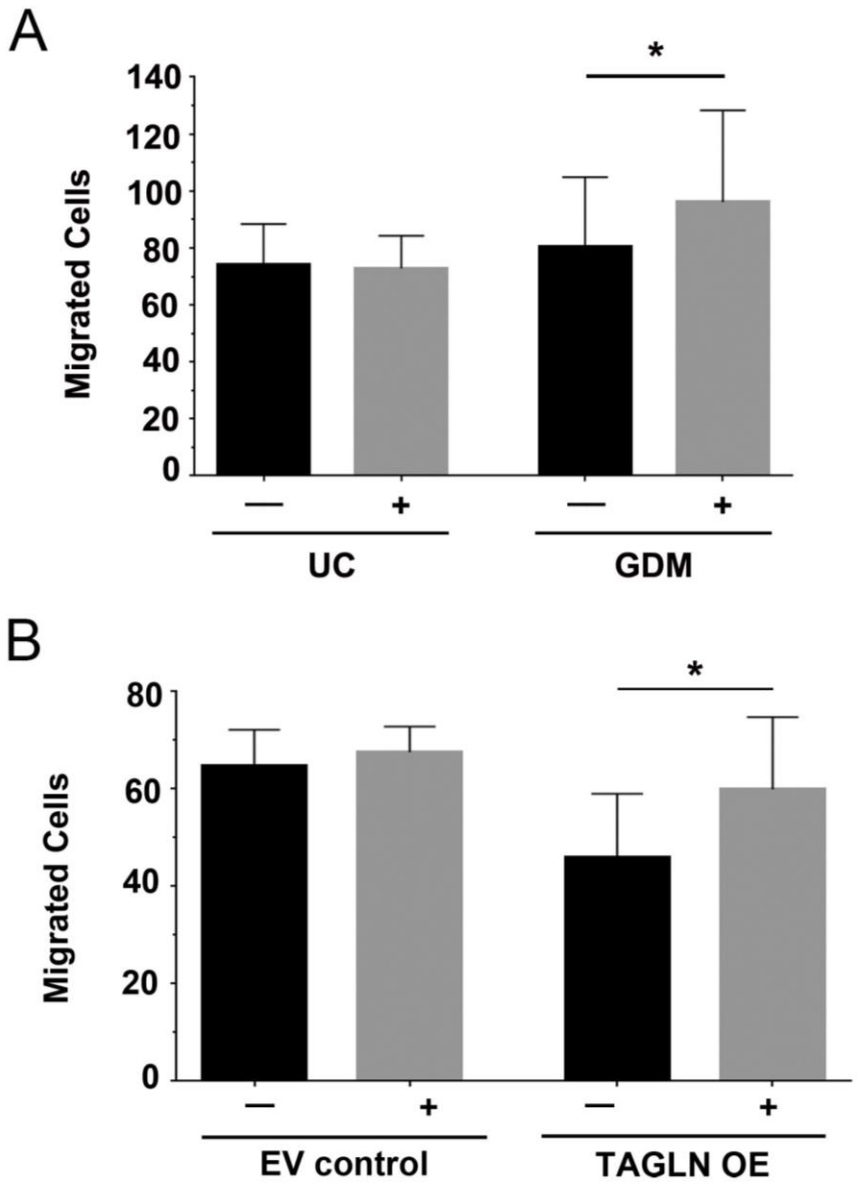

A) ECFCs from uncomplicated (UC) and GDM pregnancies were either untreated (-) or treated by adding 0.1μM Rho kinase inhibitor Y27632 (+) to the cell suspension just prior to plating in trans-well assays. After four hours, trans-wells were fixed and the number of migrated cells was quantified from eight randomized image fields per treatment group. Results were analyzed by two-way ANOVA followed by Sidak's multiple comparison test (UC n=3, GDM n=6, *p=01). **B)** ECFCs from uncomplicated pregnancies transduced with control lentivirus (EV control) or a lentivirus containing TAGLN (TAGLN OE) were untreated (-) or treated with Rho kinase inhibitor Y27632 (+) and plated in trans-well assays. After four hours, trans-wells were fixed and the number of migrated cells was quantified from eight randomized image fields per treatment group. Results were analyzed by two-way ANOVA followed by Sidak's multiple comparison test (n=5 transductions, *p=0.019).

Figure 36. Total G-actin and F-Actin Levels are Not Different Following TAGLN Overexpression

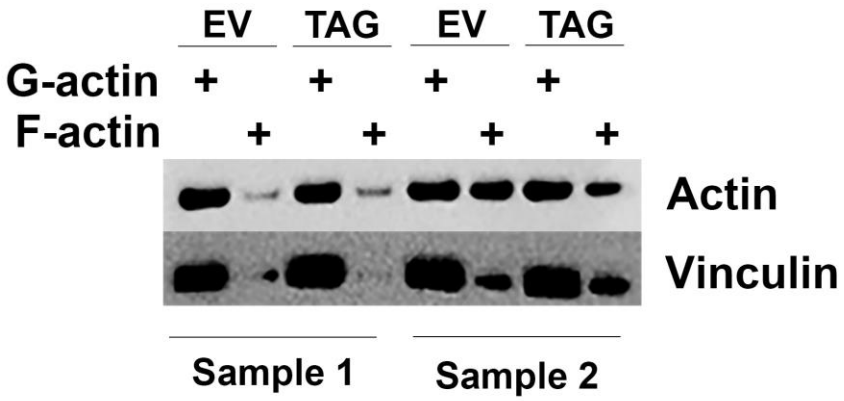

A western blot depicting lysates from two different ECFC samples (1-2) that were collected following transduction with either a control lentivirus (EV) or a lentivirus containing TAGLN (TAG). Centrifugation was performed to isolate the G-actin and F-actin fractions from the lysates. A western blot was performed using the processed lysates and the membrane was probed for Actin and Vinculin.

Figure 37. Flow Cytometric Analysis Confirms No Difference in F-actin following TAGLN Overexpression

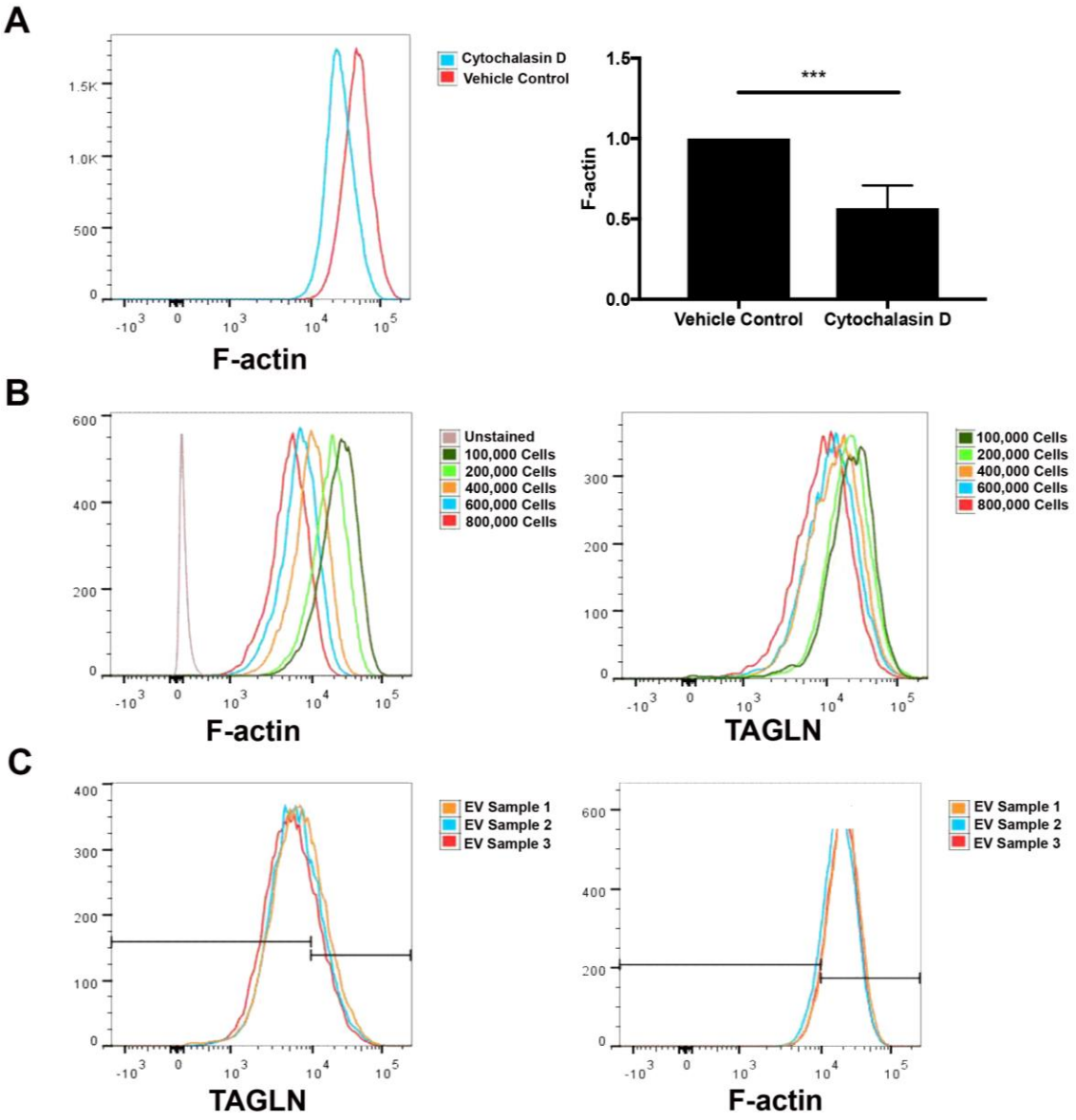

A) ECFCs from uncomplicated pregnancies were treated with DMSO (Vehicle Control, red) or 10μM Cytochalasin D (blue) for one hour. Following treatment, total F-actin was measured using flow cytometry. Cytochalasin D-treated sample values were normalized to Vehicle Control and mean (peak) values are graphed (n=4, ***p=0.0009). **B)** Five different concentrations of ECFC suspensions ranging from 100,000-800,000 cells were stained for F-actin (left) and TAGLN (right) and analyzed by flow cytometry. An unstained control (gray) is shown in the F-actin panel. **C)** Three different ECFC samples (1-3) were transduced with control lentivirus (EV) and stained for TAGLN (left) and F-actin (right). Graphs depict the amount of TAGLN and F-actin in all three samples.

Figure 37 continued:

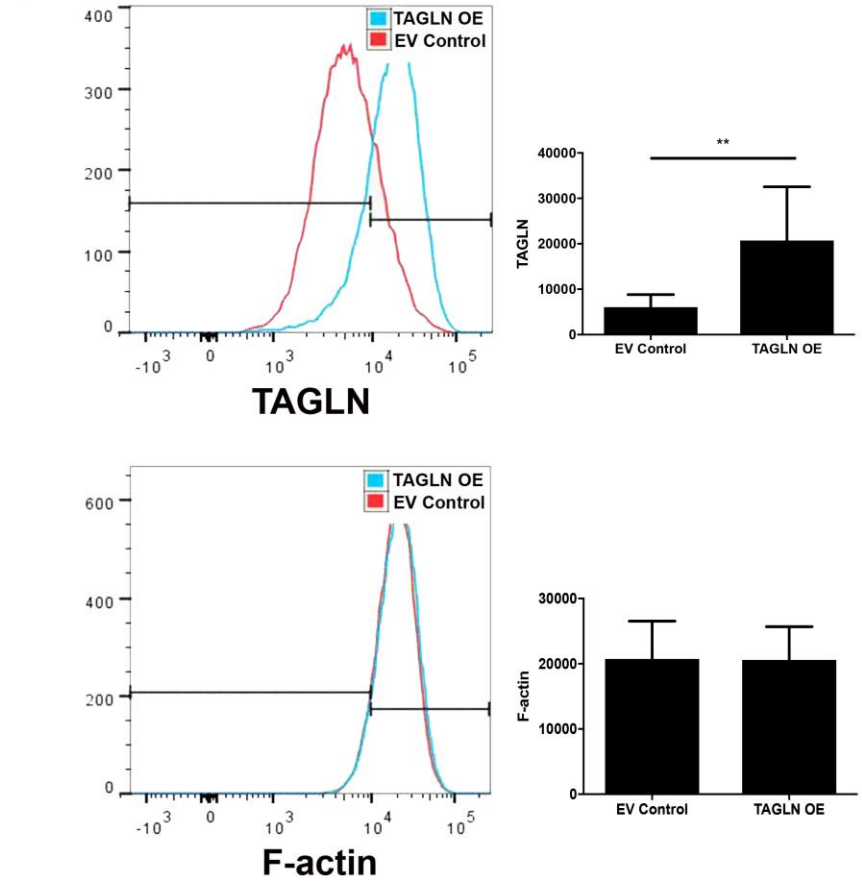

D) ECFCs from uncomplicated pregnancies were transduced with a control lentivirus (EV Control, red) or a lentivirus containing TAGLN (TAGLN OE, blue). Representative histograms are shown demonstrating the amount of TAGLN (left) and F-actin (right) in one ECFC sample. Bar graphs to the right of each histogram represent mean peak values from three separate transduced ECFC samples. (n=11 transductions, **p=0.0029)

Figure 38. TAGLN Localizes to F-actin in ECFCs

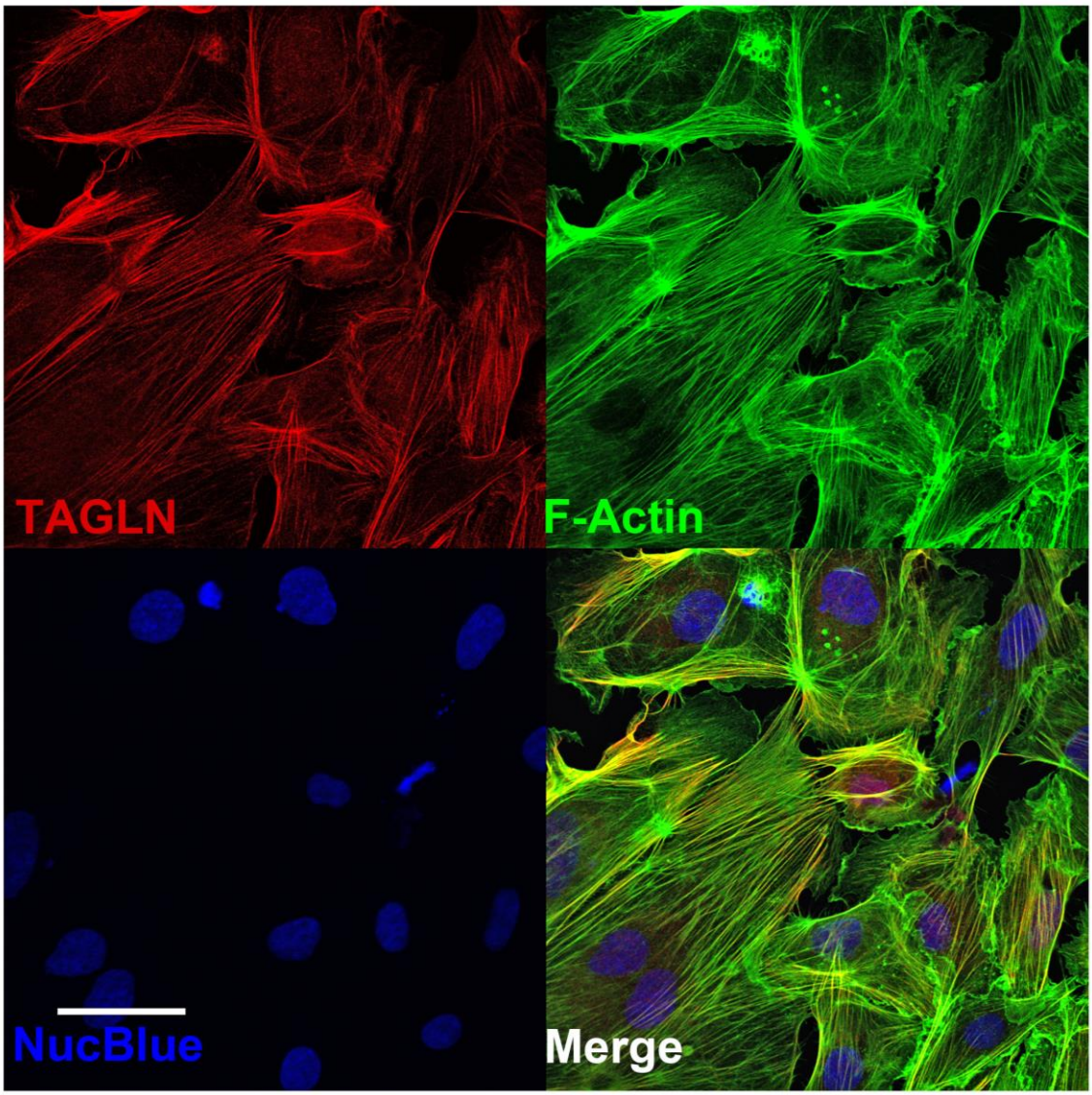

ECFCs from a GDM pregnancy were plated on type 1 collagen-coated glass slides and stained for TAGLN (red) and F-actin (green). NucBlue was used as a nuclear stain (blue) and all three channels were overlaid in the fourth panel (Merge). Images were obtained using confocal microscopy. The scale bar represents 50μm.

Figure 39. TAGLN Alters ECFC Alignment and Response to Shear Stress

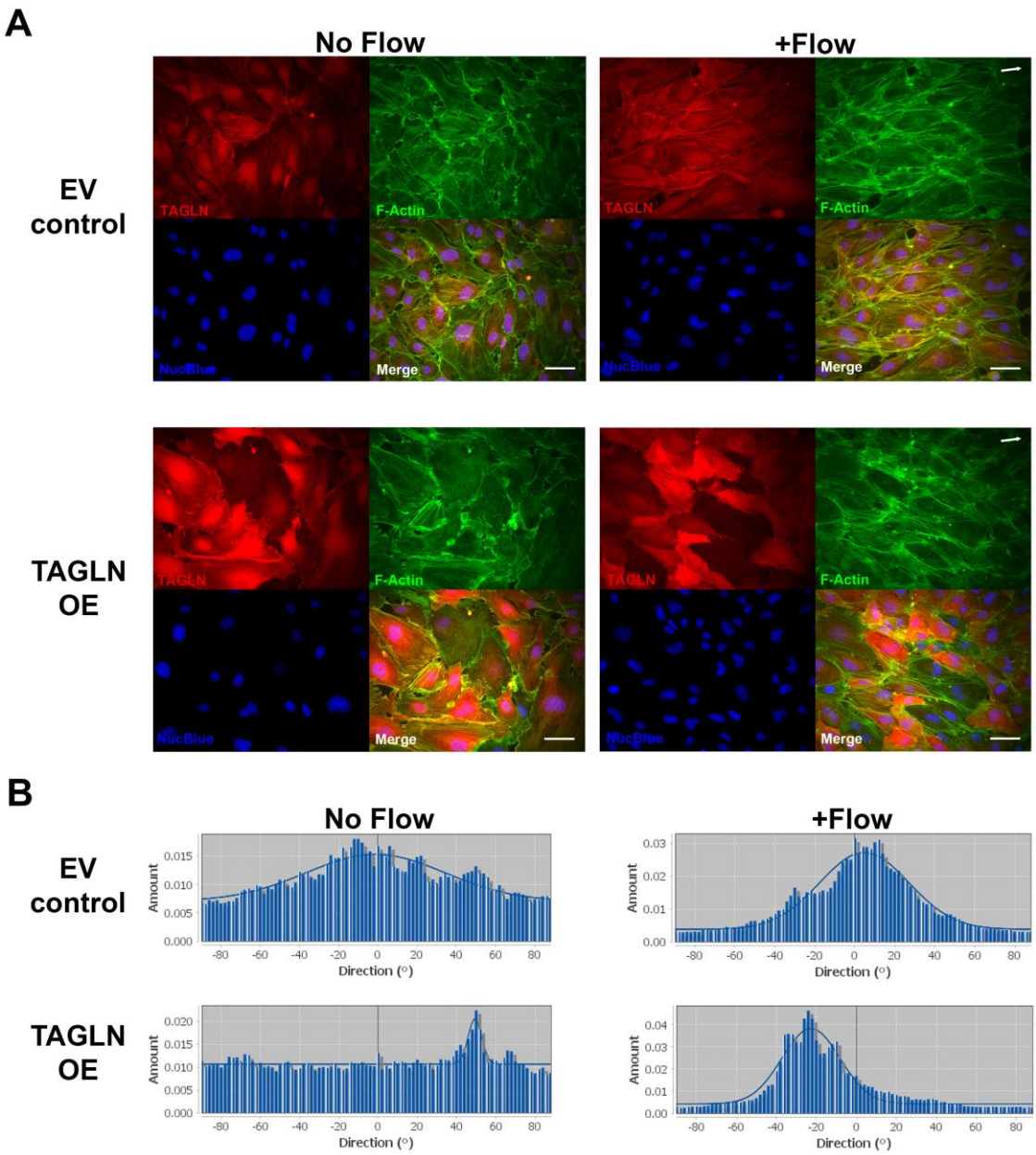

A) ECFCs from uncomplicated pregnancies were transduced with control lentivirus (EV control) or a lentivirus containing TAGLN (TAGLN OE). Transduced ECFCs were plated on type 1 collagen-coated glass slides and were maintained in static culture medium (No Flow) or exposed to 7 hours of laminar flow (+Flow) using a custom apparatus as previously described [127,128]. Direction of flow is indicated by white arrows in upper corner of images. Following treatment, ECFCs were fixed and stained for TAGLN (red), F-actin (green), and NucBlue (blue). All three channels were overlaid in the Merged image. Scale bars represent 6350μm. **B)** ECFC alignment was analyzed with the Directionality Plug-in (ImageJ). F-actin fluorescence images were used to generate the single, blue histograms representing angle distribution from the representative sample images above.

Figure 39 continued:

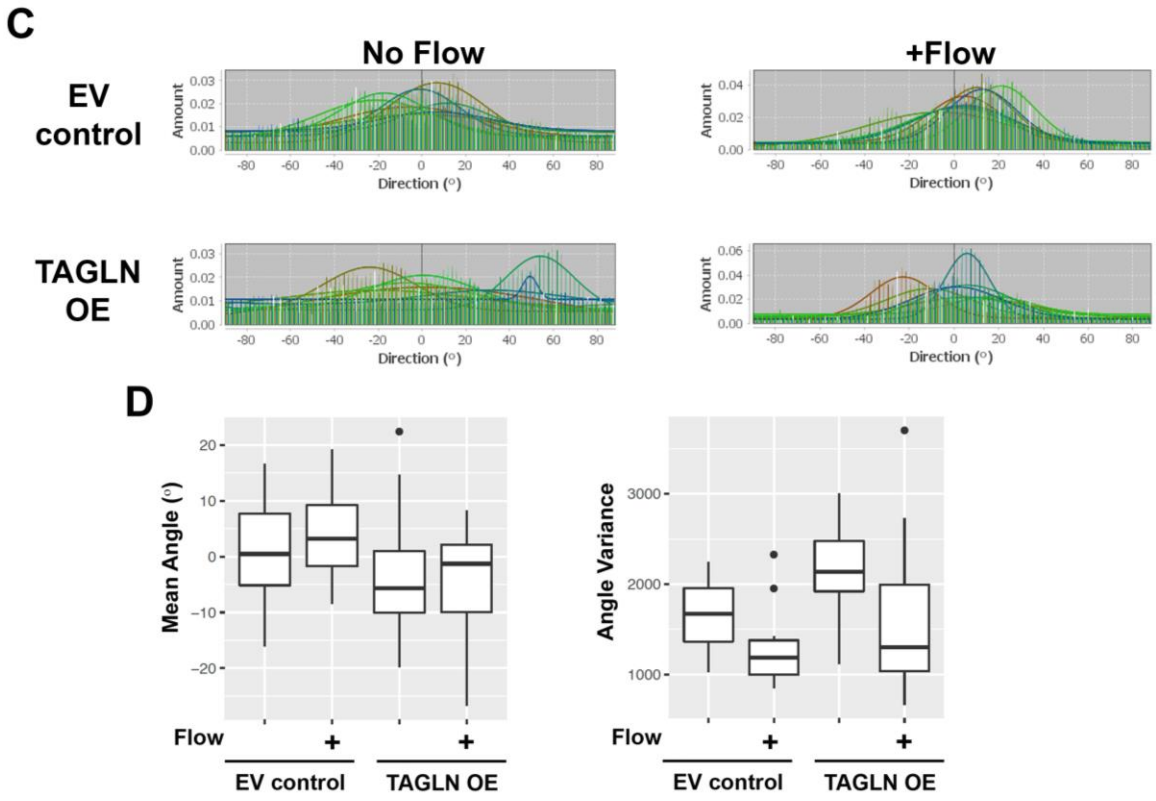

C) Histograms representing all images for each group were combined and overlaid. **D)** Box and whisker plots representing statistical analysis completed to compare the mean angle and angle variance distributions between the two treatment groups (EV control and TAGLN OE) in the presence and absence of Flow.

Figure 40. ECFCs from Uncomplicated and GDM Pregnancies Align with Laminar Flow

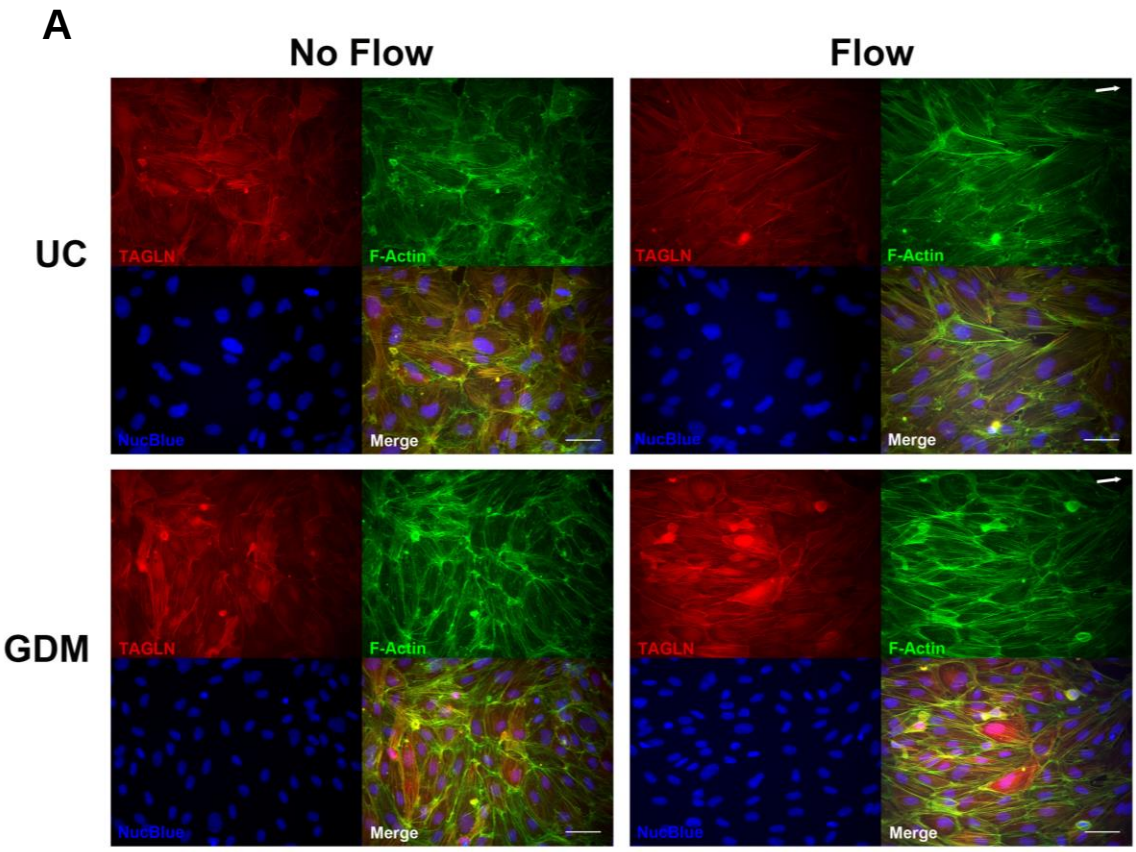

A) ECFCs from uncomplicated (UC) and GDM pregnancies were plated on type 1 collagen-coated glass slides and were maintained in static culture medium (No Flow) or exposed to 7 hours of laminar flow (Flow) using a custom apparatus as previously described [127,128]. Direction of flow is indicated by white arrows in upper corner of images. Following treatment, ECFCs were fixed and stained for TAGLN (red), F-actin (green), and NucBlue (blue). All three channels were overlaid in the Merged image. Scale bars represent 6350μm.

Figure continued on the next page.

Figure 40 continued:

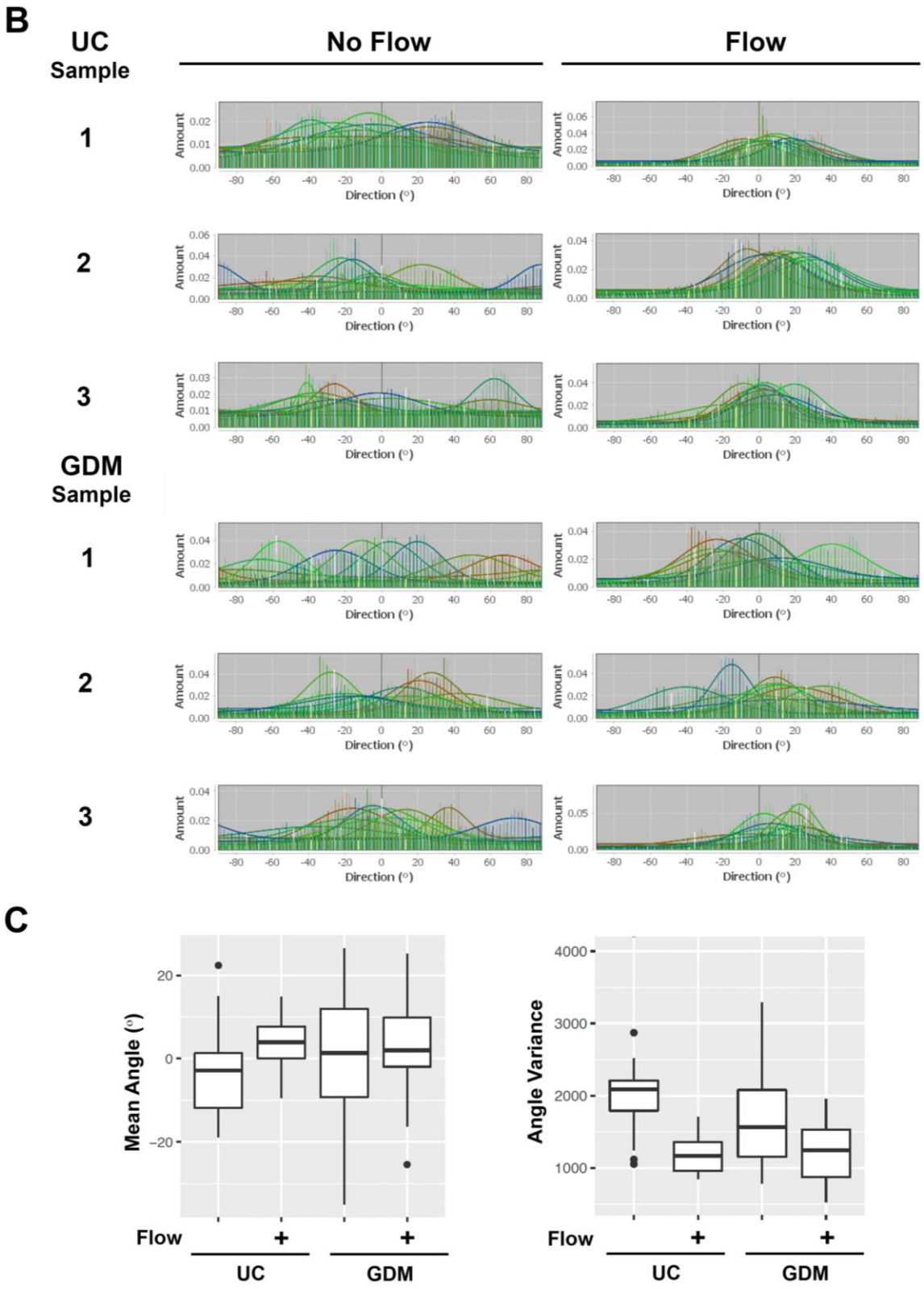

Figure 40 continued:

B) ECFC alignment was analyzed with the Directionality Plug-in (ImageJ). The F-actin fluorescence images were used to produce the histograms representing the distribution of angles measured within eight images for each group, which were combined and overlaid. **C)** Box and whisker plots representing statistical analysis completed to compare the mean angle and angle variance distributions between the two sample groups (UC and GDM) in the presence and absence of flow.

CHAPTER 4: CONCLUSION

Discussion

The objectives of this work were to identify novel phenotypes involved in vasculogenesis and to investigate the molecular mechanisms altered in fetal ECFC vasculogenesis following *in utero* maternal diabetes mellitus exposure. I made significant progress towards these objectives through the completion of several independent studies and the development of new technologies that can be applied to future studies in the field. The results of these investigations are summarized under the corresponding study aims below.

Aim 1: To develop innovative methods to quantitatively assess the kinetics of ECFC vasculogenesis *in vitro*.

Implementation of Technological Advancements to Overcome Assay Limitations

Advancements in imaging technology have created new challenges for image processing and quantitative analysis. These challenges include managing large volumes of data and deriving new biologically meaningful results that are not dependent upon manual analyses. Therefore, development of automated image analysis is crucial for maximizing information obtained from independent experiments, which in turn will provide opportunities for discovery of novel pathologic phenotypes. Automation enables multi-parametric investigation of a broad range of quantitative measures that are too difficult to detect manually [143–145]. Additionally, automation can increase assay sensitivity and reproducibility while minimizing time, labor, and bias. In the study of vasculogenesis, automation of image analysis allows for greater mechanistic understanding of the complex, kinetic process of network formation. Although some automated vasculogenic image analyses are commercially available, many technologies are cost-prohibitive for

large, kinetic studies [146]. Therefore, a primary limitation in the field is an open source platform for assessing kinetic measurements of vasculogenesis *in vitro*.

In the Aim 1 results section, new techniques were optimized to assess the kinetics of ECFC function and identify correlative vasculogenic phenotypes [133]. KAV measured numerous structural phenotypes, identifying two phases of network formation. The transition point between phases was associated with maximal network connectivity. Additionally, KAV calculated a novel and direct measure of connectivity, the branch to-node-ratio. Motility analyses determined how individual cell movement impacted network formation. Greater movement occurred during early network formation, and movement in Phase 1 directly correlated with Phase 2 movement. Future studies that assess directionality of cell movement will be important to determine whether ECFCs respond to pro-migratory stimuli with coordinated movements.

Assessment of proliferation by nuclear markers, such as histone H3 phosphorylation, is a standard technique. However, assessing proliferation during network formation is novel. Tissue Cytometry (TC) enabled identification of distinct cell populations based on fluorescence and localization. Thus, TC is an innovative and powerful tool to assess cellular events, such as proliferation, apoptosis, and senescence on a large-scale in thousands of cells. Specifically, this technique was applied to quantitate localization of proliferating ECFCs within networks at a single cell resolution. TC revealed that few ECFCs divide (2-8%) in early network formation. Dividing ECFCs are primarily in nodes where most cells reside, however ECFCs in branches are equally likely to undergo division. Importantly, this TC approach could be applied to assess the frequency and localization of a variety of cellular events that can be fluorescently labeled during vasculogenesis. Thus, the potential impact of applying this newly developed methodology

to unique biologic systems is yet to be realized. Overall, the improvements to standard imaging and quantitation strategies outlined in Aim1 provide insight into potential mechanisms contributing to altered ECFC vasculogenesis and can be applied to any vascular system or cell type.

Strengths of New Experimental Approaches

Assessing multiple phenotypes within the same biologic system provides an opportunity to identify correlative phenotypes. In our system, negative correlations were identified between KAV parameters and TC data. Samples with higher branch proliferation formed maximal closed networks quickly, though fewer total closed networks overall. KAV parameters also correlated with ECFC motility. Specifically, ECFCs that move shorter distances or at slower speeds during early network formation have a higher branch to node ratio, or reduced connectivity. We speculate that ECFCs that move less form fewer nodes, resulting in longer branches and decreased network stability. Fewer nodes and decreased network stability (i.e. reduced connectivity) would result in an increased ratio of branches to nodes.

Though *in vivo* models provide a more complete view of vasculogenic function [147], the new approaches outlined for *in vitro* studies are informative without being cost-prohibitive and can guide future *in vivo* studies. A concrete example is that the ratio of branches to nodes is not generally evaluated. However, it was the phenotype most strongly correlated with ECFC motility, and one of the most informative phenotypes in differentiating ECFC vasculogenic function. Based on these findings, future studies that focus on understanding the basis for increased branch to node ratio could be highly instructive and promote mechanistic insights into altered vasculogenesis. Furthermore, the automated imaging

analyses reported here could be applied to *in vivo* models, thereby broadening the impact of the open source resources developed in this thesis to assess vasculogenesis.

Aim 2: To identify novel phenotypic differences in ECFC vasculogenesis following exposure to intrauterine diabetes.

Intrauterine Exposure to Maternal T2DM Alters Kinetics of Fetal ECFC Vasulogenesis

The techniques developed here were implemented to identify how exposure to a maternal T2DM environment alters ECFC network formation. These new data confirm previous findings that ECFCs exposed to intrauterine T2DM have impaired vasculogenesis [79]. However, time-lapse imaging identified two phases of vasculogenesis, which was previously unappreciated. KAV methodology demonstrated that ECFCs exposed to T2DM *in utero* form (Phase 1) and maintain fewer networks (Phase 2), resulting in increased average network areas. In T2DM ECFCs, the onset of a pathologic increase in the branch to node ratio in Phase 2 is speculated to indicate network instability, or an inability to maintain branch connections.

Overall, differences in proliferation were not observed between ECFC sample groups in either of the two assays that measured proliferation acutely (Figures 16-17). Additionally, acute ECFC proliferation is not altered on collagen or Matrigel following exposure to maternal T2DM *in utero*. However, significant differences in ECFC clonogenic potential following intrauterine exposure to T2DM were identified in a more chronic, long-term assessment (Figure 18). This finding suggests that the identified ECFC defect in short-term network formation, as measured *in vitro*, is not secondary to altered proliferation. Alternatively, it is possible that current *in vitro* static measurements of proliferation during the process of vasculogenesis are insufficient to capture subtle differences in the

proliferation of ECFCs. Given the observation that T2DM-exposed ECFC samples had no HPP-ECFCs, long-term repopulating ability is predicted to be reduced. The consequences of altered repopulation capacity can't be measured by current short-term measurements of vasculogenesis *in vitro*. However, these results do support previous findings that ECFCs from T2DM pregnancies have significantly reduced vessel-forming ability *in vivo* [79]. Future studies in which associations between clonogenic capacity measured *in vitro* and vessel formation *in vivo* would be informative in understanding how functional phenotypes may be producing long-term vascular complications in offspring.

Challenges of Studying Primary Human Samples

Surprisingly, ECFC proliferation and motility were not different between the uncomplicated and T2DM ECFC groups when measured acutely. These observations suggest that differences in network structure may not be attributable to these phenotypes. However, these unexpected results could be due to T2DM sample variability, method resolution, or a relatively low sample size. Additionally, differences between population-based functional assessments versus single ECFC measurements may account for these findings. For instance, KAV, a population-based analysis, identified differences between the clinical groups. Subsequent ECFC studies (i.e. proliferation and motility) were at a single cell resolution. However, as discussed above, single cell phenotypes correlated with measures of network formation. Therefore, subtle alterations in single ECFC function may impact overall cell coordination required for optimal network formation. Future studies that correlate individual cell functions with population-based read-outs are predicted to reveal a better understanding of the complex process of vasculogenesis.

Studies using primary human stem/progenitors generate clinically relevant data. However, human samples from heterogeneous sources introduce variability, which can be a barrier

in identifying differences between groups with small sample sizes. Overall, greater variation was observed in T2DM samples; consistent with the hypothesis that ECFC samples from T2DM mothers are heterogeneous with varying functionality due to factors such as disease severity and therapeutics used during pregnancy [79,81]. Thus, more sensitive readouts are necessary to delineate meaningful differences in a disease with significant heterogeneity.

Overall, novel microscopic approaches described here were optimized to provide greater mechanistic insight into the dynamic process of vasculogenesis. KAV identified two phases of network formation and guided further mechanistic studies of proliferation and motility, which correlated with network structure parameters. These correlations provide new insight into how neonatal ECFC vasculogenesis may be altered from intrauterine T2DM exposure. Importantly, the methods outlined have broad implications beyond the scope reported here. Implementation of these approaches will enhance mechanistic assessment and improve functional readouts of vasculogenesis in numerous cell types or disease states.

Aim 3: To determine if increased Transgelin 1 expression in ECFCs from gestational diabetic pregnancies impairs vasculogenesis.

Implications of Altered TAGLN in GDM-exposed ECFCs

Transgelin was originally identified as smooth muscle cell-specific, but increasing evidence suggest that this family of proteins is expressed in a variety of cell types including mesenchymal cells, fibroblasts, and epithelial cells [90,100]. Using a broad microarray screen, elevated TAGLN was identified in ECFCs isolated from pregnancies complicated with GDM. As a result of intrauterine GDM exposure, ECFCs exhibit impaired functional

abilities including resistance to hyperglycemia-induced senescence and decreased network formation *in vitro* [79,81]. Therefore, this study aimed to determine if elevated TAGLN expression in GDM-exposed fetal ECFCs contributed to observed impairments in ECFC migration and network formation *in vitro*.

Recent published studies in the laboratory demonstrated that ECFCs from T2DM pregnancies have increased nuclear localization of the transcription factor, Mesenchyme Homeobox 2 (MEOX2), which was sufficient to increase ECFC migration and network formation [82]. Therefore, increased MEOX2 expression was speculated to be a compensatory mechanism by which fetal ECFCs from T2DM pregnancies maintain vascular function despite poor intrauterine environments. The identification of a dysregulated molecular mechanism in T2DM-exposed ECFCs prompted additional studies to identify specific molecular mechanisms altered by TAGLN expression in GDM-exposed ECFCs.

Molecular approaches were used to modify levels of TAGLN in ECFCs obtained from GDM and uncomplicated pregnancies prior to conducting functional assays. Importantly, similar TAGLN expression was observed in ECFCs from uncomplicated pregnancies and GDM-exposed ECFCs following siRNA-mediated TAGLN knockdown. Additionally, lentiviral-mediated TAGLN over-expression produced similar protein expression to levels observed endogenously in GDM-exposed ECFCs. Therefore, TAGLN expression achieved in these studies was within a physiological range. SiRNA-mediated reduction of TAGLN in GDM-exposed ECFCs increased the number of networks formed in Matrigel and the number of migrated cells in trans-well assays. These data suggest that elevated TAGLN could be responsible for impaired network formation and migration in GDM-exposed ECFCs. This is supported by the observation that lentiviral-mediated over-

expression of TAGLN in ECFCs from uncomplicated pregnancies reduced network number in Matrigel and the number of migrated cells in trans-well assays, suggesting that TAGLN alone was sufficient to impair network formation and migration. In contrast to the protective effects of MEOX2 in T2DM-exposed ECFCs, elevated TAGLN expression in ECFCs from GDM pregnancies results in pathologic changes. Therefore, TAGLN expression was not compensatory, but rather detrimental, as it reduced ECFC network formation and migration. The difference between the consequences of elevated MEOX2 and TAGLN in ECFCs could be due to the specific function of each protein, but differences could also be attributable to the severity and duration of the intrauterine diabetic microenvironment from which the cells were derived.

TAGLN Regulates Cell Migration

Two Transgelin genes, TAGLN and TAGLN2, are involved in the regulation of cell migration. TAGLN2 expression in human umbilical vein endothelial cells decreases migration through a reduction in phosphorylation of MLC [111]. In HT1080 (human fibrosarcoma cell line) cells, TAGLN regulates MMP9, a key factor involved in the breakdown of extracellular matrix proteins to enhance migration [112]. Importantly, a high sequence conservation exists between all three Transgelin genes (Transgelin 1-3), including within the actin-binding domain. Therefore, these pathways were tested to determine whether similar TAGLN-mediated mechanisms exist in ECFCS to regulate migration. Although MMP9 is not detectable at the transcript level in ECFCs, MLC phosphorylation was increased in ECFC samples from GDM pregnancies. Similarly, overexpression studies demonstrated that increased TAGLN was sufficient to enhance MLC phosphorylation in uncomplicated ECFC samples. Although these results are not consistent with previous reports on TAGLN2 in human umbilical vein endothelial cells, the apparent discrepancy may be due to differences in cell types and Transgelin genes

studied. In these overexpression studies, reduced phosphorylation of MLC, via Rho kinase inhibition, increased ECFC migration. These data suggest that elevated MLC phosphorylation is pathologic, which may be secondary to altered actin cytoskeletal rearrangement.

TAGLN Regulates ECFC Alignment Under Shear Stress

Vascular endothelial cells comprising vessel walls are constantly exposed to hemodynamic forces. Therefore, it is critical for endothelial cells to appropriately sense and respond to shear stress, most commonly laminar flow [148]. Endothelial cell alignment in the direction of laminar flow is a central feature of vascular homeostasis [149]. Given that TAGLN is an actin binding protein involved in regulating cytoskeletal reorganization, we asked whether the increased TAGLN expression in GDM-exposed ECFCs was sufficient to impair ECFC alignment to laminar flow. Initial studies demonstrated that overexpressing TAGLN altered ECFC alignment in basal as well as under flow conditions (Figure 39). Alterations in alignment under basal conditions was surprising, as it wasn't previously appreciated the extent to which ECFC organization can vary in static culture. Next, GDM-exposed ECFCs with high endogenous TAGLN levels were assessed to identify if GDM exposure resulted in baseline impairment of cell alignment. No differences in ECFC alignment were observed between samples from uncomplicated (UC) and GDM pregnancies following static culture (Figure 40). However qualitative and quantitative differences between UC and GDM-exposed ECFC alignment were evident following seven hours of laminar flow exposure (Figure 40A-B). Interestingly, the graphs depicting angle variance in the overexpression as well as the GDM experiments exhibit similar trends (Figures 39C and 40C). Although differences in UC and GDM-exposed ECFC alignment in response to laminar flow were not statistically significant, the trend was similar to the malalignment observed in ECFCs overexpressing

TAGLN. Previous functional assessments of GDM-exposed ECFCs required high sample numbers, likely due to disease heterogeneity and duration, which was evident in variability of GDM-exposed ECFC function measured *in vitro*. Therefore, this preliminary study was likely underpowered to interrogate the question adequately. Additional studies in which higher sample numbers are assessed will provide meaningful outcomes from which conclusions can be properly derived.

Successful completion of the following experimental aims will provide further insight into genetic and mechanistic changes occurring in ECFCs following exposure to maternal diabetes *in utero*.

1. To further evaluate how elevated TAGLN expression in GDM-exposed ECFCs impairs migration and network formation.

Increasing Sample Size

Although results from studies outlined in Aim 3 provide strong evidence that increased TAGLN expression in GDM-exposed ECFCs reduces migration and network formation, additional studies will strengthen the conclusions reported above. Since assessment of GDM-exposed ECFC alignment to laminar flow was likely underpowered, additional studies testing greater sample numbers will be more convincing and enable formulation of stronger conclusions. Simultaneous to testing additional samples in shear assays, KAV assays could be performed with GDM-exposed ECFC samples. Several samples from T2DM pregnancies were assessed (Aim 2), however few samples from GDM pregnancies have been assessed in kinetic network formation assays. Based on preliminary studies using three GDM samples (Figure 44), great heterogeneity in network formation kinetics was observed in GDM samples. In our experience in the laboratory, heterogeneity is common in functional *in vitro* assessments of GDM-exposed ECFCs. Therefore, testing a greater sample number will aid formulation of conclusions that pertain to a majority, if not all samples in that clinical group.

Conducting Assessments on Matrigel

ECFC gene expression, including TAGLN, is contingent on extracellular matrix composition (Figures 29 and 41). Therefore, assessment of TAGLN expression on Matrigel will provide a more accurate measure of TAGLN levels, which would better inform network formation outcomes. Therefore, TAGLN expression should be evaluated in additional ECFC samples on Matrigel, including ECFCs from uncomplicated and GDM pregnancies as well as those transfected with siRNA for knockdown studies and transduced with lentivirus for overexpression studies. Similarly, trans-well studies outlined in Aim 3 results were conducted using type 1 collagen. However, given that ECFC gene expression and function is altered on different extracellular matrices, it would be informative to conduct trans-well invasion assays in which trans-wells are coated with Matrigel instead of collagen, requiring ECFCs to "invade" the gel to migrate. Given that differences in migration were not observed in GDM-exposed ECFCs plated on collagen (Figure 24), and previous assessments of GDM-exposed ECFCs reported altered performance under conditions of stress [81], perhaps conducting a different version of the trans-well assay using Matrigel would capture a new, biologically meaningful readout.

Requirement of Actin Binding in TAGLN-mediated Effects

Although it seems likely that TAGLN is altering ECFC cytoskeletal rearrangement, and thus migration, through binding to F-actin, it is unclear whether actin binding is required for TAGLN-mediated reductions in network formation, migration, and cell alignment. To determine how disrupting actin binding impacts TAGLN-mediated dysfunction, site-directed mutagenesis could be used to alter the actin-binding domain in the TAGLN sequence used for overexpression. Based on foundational work in the literature characterizing TAGLN amino acids critical for actin binding [108], I propose three mutations, including two deletions and one in which 4 amino acids are altered (Delta 154-

161, Delta 170-186, K154L/K155L/K160L/R161L). I hypothesize that the TAGLN-mediated effects on ECFC migration require actin binding, therefore overexpressing a mutant form of TAGLN unable to bind actin will not reduce ECFC migration or MLC phosphorylation. Overexpression and MLC phosphorylation could be assessed by Western blotting and F-actin binding could be assessed by immunofluorescence and co-immunoprecipitation assays.

Centrifugation and flow cytometric assays were performed to assess total F-actin following TAGLN overexpression. Using these approaches, no differences in total F-actin were identified, however the functional organization of F-actin into stress fibers was not assessed. I hypothesize that TAGLN expression increases F-actin bundling, resulting in the formation of stress fibers. To assess F-actin bundling, I propose to use fluorescence anisotropy as described by Koskinen et al. [150]. Briefly, inter-filament Förster resonance energy transfer (FRET) would be used to detect proximity of individual actin filaments, or actin bundling, following GFP labeling of actin monomers. Increased bundling would result in increased local F-actin concentration and therefore, GFP-actin monomers. Increased proximity of GFP-actin monomers would result in increased FRET, which would be quantitated to provide a measurable readout indicative of F-actin bundling.

Assessing MLC Phosphorylation following TAGLN Knockdown

Additional studies are needed to confirm MLC phosphorylation following siRNA-mediated TAGLN knockdown in GDM-exposed ECFCs. Although differences in MLC phosphorylation were not observed under standard culture conditions following TAGLN reduction (Figure 32), these results are not conclusive. As discussed in the Results, the timing of analysis may not have captured alterations in MLC phosphorylation. Time course studies in which MLC phosphorylation was evaluated at multiple times spanning several

days would provide a more comprehensive analysis of the impact of knockdown duration on MLC phosphorylation. Stress conditions that increase MLC phosphorylation, such as ionomycin treatment, could also be used as a terminal treatment to increase basal levels of MLC phosphorylation, resulting in a readout of greater differences in MLC phosphorylation following TAGLN knockdown. Finally, knockdown of TAGLN was not complete, making it possible that residual TAGLN obscured detection of this phenotype. A CRISPR/Cas method to genetically delete TAGLN could be used to explore this possibility in the future. Although it is also important to consider the possibility that TAGLN knockdown may not alter MLC phosphorylation due to activation of a compensatory mechanism in GDM-exposed ECFCs, which could be explored in future studies following the outcome of the additional analyses outlined above.

2. To determine if TAGLN expression is regulated by methylation.

Our data demonstrate that increased TAGLN expression in GDM-exposed ECFCs results in substantial functional deficits. Our previous focus was on identifying the downstream consequences of increased TAGLN expression in ECFCs. Future studies are necessary to dissect molecular mechanisms that promote increased TAGLN expression in order to discover potential therapeutics to overcome these changes. To accomplish this goal, it is imperative to understand how TAGLN expression is regulated.

In the Haneline laboratory, an RNA microarray (Affymetrix GeneChip) and a DNA methylation array (Illumina Infinium 450K) were conducted to identify differential gene expression and methylation between ECFCs isolated from uncomplicated pregnancies and those complicated by T2DM or GDM. An inverse correlation was identified between DNA methylation in the TAGLN gene promoter region and TAGLN gene expression (r =-

0.72, p=0.02, FDR=0.28, Emily Blue, unpublished data). These data suggest that TAGLN expression in ECFCs may be regulated at the epigenetic level by DNA methylation, similar to recent published studies by Dr. Blue for placenta-specific 8 (PLAC8) [83]. Therefore, I hypothesize that decreased methylation in the TAGLN promoter region in GDM-exposed ECFCs leads to increased TAGLN gene expression. To test this hypothesis, I would assess methylation status of the 10 CpG sites in the TAGLN promoter identified in the methylation array in ECFCs from uncomplicated and GDM pregnancies. Confirmation of differential methylation in the TAGLN promoter would further support the hypothesis that intrauterine exposure to GDM induces epigenetic alterations in neonatal ECFCs that modify gene expression leading to altered ECFC function.

3. Explore the mechanism(s) responsible for increased Notch signaling in GDM-exposed ECFCs and determine whether altered Notch signaling impairs ECFC vasculogenesis.

Diabetes Alters Notch and VEGF Signaling: Rationale for Targeted, Mechanistic Studies in GDM-exposed ECFCs

Development of endothelial dysfunction resulting from diabetes mellitus is complex. Therefore, the molecular mechanisms underlying vascular disease progression are not fully understood [151]. One mechanism previously identified involved peroxisome proliferator-activated receptor-gamma co-activator 1 alpha (PGC-1α), a transcriptional co-activator involved in regulation of energy metabolism. In rodents and humans with diabetes mellitus, PGC-1α was elevated in endothelial cells and caused impairment of migration *in vitro* and vasculogenesis *in vivo*. Importantly, the mechanisms responsible for these pathologic phenotypes were altered PGC-1α-induced Rac/Akt/eNOS signaling and Notch signaling [152]. Additional studies reported a deleterious effect of diabetes on

Notch activation contributing to abnormal vasculogenesis [153–155]. For example, in aortic endothelial cells obtained from streptozotocin-induced diabetic mice, cell migration, proliferation, and sprouting were rescued through inhibition of Notch signaling *in vitro* [153]. Moreover, inhibition of Notch signaling combined with VEGF stimulation in the hind limb ischemia model increased blood vessel density and perfusion in diabetic mice *in vivo* [153]. Additionally, in a spheroid model of endothelial cells on smooth muscle cell monolayers, high glucose treatment increased sprouting and branching and resulted in an increased number of tubes with small diameters. However, the small tubes formed in high glucose conditions regressed and eventually disconnected [6]. The high glucose treatment induced JAGGED1 and suppressed NOTCH1 in this model. Therefore, not only is Notch signaling up-regulated in endothelial cells from diabetic animals and humans, but Notch activation results in impairment of vasculogenesis.

In addition to Notch signaling, VEGF signaling is also critical during vasculogenesis [4]. VEGF regulates cellular processes primarily through ligand binding at surface receptors and subsequent signal transduction and activation of intracellular pathways. Therefore, it is critical that vascular cells, such as endothelial cells, receive and respond appropriately to the external stimuli. Diabetic patients exhibit VEGF resistance, in which reduced signaling occurs despite normal, or even elevated VEGF ligand expression [156]. Specifically, diabetic patients have elevated levels of soluble VEGF, but no concomitant increase in VEGFR expression in the myocardium. In fact, VEGFR1 and VEGFR2 levels were decreased in the samples from diabetic patients compared to samples from non-diabetic patients. Although these studies were carried out in cardiomyocytes and not endothelial cells, the impact of the diabetic environment on VEGF signaling is an important component to vascular health. Our recent studies indicate that ECFCs isolated from the umbilical cord blood of diabetic mothers have altered network formation kinetics [133].

Since the process of vasculogenesis is tightly regulated by crosstalk between the Notch and VEGF pathways, and Notch signaling is altered in response to high glucose [152,153,156], I hypothesize that these pathways are altered in diabetes-exposed ECFCs.

Altered Notch Signaling in GDM-exposed ECFCs

Previous gene expression studies conducted on ECFC samples from uncomplicated and diabetic pregnancies did not identify alterations in members of the Notch or VEGF signaling pathways. However, those studies were conducted on a limited number of samples and ECFCs were plated on collagen, not Matrigel prior to RNA isolation. ECFCs plated on collagen grow in a monolayer; whereas, ECFCs on Matrigel form complex network structures. Additionally, different extracellular matrices engage and bind distinct integrins to induce specific intracellular interactions with cytoskeletal proteins and signaling cascades [157]. Therefore, preliminary studies were conducted to determine if the observed functional differences of ECFCs on Matrigel compared to collagen were accompanied by changes in Notch activation, including *HEY1* and *DLL4* expression. *HEY1* is a transcriptional target of the Notch pathway that is commonly used as a measure of Notch pathway activation, and DLL4 is a membrane-bound ligand for multiple Notch receptors. Analysis by qRT-PCR revealed a large increase in *HEY1* and *DLL4* on Matrigel compared to collagen in all samples tested (Figure 41). Increases in both *HEY1* and *DLL4* appear to be larger in the samples from T2DM and GDM pregnancies compared to the sample from an uncomplicated pregnancy (Figure 41-42). These preliminary data suggest that the T2DM and GDM-exposed ECFCs may have an elevated response to a component in the Matrigel. These results also emphasize the importance of assessing ECFC functionality in the context of network formation on Matrigel, as it likely results in the activation of different pathways. Therefore, previous analyses of gene expression using samples plated on collagen may not reflect gene expression differences during ECFC

vasculogenesis. In addition to following up on specific targets, such as Notch signaling ligands and receptors, it would also be worthwhile to repeat a broad gene expression survey using RNA samples from ECFCs on Matrigel.

Differences in VEGFR2 Expression and Localization in GDM-exposed ECFCs

While alterations in gene expression profiles on Matrigel are important, confirmatory protein analyses are challenging because the commonly used methods for collecting protein lysates are not feasible on Matrigel matrix due to the high protein concentration in the gel. Therefore, to assess receptor and ligand expression at the protein level while ECFCs are actively forming networks, a protocol for immunofluorescence staining on Matrigel matrix was implemented in pilot studies. This method is extremely powerful as it allows observation of changes in protein expression at a single cell level and identification of the location of those cells within the overall network structure. Preliminary studies demonstrate differences in VEGFR2 expression between control and GDM-exposed ECFCs. Two hours post-plating control ECFCs express predominantly VEGFR1 on the cell membrane in the node structures, and VEGFR2 on the tip, or extending cells (Figure 43). Conversely, the GDM-exposed ECFCs predominantly express VEGFR2 on the cell membrane of every cell in the network structure including the nodes (Figure 43). Increased VEGFR2 expression in the GDM-exposed ECFCs is consistent with increased Notch activity because VEGFR2 up-regulates *DLL4,* stimulating Notch activation [158] (Background Figure 2). This observation provides insight into a possible mechanism by which GDM-exposed ECFCs form altered network structures.

Overall, Notch and VEGF signaling play a critical role in vasculogenesis. Importantly, hyperglycemia and diabetes mellitus alter activation of these signaling pathways, however no studies have investigated whether similar dysfunction occurs following intrauterine

diabetes mellitus exposure. Based on these preliminary data, I hypothesize that intrauterine exposure to diabetes may be causing differential activation of these pathways during network formation. These studies are critical to pursue, to evaluate a potential molecular mechanism underlying altered network formation kinetics identified by KAV (Figure 44). Based on this contention, next steps would include broadly surveying Notch pathway components including Notch receptors (NOTCH1-4), Notch ligands (DLL1, DLL4, JAGGED1, JAGGED2), Notch transcriptional targets (Hey1, Hey1, Hes1), and VEGF receptors (VEGFR1-2) in ECFC patient samples from uncomplicated and GDM pregnancies plated on Matrigel. Assessing expression of key components of the Notch and VEGF signaling pathways would provide evidence of Notch pathway activation and the specific ligands and receptors altered in GDM-exposed ECFCs. Additionally, since conducting initial studies to assess expression of VEGFR1 and VEGFR2 on ECFCs in Matrigel, immunofluorescence techniques were optimized to enable large scale imaging of whole networks (Figure 11), and Tissue Cytometry (TC) was developed to quantitate localization of protein expression within network structures (Figure 12). Therefore, to build on preliminary data shown in Figure 43, and to determine if GDM-exposed ECFCs exhibit increased VEGFR2 expression compared to uncomplicated controls, VEGFR1 and VEGFR2 expression should be analyzed in additional ECFC samples using optimized immunofluorescence techniques combined with TC analysis. One of the strengths of TC is the ability to analyze expression and localization of multiple proteins simultaneously. Therefore, the staining strategy employed in the preliminary studies of VEGFR1 and VEGFR2 could be expanded to include co-staining with other Notch pathway receptors or ligands identified in the broad expression analysis on Matrigel. Specifically, inclusion of a fluorescent probe for DLL4 in the VEGFR1 and VEGFR2 staining protocol would be informative since VEGFR2 up-regulates DLL4 *and* stimulates Notch activation. An immunofluorescence approach might identify how crosstalk between the Notch and VEGF

pathways regulate ECFC vasculogenesis, and if those mechanisms are altered following intrauterine GDM exposure. Upon identification of altered expression of specific Notch receptors or ligands in GDM-exposed ECFCs, targeted knockdown and lentiviral-mediated overexpression approaches could be implemented to determine whether reductions in a specific protein are required to impair network formation or whether increased expression was sufficient to induce impaired network formation.

Closing Remarks on Broad Translational Implications of Research on ECFCs

TAGLN: A Promising Target in Anti-Cancer Therapies

Due to the unique proliferative and vasculogenic properties of ECFCs, increasing numbers of studies have explored potential applications of ECFCs for tissue regeneration, as biomarkers for vascular disease, and in anti-angiogenic cancer therapies [24,159]. During cancer progression, a common mechanism by which tumor suppressors achieve gene silencing is through CpG hyper-methylation in gene promoter regions [160,161]. Therefore, to identify which genes are hyper-methylated in breast cancer tissues, Sayar et al. conducted a comprehensive microarray expression profiling analysis [162]. Based on results of the microarray analysis, TAGLN was identified as a primary target of DNA hyper-methylation. Specifically, TAGLN expression was decreased in approximately 62% of breast tumors, compared to matched tissue [162]. Analysis of additional, public microarray methylation data (GSE201713 and GSE31979) identified TAGLN hyper-methylation in approximately 63% of tumors tested [162]. Thus, methylation patterns in the TAGLN promoter region could serve as a diagnostic or prognostic biomarker in cancer.

Decreased TAGLN has been identified in several different types of cancer, including breast, colon, lung, bladder, and prostate cancer [163–171]. Therefore, increasing studies are focused on targeting TAGLN in the development of anti-cancer therapies [172]. Specifically, actin stabilization and MMP9 regulation are two TAGLN-mediated mechanisms thought to be critical in cancer progression. One of the common cancer cell phenotypes is actin disorganization. Since TAGLN is an actin stabilizing protein, it acts like a tumor suppressor by protecting against cellular depolarization through induction of rigid actin stress fibers [172]. Secondly, TAGLN may act as a tumor suppressor through regulation of MMP9 expression [173,174]. MMP9 is a matrix metalloproteinase required

for extracellular matrix degradation in the processes of cell migration and invasion [175]. Therefore, in addition to the implications of TAGLN in diabetes, it may also be a useful target in the development of anti-cancer therapies.

Translational Propositions: ECFCs as Therapeutic Agents

Despite promising functional efficacy, isolation of sufficient cell numbers remains a prominent challenge in using ECFCs for angiogenic therapy [39]. To overcome this challenge, a protocol was developed to convert human induced pluripotent stem cells (hiPSCs) or embryonic stem cells (hESCs) into cord-blood-like ECFCs [135]. Importantly, the cord-blood-like cells express a stable endothelial phenotype, exhibit high clonal proliferative potential, and form perfused vessels in ischemia reperfusion models. Successfully recapitulating the functional phenotypes critical to ECFC vascular formation and repair using hiPSCs provides a unique opportunity to obtain clinically relevant cell numbers for the development of angiogenic therapies.

Complementary to efforts in obtaining sufficient ECFCs for therapeutic use, recent studies confirmed sufficient recovery of ECFCs from cryopreserved cell samples up to 21 years old, which is key for future feasibility of transplanting ECFCs clinically [176]. Although the ECFC colonies were smaller in size following many years of cryopreservation, these studies support regenerative medicine efforts using banked ECFC samples. ECFC isolation protocols have even been established in different model systems, such as rat, to enable assessment of function resulting from different pathophysiological states [159,177]. In an acute kidney injury rat model, administration of rat pulmonary microvascular ECFCs was sufficient to reduce renal injury and increase recovery speed [159]. Interestingly, the microvascular ECFCs administered achieved renal protection despite ineffective homing to the site of ischemic injury in the kidney. This finding suggests

that ECFCs may secrete factors that enhance recovery following ischemia through preservation of microvascular function in the damaged tissue.

Utilizing Measurements of ECFC Function at Birth to Predict Future Disease Risk.

In addition to therapeutic applications, ECFCs are also being explored for use as biomarkers of diseases, especially cardiovascular-related diseases [178,179]. Generally, endothelial cell populations are considered useful biomarkers for cardiovascular disease due to their role in maintaining homeostasis by modulating vascular integrity and blood fluidity [180,181]. Alvarado-Moreno et al. conducted a broad study in which they evaluated ECFC number, frequency, and functional phenotypes in the setting of venous thromboembolic disease (VTD). They detected a higher number of ECFCs in patients with VTD, and the ECFCs isolated from those patients had increased production of free radicals, reactive oxygen species (ROS), and inflammatory mediators such as tumor necrosis factor alpha (TNF-α) and interferon gamma (INF-γ) [179]. These functional deficits are like other previously identified characteristics of dysfunctional endothelium [182]. However, unlike differentiated endothelium, deficits in undifferentiated progenitor cell populations, like ECFCs, may aid in the understanding of how chronic diseases, like VTD, persist.

In addition to biomarkers for adult cardiovascular diseases, ECFCs are good candidates for assessing disease risk in children. The study of fetal progenitor cell populations that are enriched in umbilical cord blood provides a unique, translational research opportunity to understand the impact of suboptimal intrauterine environments, such as maternal diabetes mellitus, on the development of future offspring morbidities [37,79,183]. Importantly, not all forms of maternal diabetes mellitus, whether acquired prior to or during pregnancy, are equivalent. By obtaining pertinent patient data from individuals with a

variety of clinical backgrounds (i.e. HgA1C values, medications, etc.), a more comprehensive understanding of how disease management impacts fetal development can be achieved.

In vitro studies of ECFC function indicated that exposure to hyperglycemia impaired the ability of ECFCs to undergo vasculogenesis [79]. However, since both the duration of diabetes exposure and the severity of hyperglycemia are different in GDM and T2DM, it is not surprising that these conditions result in different health outcomes. Therefore, it is important for future studies to assess pre-gestational (T2DM) and gestational (GDM) diabetic pregnancies. Currently limited clinical readouts are available to identify children at greatest risk of developing complications later in life following intrauterine T2DM and GDM exposure. Therefore, if a mechanism was identified to link severity of intrauterine diabetic exposure with development of chronic vascular complications, new preventative strategies aimed at delaying or decreasing disease progression would be possible. Ultimately, longitudinal studies in which long-term health outcomes are assessed following intrauterine diabetes exposure would provide important validation for *in vitro* measures acquired at birth.

Although these studies provide novel insights into ECFC vasculogenesis, additional studies are needed to determine the accuracy with which the *in vitro* assays recapitulate functional deficits *in vivo*. Confirming long-term ECFC dysfunction resulting from developmental exposure to maternal diabetes would provide a strong link between progenitor cell dysfunction and subsequent development of vascular complications. Overall, ECFCs could be useful candidates for future preventative therapies. The development of a useful, non-invasive platform for assessing severity of exposure at the time of birth would increase the accuracy of health assessments to enable more informed

predictions of long-term health outcomes. Importantly, an *in vitro* platform assessing vascular cell function could be applied to evaluate health risk following exposure to a variety of abnormal gestational environments.

Figures (41-44)

Figure 41. Enhanced Expression of *Hey1* and *DLL4* on Matrigel

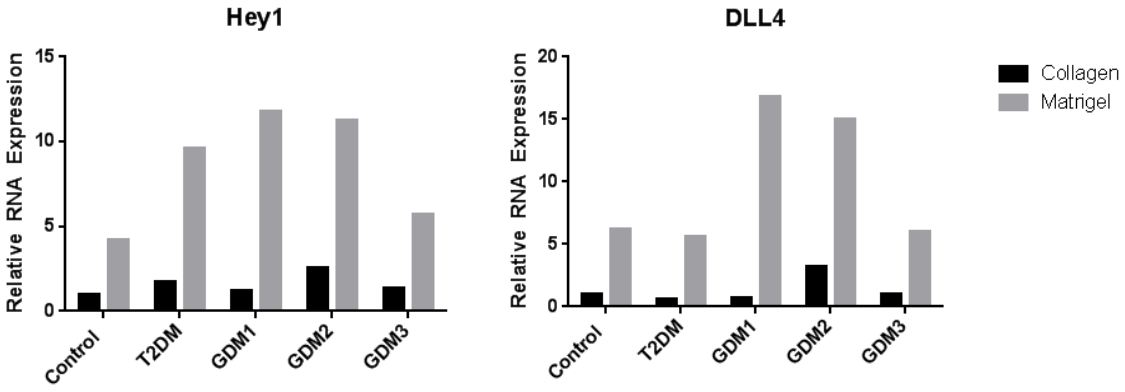

Graphs representing *HEY1* and *DLL4* mRNA expression in individual ECFC samples plated on collagen (black) and Matrigel matrix (gray). All values are relative to the uncomplicated ECFC sample (Control) value on collagen following normalization with HPRT. (n=1)

Figure 42. Notch Signaling may be Increased in GDM-exposed ECFCs

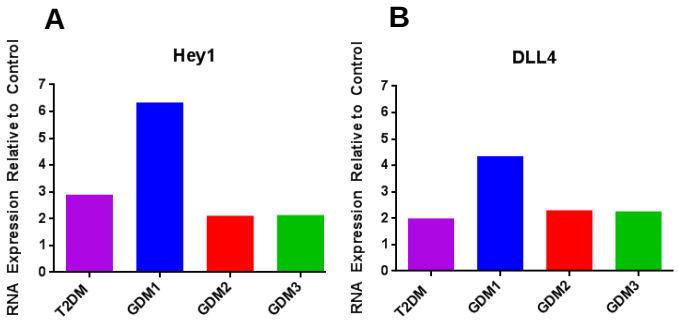

HEY1 **(A)** and *DLL4* **(B)** mRNA were measured in individual ECFC samples isolated from Matrigel matrix during network formation. Values were normalized to HPRT and are shown relative to uncomplicated ECFC expression levels (Control). (n=1)

Figure 43. VEGFR2 Expression may be Altered in GDM-exposed ECFCs

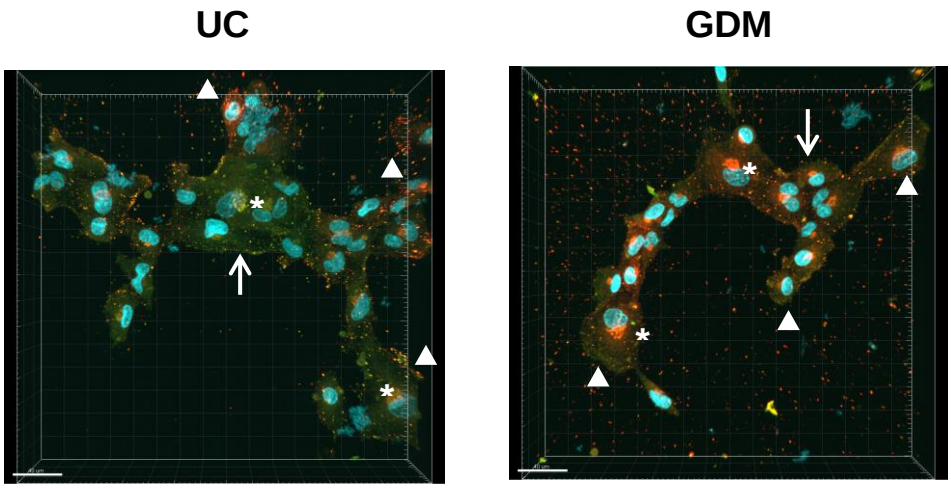

Immunofluorescence images illustrating expression of VEGFR1 and VEGFR2 in uncomplicated (UC) and GDM-exposed ECFCS plated on Matrigel matrix for two hours. Nuclei are shown in blue, VEGFR1 in green, and VEGFR2 in red. Asterisks (*) indicate staining in the Golgi apparatus while arrowheads indicate tip cells and arrows mark the nodes. Scale bars represent 40 μm.

Figure 44. Preliminary Kinetic Analysis of GDM-exposed ECFCs

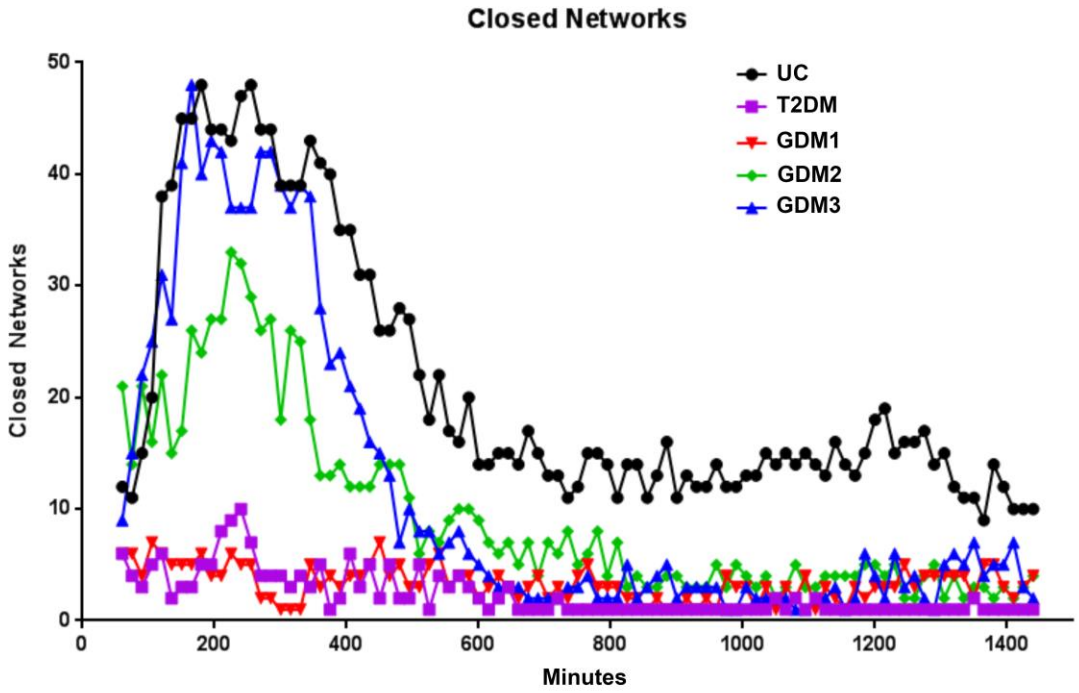

Representative average trace graphs of the number of closed networks over 24 hours. Images were acquired in 15 minute intervals, combined into video and analyzed by Kinetic Analysis of Vasculogenesis (KAV) software. The color-coded key identifies the individual cell samples used in three separate experiments (n=3).

LIST OF APPENDICES

APPENDIX A: Protocol for Analyzing Immunofluorescence Mitotic Index Images

1) Open FIJI
2) Open Image Files
    a. Import→Bioformats
    b. Check “Open All Series”
3) Create Maximum Intensity Projection Images
    a. Image→Stack→Z projection
    b. Dropdown (Max Intensity)
4) Adjust brightness and contrast in all open images at once
    a. Image→Adjust Brightness Contrast
    b. Click Set→ “Prop to all”
5) Save versions of all files at this point—label MIPs
6) View all images at once
    a. Window→Tile
7) Open Cell Counter
    a. Plugins→Analyze→Cell Counter
8) Open ROI Manager
    a. Analyze→Tools→ROI Manager
    b. Click polygon tool in main FIJI menu
    c. Use “Add,” “Show All,” and “Labels” in the ROI manager window to add ROIs, see all ROIs, and label individual ROIs within an image
9) Identify Nodes, outline with ROI (Best to do one image at a time)
10) Area Measurements
    a. Analyze→Set Measurements→ Check Area
    b. Select area on image and click Ctrl+M to get area in data table
    c. Record measurements in an excel data table
11) Count nuclei/node, mitotic cells/node, and tubular mitotic cells with Cell counter and record in excel data table.

APPENDIX B: Protocol for Processing Fluorescence Images in FIJI (ImageJ) for TrackMate

Opening a File:
Open image in FIJI (Image J) by clicking File → Open or by dragging file to gray bar at base of FIJI program.

Making a Selection:
Use square or circle tool (2nd from left) to make selection around region or entire well. You can hold 'Shift' while dragging the selection tools to make a perfect square or circle. The white anchor points on the selection can be dragged to make the region larger/smaller.

Manage Selections:
Analyze → Tools → ROI Manager
You can use the ROI manager to save selections (size and shape).
'Add': Adds a selection to the manager that you have just drawn on the image.
'More': You can save your ROIs and use for future image analysis

Crop:
Once your selection is the correct size and is in the correct location you can crop.
Image→ Crop
**However, for circles you will still have the original image in the corners after cropping.
Edit→Clear Outside
This will delete any information outside of the selection, and should default to black.

Background Subtract:
Process→ Subtract Background
This is useful for cleaning up fluorescent images.

Removing ROI:
Click outside the region of the ROI to remove. If that doesn't work, can do Image→Overlay→Hide Overlay

Removing circle for TrackMate Spot analysis:
After cropping, clearing the outside, and the background subtract, you will still have a circle outline that will get picked up through the Trackmate analysis. To get rid of that just create a smaller circle ROI that excludes just that line. Use the techniques/tools described in "Making a Selection" above.
Then repeat: Edit→Clear Outside
This will delete any information outside of the selection, and should default to black.
Adjust brightness and contrast as needed.
Image→Adjust→Brightness/Contrast

Open TrackMate:
Plugins→Tracking→TrackMate
New Screen should pop up that is labeled "TrackMate v2.0.4" or whichever version you are using. Click "Next".

For image analysis the following settings were used, however these may need to be adjusted based on image size and quality:
DOG
Average spot size 25
Threshold 2
Check ‘Use average threshold box’
Linking distances: 50, 90, 4
Frame depth: 20

APPENDIX C: Protocol for Overlapping Separate Images in Photoshop

1) Open the two images you wish to overlap in Photoshop (Image A and Image B)
2) Select the frame of the image you wish to transfer (Image B)
3) Type Ctrl+A to select the entire image
4) Copy and Paste that image into the frame of the second image (Image A)
5) With the new layer (Image B) selected in the Layers menu, click the arrow for the dropdown menu and select 'Difference'
6) This should overlap the two photos.

*You can adjust the levels prior to overlapping the images if necessary. To do that, click on the 'IMAGE' tab at the top of the screen. Then select 'Adjustments' and then 'Levels'.

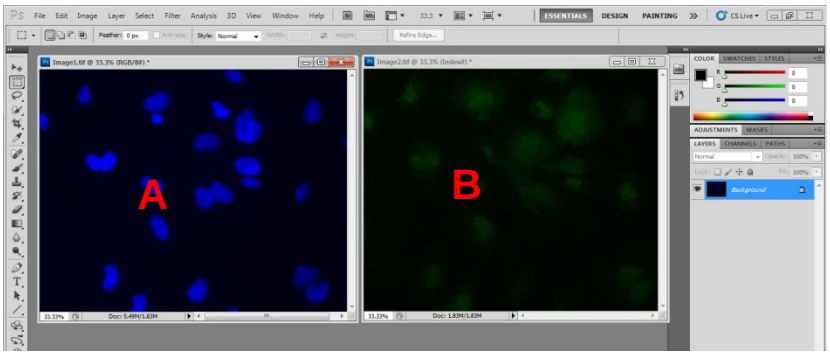

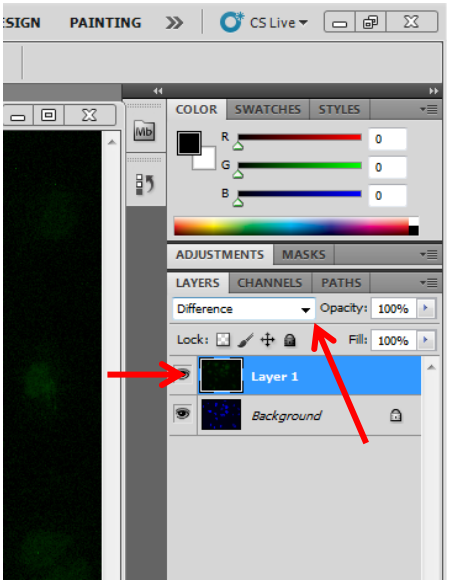

APPENDIX D: Protocol for Merging Images in Photoshop

Select

File→Automate→Photomerge

Make sure all settings in the Photomerge screen match the settings outlined in yellow (right).

Select Browse (red arrow)

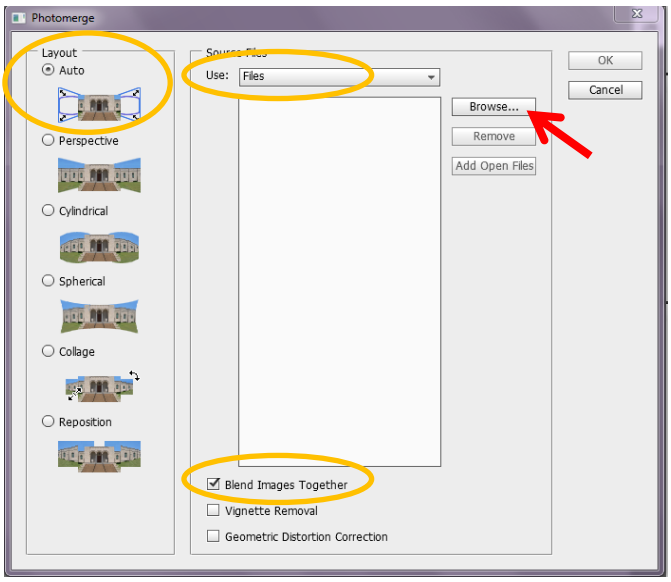

Highlight all images you would like to merge by holding down Shift (images in series) or Ctrl (images not in series) and click Open.

The names of the images you selected should appear in the white box on the Photomerge screen.

Click OK.

Photoshop will attempt to merge all of the selected images together, hopefully resulting in one completely photomerged image.

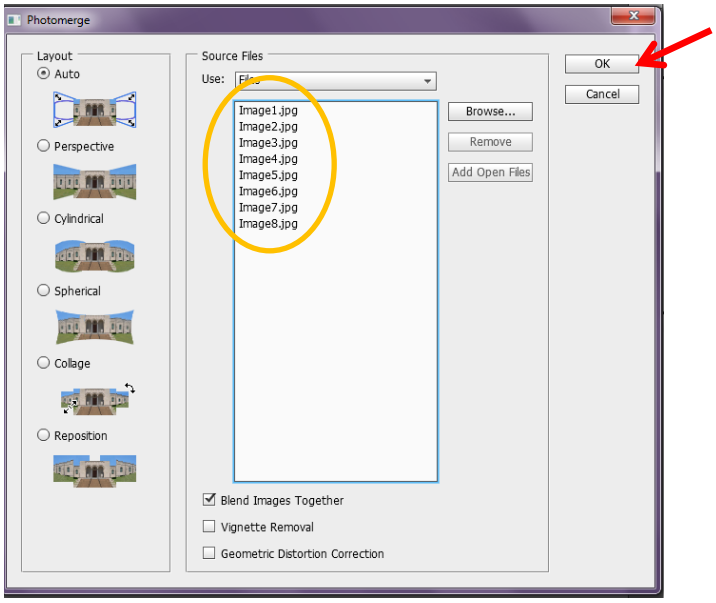

If the photomerge is incomplete, select and drag the different layers so that they overlap and form one completely photomerged image.

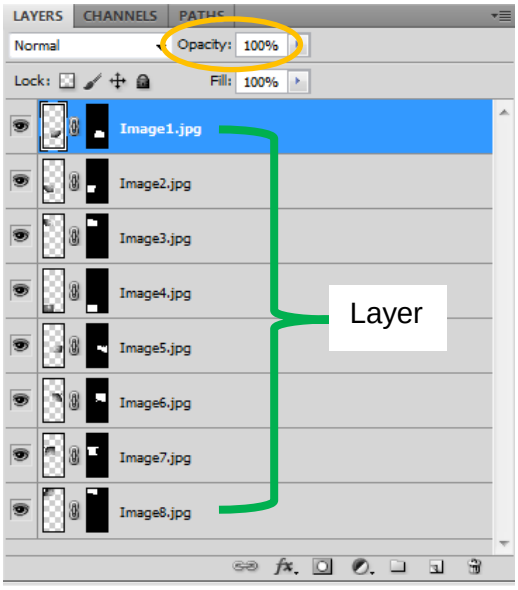

Select the layer(s) you wish to move (hold Shift or Ctrl to select multiple) and then select the black arrow tool from the tool window to move the images within the canvas.

Sometimes altering the Opacity in the 'Layers' window is helpful when aligning the images.

To create a larger canvas (work space) select Click Image→Canvas Size to make adjustments as needed.

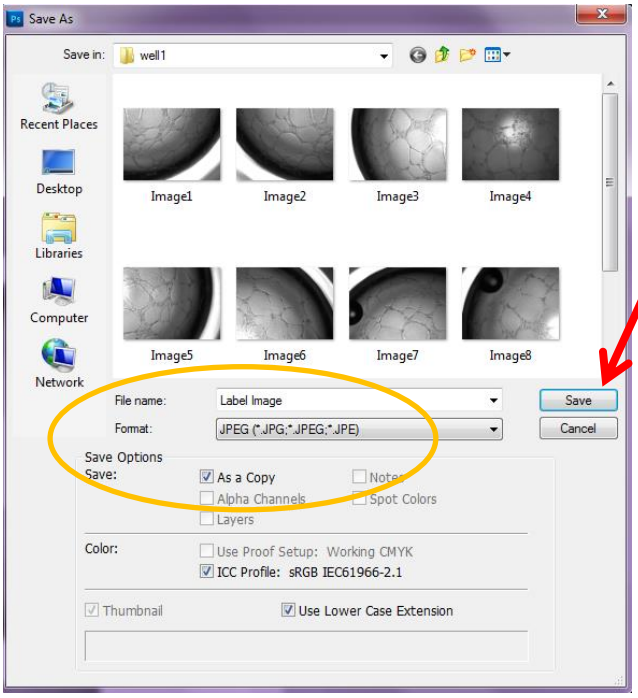

Once the photomerge is complete, Click Layer→Flatten Image

Once the image is flattened Click File→Save As

Label the merged image and under Save Options select “As a Copy” and Format as “JPEG”

Click Save

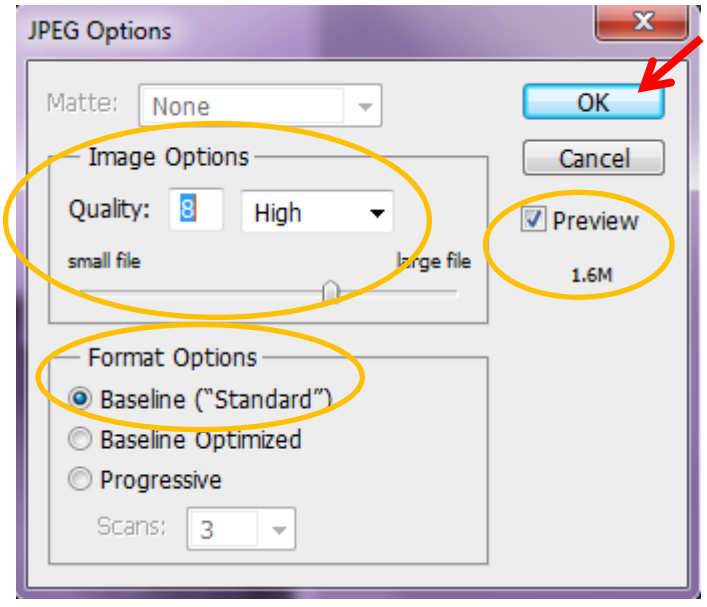

In the JPEG Options window under Image Options make sure the Quality is set to 8 / High and the Format is set at Baseline (“Standard”). Click the Preview box and then click OK.

If the file size is too large to open in Image J, etc. you can adjust the image size by clicking on Image→Image size In the Image size window adjust the number of pixels for the width and the ratio for the height will automatically adjust. Then click OK.

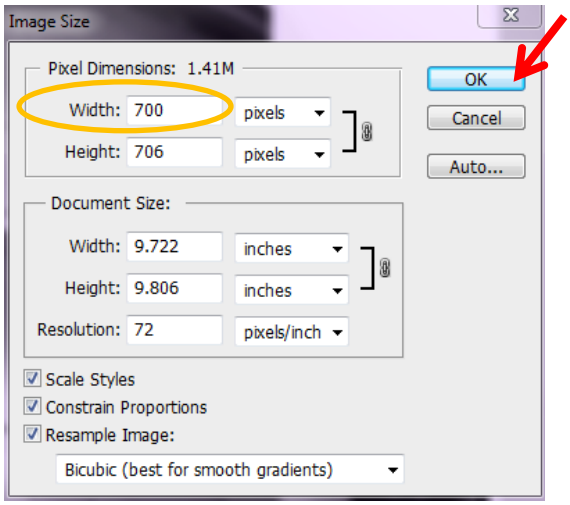

For opening the Photomerged images in Image J to count closed networks for Matrigel typically 700 pixels (width) is a good size to use.

APPENDIX E: Protocol for Automated Matrigel Counting Using ImageJ (Quick Version)

1) Open FIJI (ImageJ)

Creating ROI

2) Analyze→Tools→ROI Manager
3) Drag saved ROIs (zipped folder) into the 'Drag and Drop' bar to open in Manager
    a. OR create a new ROI using the circle selection tool in the tool bar

Opening and Converting Image

4) Drag JPEG image into 'Drag and Drop' bar to open
5) Image→Type→8 bit

Running Plug-IN

6) Click on ROI to view it on image
7) Align ROI if needed
8) Edit→Clear Outside
9) Plug-Ins→Analyze Network

Saving Files

10) Two windows will open
    a. File→Save As→JPEG for the fused skeleton/mask image
    b. Edit→Copy data table into excel document
    c. File→Save As→Original image with ROI on it with _ROI added onto end of name

APPENDIX F: Protocol for Automated Network Analysis in FIJI (ImageJ)

Open FIJI (Version from July 15, 2013)

Drag the Plug-In (Analyze Networks 0.6.5) into the gray bar at the bottom of the software window.

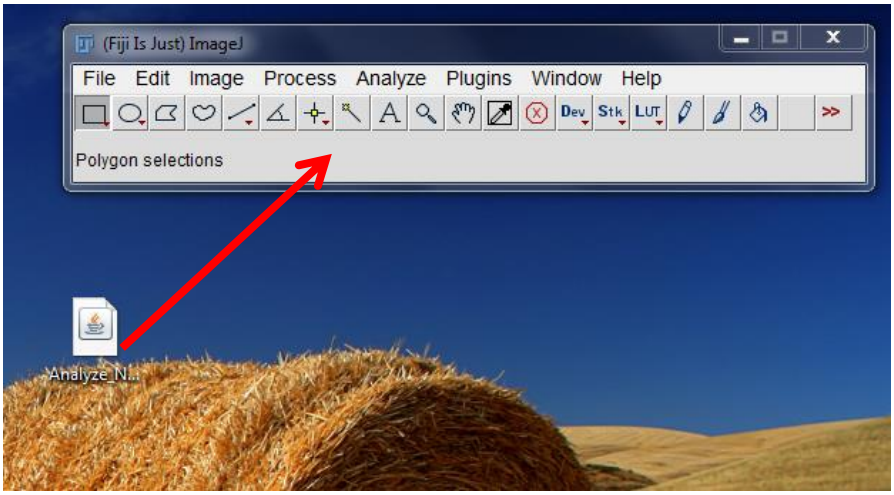

Then Click Save to add the Plug-In to the list.

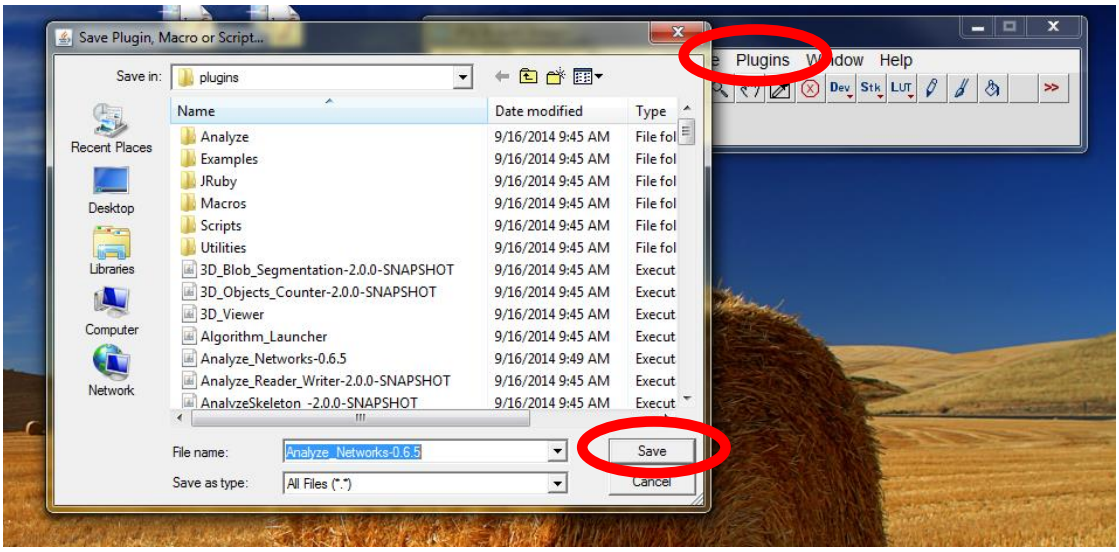

Open the image you want to analyze in FIJI. You can either click File->Open through the dropdown menu or you can drag the image file into the grey bar as in step 1.

Create an ROI by first opening the ROI Manager. Click on Analyze→Tools→ROI Manager.

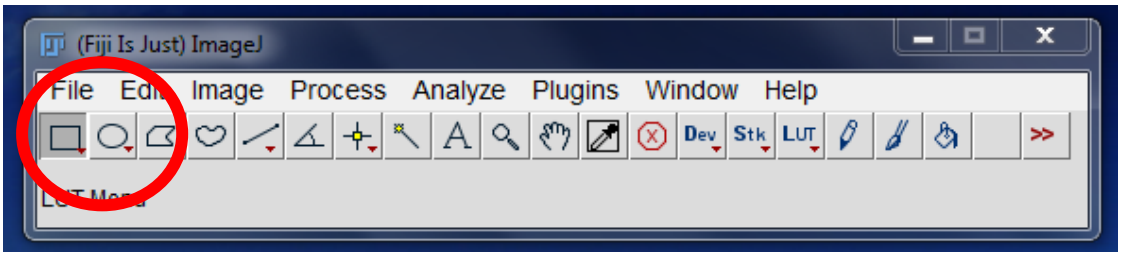

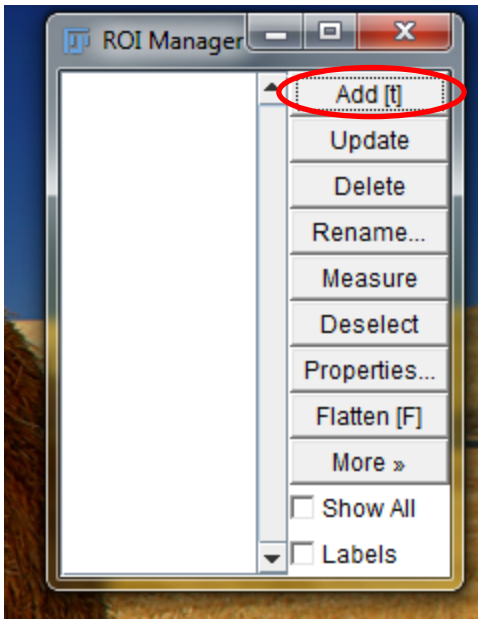

Draw the shape on your image using the rectangle or circle tool.

Click Add in the ROI manager window.

(There is a quirk with the ROI manager—sometimes you have to create a second ROI and Add it to the manager in order to click back and forth between the two in order to get the desired ROI to show up on your image).

Once you have the ROI placed on your image in the desired location, go the Menu and Click Edit->Clear Outside. This will delete the image outside of your ROI (useful for non rectangle shapes). You can also go to Image→Crop if you are using a rectangular ROI.

Then you are ready to run the Plug-In!

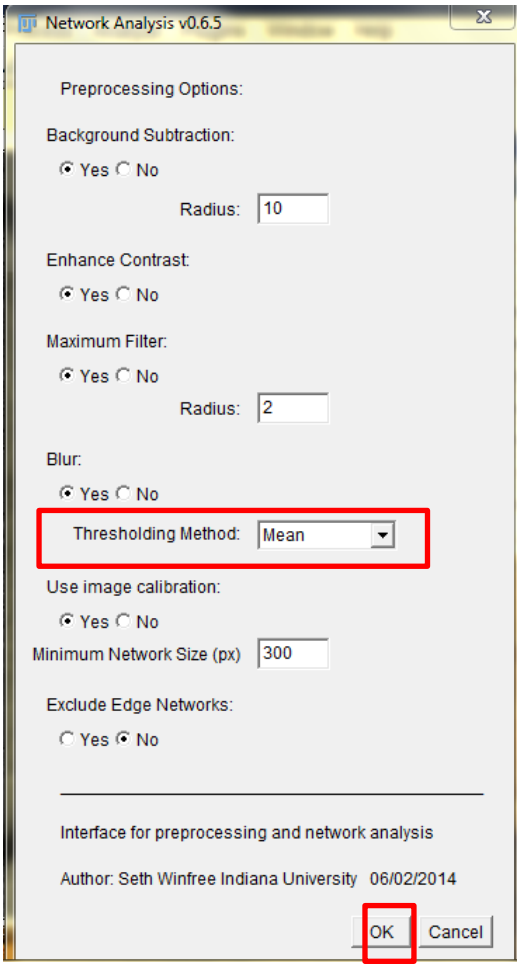

Go to the Menu Bar and click Plug-Ins→Analyze Networks.

This will open up a window with options to alter the settings in the Plugin. You can change the Thresholding method using the drop down arrow which is the most common adjustment. Then Click OK.

Once the Plug-In has finished the analysis, two windows will pop up.

1) Data Table with values
2) Image of the skeleton and mask

On the Data Table, go to Edit→Cut and then paste those values into an excel spreadsheet.

Save the skeleton/mask image as a TIFF.

File→ Save As→TIFF

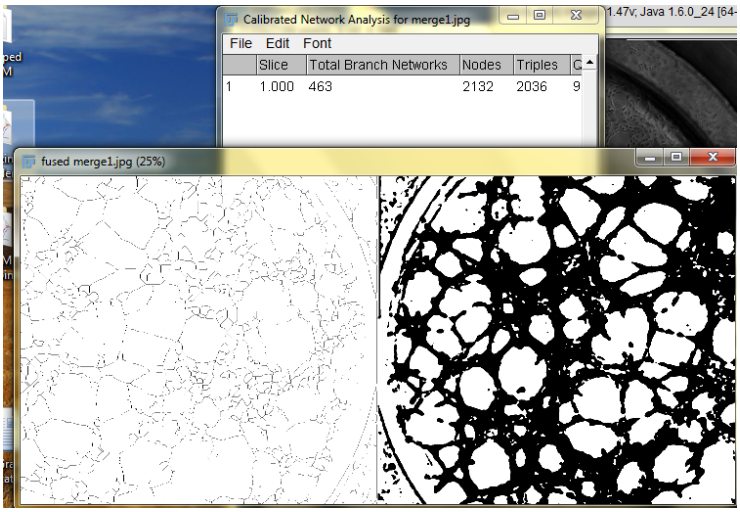

I typically save the corresponding images in the correct subfolders.

Save the cropped image (that you used the ROI to create) by going to File→Save As→TIFF also in the matching subfolder.

REFERENCES

1. Swift MR, Weinstein BM. Arterial–Venous Specification During Development. Circ Res. 2009;104: 576–588. doi:10.1161/CIRCRESAHA.108.188805

2. Carmeliet P, Jain RK. Molecular mechanisms and clinical applications of angiogenesis. Nature. 2011;473: 298. doi:10.1038/nature10144

3. Sewduth R, Santoro MM. “Decoding” Angiogenesis: New Facets Controlling Endothelial Cell Behavior. Front Physiol. 2016;7. doi:10.3389/fphys.2016.00306

4. Tung JJ, Tattersall IW, Kitajewski J. Tips, stalks, tubes: notch-mediated cell fate determination and mechanisms of tubulogenesis during angiogenesis. Cold Spring Harb Perspect Med. 2012;2: a006601. doi:10.1101/cshperspect.a006601

5. Lawson ND, Vogel AM, Weinstein BM. sonic hedgehog and vascular endothelial growth factor act upstream of the Notch pathway during arterial endothelial differentiation. Dev Cell. 2002;3: 127–136.

6. Yoon C-H, Choi Y-E, Koh S-J, Choi J-I, Park Y-B, Kim H-S. High glucose-induced jagged 1 in endothelial cells disturbs notch signaling for angiogenesis: a novel mechanism of diabetic vasculopathy. J Mol Cell Cardiol. 2014;69: 52–66. doi:10.1016/j.yjmcc.2013.12.006

7. Suchting S, Freitas C, le Noble F, Benedito R, Bréant C, Duarte A, et al. The Notch ligand Delta-like 4 negatively regulates endothelial tip cell formation and vessel branching. Proc Natl Acad Sci U S A. 2007;104: 3225–3230. doi:10.1073/pnas.0611177104

8. Hellström M, Phng L-K, Hofmann JJ, Wallgard E, Coultas L, Lindblom P, et al. Dll4 signalling through Notch1 regulates formation of tip cells during angiogenesis. Nature. 2007;445: 776–780. doi:10.1038/nature05571

9. Bozkulak EC, Weinmaster G. Selective use of ADAM10 and ADAM17 in activation of Notch1 signaling. Mol Cell Biol. 2009;29: 5679–5695. doi:10.1128/MCB.00406-09

10. De Strooper B, Annaert W, Cupers P, Saftig P, Craessaerts K, Mumm JS, et al. A presenilin-1-dependent gamma-secretase-like protease mediates release of Notch intracellular domain. Nature. 1999;398: 518–522. doi:10.1038/19083

11. Henderson AM, Wang SJ, Taylor AC, Aitkenhead M, Hughes CC. The basic helix-loop-helix transcription factor HESR1 regulates endothelial cell tube formation. J Biol Chem. 2001;276: 6169–6176. doi:10.1074/jbc.M008506200

12. Jakobsson L, Franco CA, Bentley K, Collins RT, Ponsioen B, Aspalter IM, et al. Endothelial cells dynamically compete for the tip cell position during angiogenic sprouting. Nat Cell Biol. 2010;12: 943–953. doi:10.1038/ncb2103

13. Funahashi Y, Shawber CJ, Vorontchikhina M, Sharma A, Outtz HH, Kitajewski J. Notch regulates the angiogenic response via induction of VEGFR-1. J Angiogenesis Res. 2010;2: 3. doi:10.1186/2040-2384-2-3

14. Williams CK, Li J-L, Murga M, Harris AL, Tosato G. Up-regulation of the Notch ligand Delta-like 4 inhibits VEGF-induced endothelial cell function. Blood. 2006;107: 931–939. doi:10.1182/blood-2005-03-1000

15. Gerhardt H, Golding M, Fruttiger M, Ruhrberg C, Lundkvist A, Abramsson A, et al. VEGF guides angiogenic sprouting utilizing endothelial tip cell filopodia. J Cell Biol. 2003;161: 1163–1177. doi:10.1083/jcb.200302047

16. Sahara M, Hansson EM, Wernet O, Lui KO, Später D, Chien KR. Manipulation of a VEGF-Notch signaling circuit drives formation of functional vascular endothelial progenitors from human pluripotent stem cells. Cell Res. 2014;24: 820–841. doi:10.1038/cr.2014.59

17. Ingram DA, Mead LE, Moore DB, Woodard W, Fenoglio A, Yoder MC. Vessel wall-derived endothelial cells rapidly proliferate because they contain a complete hierarchy of endothelial progenitor cells. Blood. 2005;105: 2783–2786. doi:10.1182/blood-2004-08-3057

18. Asahara T. Cell therapy and gene therapy using endothelial progenitor cells for vascular regeneration. Handb Exp Pharmacol. 2007; 181–194. doi:10.1007/978-3-540-68976-8_8

19. Georgescu A. Vascular dysfunction in diabetes: The endothelial progenitor cells as new therapeutic strategy. World J Diabetes. 2011;2: 92–97. doi:10.4239/wjd.v2.i6.92

20. Kirton JP, Xu Q. Endothelial precursors in vascular repair. Microvasc Res. 2010;79: 193–199. doi:10.1016/j.mvr.2010.02.009

21. Vasa M, Fichtlscherer S, Aicher A, Adler K, Urbich C, Martin H, et al. Number and migratory activity of circulating endothelial progenitor cells inversely correlate with risk factors for coronary artery disease. Circ Res. 2001;89: E1-7.

22. Watt SM, Athanassopoulos A, Harris AL, Tsaknakis G. Human endothelial stem/progenitor cells, angiogenic factors and vascular repair. J R Soc Interface. 2010;7 Suppl 6: S731-751. doi:10.1098/rsif.2010.0377.focus

23. Asahara T, Murohara T, Sullivan A, Silver M, Zee R van der, Li T, et al. Isolation of Putative Progenitor Endothelial Cells for Angiogenesis. Science. 1997;275: 964–966. doi:10.1126/science.275.5302.964

24. Critser PJ, Yoder MC. Endothelial colony-forming cell role in neoangiogenesis and tissue repair. Curr Opin Organ Transplant. 2010;15: 68–72. doi:10.1097/MOT.0b013e32833454b5

25. Basile DP, Yoder MC. Circulating and tissue resident endothelial progenitor cells. J Cell Physiol. 2014;229: 10–16. doi:10.1002/jcp.24423

26. Prater DN, Case J, Ingram DA, Yoder MC. Working hypothesis to redefine endothelial progenitor cells. Leukemia. 2007;21: 1141–1149. doi:10.1038/sj.leu.2404676

27. Yoder MC. Endothelial progenitor cell: A blood cell by many other names may serve similar functions. J Mol Med Berl Ger. 2013;91: 285–295. doi:10.1007/s00109-013-1002-8

28. Rafii S, Lyden D. Therapeutic stem and progenitor cell transplantation for organ vascularization and regeneration. Nat Med. 2003;9: 702–712. doi:10.1038/nm0603-702

29. Mead LE, Prater D, Yoder MC, Ingram DA. Isolation and characterization of endothelial progenitor cells from human blood. Curr Protoc Stem Cell Biol. 2008;Chapter 2: Unit 2C.1. doi:10.1002/9780470151808.sc02c01s6

30. Yoder MC. Human Endothelial Progenitor Cells. Cold Spring Harb Perspect Med. 2012;2: a006692. doi:10.1101/cshperspect.a006692

31. Ingram DA, Mead LE, Tanaka H, Meade V, Fenoglio A, Mortell K, et al. Identification of a novel hierarchy of endothelial progenitor cells using human peripheral and umbilical cord blood. Blood. 2004;104: 2752–2760. doi:10.1182/blood-2004-04-1396

32. Yoder MC, Mead LE, Prater D, Krier TR, Mroueh KN, Li F, et al. Redefining endothelial progenitor cells via clonal analysis and hematopoietic stem/progenitor cell principals. Blood. 2007;109: 1801–1809. doi:10.1182/blood-2006-08-043471

33. Mund JA, Estes ML, Yoder MC, Ingram DA, Case J. Flow cytometric identification and functional characterization of immature and mature circulating endothelial cells. Arterioscler Thromb Vasc Biol. 2012;32: 1045–1053. doi:10.1161/ATVBAHA.111.244210

34. Yoder MC. Is endothelium the origin of endothelial progenitor cells? Arterioscler Thromb Vasc Biol. 2010;30: 1094–1103. doi:10.1161/ATVBAHA.109.191635

35. Yoder MC. Progenitor cells in the pulmonary circulation. Proc Am Thorac Soc. 2011;8: 466–470. doi:10.1513/pats.201101-006MW

36. Prasain N, Meador JL, Yoder MC. Phenotypic and Functional Characterization of Endothelial Colony Forming Cells Derived from Human Umbilical Cord Blood. J Vis Exp JoVE. 2012; doi:10.3791/3872

37. Javed MJ, Mead LE, Prater D, Bessler WK, Foster D, Case J, et al. Endothelial colony forming cells and mesenchymal stem cells are enriched at different gestational ages in human umbilical cord blood. Pediatr Res. 2008;64: 68–73. doi:10.1203/PDR.0b013e31817445e9

38. Ingram DA, Mead LE, Tanaka H, Meade V, Fenoglio A, Mortell K, et al. Identification of a novel hierarchy of endothelial progenitor cells using human peripheral and umbilical cord blood. Blood. 2004;104: 2752–2760. doi:10.1182/blood-2004-04-1396

39. Critser P, Kreger S, Voytik-Harbin S, Yoder M. Collagen matrix physical properties modulate endothelial colony forming cell derived vessels in vivo. Microvasc Res. 2010;80: 23–30. doi:10.1016/j.mvr.2010.03.001

40. Melero-Martin JM, Obaldia MED, Kang S-Y, Khan ZA, Yuan L, Oettgen P, et al. Engineering Robust and Functional Vascular Networks In Vivo With Human Adult and Cord Blood–Derived Progenitor Cells. Circ Res. 2008;103: 194–202. doi:10.1161/CIRCRESAHA.108.178590

41. Melero-Martin JM, Khan ZA, Picard A, Wu X, Paruchuri S, Bischoff J. In vivo vasculogenic potential of human blood-derived endothelial progenitor cells. Blood. 2007;109: 4761–4768. doi:10.1182/blood-2006-12-062471

42. Critser PJ, Voytik-Harbin SL, Yoder MC. Isolating and defining cells to engineer human blood vessels. Cell Prolif. 2011;44: 15–21. doi:10.1111/j.1365-2184.2010.00719.x

43. Solomon I, O'Reilly M, Ionescu L, Alphonse RS, Rajabali S, Zhong S, et al. Functional Differences Between Placental Micro- and Macrovascular Endothelial Colony-Forming Cells. Stem Cells Transl Med. 2016;5: 291–300. doi:10.5966/sctm.2014-0162

44. Au P, Daheron LM, Duda DG, Cohen KS, Tyrrell JA, Lanning RM, et al. Differential in vivo potential of endothelial progenitor cells from human umbilical cord blood and adult peripheral blood to form functional long-lasting vessels. Blood. 2008;111: 1302–1305. doi:10.1182/blood-2007-06-094318

45. Broxmeyer HE, Douglas GW, Hangoc G, Cooper S, Bard J, English D, et al. Human umbilical cord blood as a potential source of transplantable hematopoietic stem/progenitor cells. Proc Natl Acad Sci U S A. 1989;86: 3828–3832.

46. Lu L, Xiao M, Shen RN, Grigsby S, Broxmeyer HE. Enrichment, characterization, and responsiveness of single primitive CD34 human umbilical cord blood hematopoietic progenitors with high proliferative and replating potential. Blood. 1993;81: 41–48.

47. Broxmeyer HE. Biology of cord blood cells and future prospects for enhanced clinical benefit. Cytotherapy. 2005;7: 209–218. doi:10.1080/14653240510027190

48. Broxmeyer HE, Hangoc G, Cooper S, Ribeiro RC, Graves V, Yoder M, et al. Growth characteristics and expansion of human umbilical cord blood and estimation of its potential for transplantation in adults. Proc Natl Acad Sci U S A. 1992;89: 4109–4113.

49. Cardoso AA, Li ML, Batard P, Hatzfeld A, Brown EL, Levesque JP, et al. Release from quiescence of CD34+ CD38- human umbilical cord blood cells reveals their potentiality to engraft adults. Proc Natl Acad Sci U S A. 1993;90: 8707–8711.

50. Carow CE, Hangoc G, Broxmeyer HE. Human multipotential progenitor cells (CFU-GEMM) have extensive replating capacity for secondary CFU-GEMM: an effect enhanced by cord blood plasma. Blood. 1993;81: 942–949.

51. Barker DJ, Winter PD, Osmond C, Margetts B, Simmonds SJ. Weight in infancy and death from ischaemic heart disease. Lancet Lond Engl. 1989;2: 577–580.

52. Calkins K, Devaskar SU. Fetal origins of adult disease. Curr Probl Pediatr Adolesc Health Care. 2011;41: 158–176. doi:10.1016/j.cppeds.2011.01.001

53. Mercuro G, Bassareo PP, Flore G, Fanos V, Dentamaro I, Scicchitano P, et al. Prematurity and low weight at birth as new conditions predisposing to an increased cardiovascular risk. Eur J Prev Cardiol. 2013;20: 357–367. doi:10.1177/2047487312437058

54. Pettitt DJ, Aleck KA, Baird HR, Carraher MJ, Bennett PH, Knowler WC. Congenital susceptibility to NIDDM. Role of intrauterine environment. Diabetes. 1988;37: 622–628.

55. WHO | Diabetes. In: WHO [Internet]. [cited 11 Apr 2017]. Available: http://www.who.int/topics/diabetes_mellitus/en/

56. Hay WW. Placental-Fetal Glucose Exchange and Fetal Glucose Metabolism. Trans Am Clin Climatol Assoc. 2006;117: 321–340.

57. Pettitt DJ, Bennett PH, Saad MF, Charles MA, Nelson RG, Knowler WC. Abnormal Glucose Tolerance During Pregnancy in Pima Indian Women: Long-Term Effects on Offspring. Diabetes. 1991;40: 126–130. doi:10.2337/diab.40.2.S126

58. Pettitt DJ, Nelson RG, Saad MF, Bennett PH, Knowler WC. Diabetes and Obesity in the Offspring of Pima Indian Women With Diabetes During Pregnancy. Diabetes Care. 1993;16: 310–314. doi:10.2337/diacare.16.1.310

59. Absence of glutamic acid decarboxylase antibodies in Pima Indian children with diabetes mellitus. Diabetologia. 1999;42: 1265–1266. doi:10.1007/s001250051303

60. Bunt JC, Tataranni PA, Salbe AD. Intrauterine exposure to diabetes is a determinant of hemoglobin A(1)c and systolic blood pressure in pima Indian children. J Clin Endocrinol Metab. 2005;90: 3225–3229. doi:10.1210/jc.2005-0007

61. Franks PW, Looker HC, Kobes S, Touger L, Tataranni PA, Hanson RL, et al. Gestational glucose tolerance and risk of type 2 diabetes in young Pima Indian offspring. Diabetes. 2006;55: 460–465.

62. Krishnaveni GV, Veena SR, Hill JC, Kehoe S, Karat SC, Fall CHD. Intrauterine exposure to maternal diabetes is associated with higher adiposity and insulin resistance and clustering of cardiovascular risk markers in Indian children. Diabetes Care. 2010;33: 402–404. doi:10.2337/dc09-1393

63. Cho NH, Silverman BL, Rizzo TA, Metzger BE. Correlations between the intrauterine metabolic environment and blood pressure in adolescent offspring of diabetic mothers. J Pediatr. 2000;136: 587–592. doi:10.1067/mpd.2000.105129

64. Crume TL, Ogden L, Daniels S, Hamman RF, Norris JM, Dabelea D. The impact of in utero exposure to diabetes on childhood body mass index growth trajectories: the EPOCH study. J Pediatr. 2011;158: 941–946. doi:10.1016/j.jpeds.2010.12.007

65. Dabelea D, Hanson RL, Lindsay RS, Pettitt DJ, Imperatore G, Gabir MM, et al. Intrauterine exposure to diabetes conveys risks for type 2 diabetes and obesity: a study of discordant sibships. Diabetes. 2000;49: 2208–2211.

66. Boney CM, Verma A, Tucker R, Vohr BR. Metabolic syndrome in childhood: association with birth weight, maternal obesity, and gestational diabetes mellitus. Pediatrics. 2005;115: e290-296. doi:10.1542/peds.2004-1808

67. Lawlor DA, Lichtenstein P, Långström N. Association of maternal diabetes mellitus in pregnancy with offspring adiposity into early adulthood: sibling study in a prospective cohort of 280,866 men from 248,293 families. Circulation. 2011;123: 258–265. doi:10.1161/CIRCULATIONAHA.110.980169

68. WHO | Obesity and overweight. In: WHO [Internet]. [cited 19 Mar 2017]. Available: http://www.who.int/mediacentre/factsheets/fs311/en/

69. Ogden C, Carroll M. Prevalence of Obesity Among Children and Adolescents: United States, Trends 1963-1965 Through 2007-2008 [Internet]. CDC National Center for Health Statistics; 2010 Jun. Available: https://www.cdc.gov/nchs/data/hestat/obesity_child_07_08/obesity_child_07_08.htm

70. Galtier-Dereure F, Boegner C, Bringer J. Obesity and pregnancy: complications and cost. Am J Clin Nutr. 2000;71: 1242S–8S.

71. Guelinckx I, Devlieger R, Beckers K, Vansant G. Maternal obesity: pregnancy complications, gestational weight gain and nutrition. Obes Rev. 2008;9: 140–150. doi:10.1111/j.1467-789X.2007.00464.x

72. Mathews TJ, Hamilton BE. Mean Age of Mothers is on teh Rise: United States, 2000-2014. CDC National Center for Health Statistics; 2016 Jan. Report No.: 232.

73. Getahun D, Nath C, Ananth CV, Chavez MR, Smulian JC. Gestational diabetes in the United States: temporal trends 1989 through 2004. Am J Obstet Gynecol. 2008;198: 525.e1-525.e5. doi:10.1016/j.ajog.2007.11.017

74. Chu SY, Callaghan WM, Kim SY, Schmid CH, Lau J, England LJ, et al. Maternal Obesity and Risk of Gestational Diabetes Mellitus. Diabetes Care. 2007;30: 2070–2076. doi:10.2337/dc06-2559a

75. Eisenberg Center at Oregon Health & Science University. Gestational Diabetes: A Guide for Pregnant Women. Comparative Effectiveness Review Summary Guides for Consumers. Rockville (MD): Agency for Healthcare Research and Quality (US); 2005. Available: http://www.ncbi.nlm.nih.gov/books/NBK45608/

76. DeSisto CL, Kim SY, Sharma AJ. Prevalence estimates of gestational diabetes mellitus in the United States, Pregnancy Risk Assessment Monitoring System

(PRAMS), 2007-2010. Prev Chronic Dis. 2014;11: E104. doi:10.5888/pcd11.130415

77. Simmons D. Diabetes and obesity in pregnancy. Best Pract Res Clin Obstet Gynaecol. 2011;25: 25–36. doi:10.1016/j.bpobgyn.2010.10.006

78. Ingram DA, Lien IZ, Mead LE, Estes M, Prater DN, Derr-Yellin E, et al. In vitro hyperglycemia or a diabetic intrauterine environment reduces neonatal endothelial colony-forming cell numbers and function. Diabetes. 2008;57: 724–731. doi:10.2337/db07-1507

79. Acosta JC, Haas DM, Saha CK, Dimeglio LA, Ingram DA, Haneline LS. Gestational diabetes mellitus alters maternal and neonatal circulating endothelial progenitor cell subsets. Am J Obstet Gynecol. 2011;204: 254.e8-254.e15. doi:10.1016/j.ajog.2010.10.913

80. Blue EK, DiGiuseppe R, Derr-Yellin E, Acosta JC, Pay SL, Hanenberg H, et al. Gestational diabetes induces alterations in the function of neonatal endothelial colony-forming cells. Pediatr Res. 2014;75: 266–272. doi:10.1038/pr.2013.224

81. Gohn CR, Blue EK, Sheehan BM, Varberg KM, Haneline LS. Mesenchyme Homeobox 2 Enhances Migration of Endothelial Colony Forming Cells Exposed to Intrauterine Diabetes Mellitus. J Cell Physiol. 2016; doi:10.1002/jcp.25734

82. Blue EK, Sheehan BM, Nuss ZV, Boyle FA, Hocutt CM, Gohn CR, et al. Epigenetic Regulation of Placenta-Specific 8 Contributes to Altered Function of Endothelial Colony-Forming Cells Exposed to Intrauterine Gestational Diabetes Mellitus. Diabetes. 2015;64: 2664–2675. doi:10.2337/db14-1709

83. Jones EAV, Noble F le, Eichmann A. What Determines Blood Vessel Structure? Genetic Prespecification vs. Hemodynamics. Physiology. 2006;21: 388–395. doi:10.1152/physiol.00020.2006

84. del Rosario MC, Ossowski V, Knowler WC, Bogardus C, Baier LJ, Hanson RL. Potential epigenetic dysregulation of genes associated with MODY and type 2 diabetes in humans exposed to a diabetic intrauterine environment: an analysis of genome-wide DNA methylation. Metabolism. 2014;63: 654–660. doi:10.1016/j.metabol.2014.01.007

85. Nomura Y, Lambertini L, Rialdi A, Lee M, Mystal EY, Grabie M, et al. Global Methylation in the Placenta and Umbilical Cord Blood From Pregnancies With Maternal Gestational Diabetes, Preeclampsia, and Obesity. Reprod Sci. 2014;21: 131. doi:10.1177/1933719113492206

86. Hajj NE, Pliushch G, Schneider E, Dittrich M, Müller T, Korenkov M, et al. Metabolic Programming of MEST DNA Methylation by Intrauterine Exposure to Gestational Diabetes Mellitus. Diabetes. 2013;62: 1320. doi:10.2337/db12-0289

87. Zilbauer M, Rayner TF, Clark C, Coffey AJ, Joyce CJ, Palta P, et al. Genome-wide methylation analyses of primary human leukocyte subsets identifies functionally

important cell-type–specific hypomethylated regions. Blood. 2013;122: e52–e60. doi:10.1182/blood-2013-05-503201

88. Lees-Miller JP, Heeley DH, Smillie LB, Kay CM. Isolation and characterization of an abundant and novel 22-kDa protein (SM22) from chicken gizzard smooth muscle. J Biol Chem. 1987;262: 2988–2993.

89. Shapland C, Hsuan JJ, Totty NF, Lawson D. Purification and properties of transgelin: a transformation and shape change sensitive actin-gelling protein. J Cell Biol. 1993;121: 1065–1073.

90. Lawson D, Harrison M, Shapland C. Fibroblast transgelin and smooth muscle SM22alpha are the same protein, the expression of which is down-regulated in many cell lines. Cell Motil Cytoskeleton. 1997;38: 250–257. doi:10.1002/(SICI)1097-0169(1997)38:3<250::AID-CM3>3.0.CO;2-9

91. Radaelli T, Varastehpour A, Catalano P, Hauguel-de Mouzon S. Gestational diabetes induces placental genes for chronic stress and inflammatory pathways. Diabetes. 2003;52: 2951–2958.

92. Wright CS, Rifas-Shiman SL, Rich-Edwards JW, Taveras EM, Gillman MW, Oken E. Intrauterine exposure to gestational diabetes, child adiposity, and blood pressure. Am J Hypertens. 2009;22: 215–220. doi:10.1038/ajh.2008.326

93. Li-Hua Dong PL and MH. Roles of SM22α in Cellular Plasticity and Vascular Diseases. In: http://www.eurekaselect.com [Internet]. [cited 19 Mar 2017]. Available: http://www.eurekaselect.com/104647/article

94. Stanier P, Abu-Hayyeh S, Murdoch JN, Eddleston J, Copp AJ. ParalogousSm22α (Tagln) Genes Map to Mouse Chromosomes 1 and 9: Further Evidence for a Paralogous Relationship. Genomics. 1998;51: 144–147. doi:10.1006/geno.1998.5381

95. Ren W-Z, Ng GYK, Wang R-X, Wu PH, O'Dowd BF, Osmond DH, et al. The identification of NP25: a novel protein that is differentially expressed by neuronal subpopulations. Mol Brain Res. 1994;22: 173–185. doi:10.1016/0169-328X(94)90045-0

96. Li S, Sims S, Jiao Y, Chow LH, Pickering JG. Evidence from a novel human cell clone that adult vascular smooth muscle cells can convert reversibly between noncontractile and contractile phenotypes. Circ Res. 1999;85: 338–348.

97. Shanahan CM, Weissberg PL. Smooth Muscle Cell Heterogeneity. Arterioscler Thromb Vasc Biol. 1998;18: 333–338. doi:10.1161/01.ATV.18.3.333

98. Alexander MR, Owens GK. Epigenetic control of smooth muscle cell differentiation and phenotypic switching in vascular development and disease. Annu Rev Physiol. 2012;74: 13–40. doi:10.1146/annurev-physiol-012110-142315

99. Owens GK. Regulation of differentiation of vascular smooth muscle cells. Physiol Rev. 1995;75: 487–517.

100. Chistiakov DA, Orekhov AN, Bobryshev YV. Vascular smooth muscle cell in atherosclerosis. Acta Physiol Oxf Engl. 2015;214: 33–50. doi:10.1111/apha.12466

101. Vo E, Hanjaya-Putra D, Zha Y, Kusuma S, Gerecht S. Smooth-muscle-like cells derived from human embryonic stem cells support and augment cord-like structures in vitro. Stem Cell Rev. 2010;6: 237–247. doi:10.1007/s12015-010-9144-3

102. Ji H, Atchison L, Chen Z, Chakraborty S, Jung Y, Truskey GA, et al. Transdifferentiation of human endothelial progenitors into smooth muscle cells. Biomaterials. 2016;85: 180–194. doi:10.1016/j.biomaterials.2016.01.066

103. Chiavegato A, Roelofs M, Franch R, Castellucci E, Sarinella F, Sartore S. Differential expression of SM22 isoforms in myofibroblasts and smooth muscle cells from rabbit bladder. J Muscle Res Cell Motil. 1999;20: 133–146.

104. Gimona M, Djinovic-Carugo K, Kranewitter WJ, Winder SJ. Functional plasticity of CH domains. FEBS Lett. 2002;513: 98–106.

105. Gimona M, Kaverina I, Resch GP, Vignal E, Burgstaller G. Calponin repeats regulate actin filament stability and formation of podosomes in smooth muscle cells. Mol Biol Cell. 2003;14: 2482–2491. doi:10.1091/mbc.E02-11-0743

106. Han M, Dong L-H, Zheng B, Shi J-H, Wen J-K, Cheng Y. Smooth muscle 22 alpha maintains the differentiated phenotype of vascular smooth muscle cells by inducing filamentous actin bundling. Life Sci. 2009;84: 394–401. doi:10.1016/j.lfs.2008.11.017

107. Fu Y, Liu HW, Forsythe SM, Kogut P, McConville JF, Halayko AJ, et al. Mutagenesis analysis of human SM22: characterization of actin binding. J Appl Physiol Bethesda Md 1985. 2000;89: 1985–1990.

108. Wen J, Shi J, Zheng B, Meng F, Han M. [The molecular mechanisms of SM22alpha in cytoskeleton remodeling of vascular smooth muscle cells]. Zhongguo Ying Yong Sheng Li Xue Za Zhi Zhongguo Yingyong Shenglixue Zazhi Chin J Appl Physiol. 2008;24: 393–397.

109. Chien S. Effects of Disturbed Flow on Endothelial Cells. Ann Biomed Eng. 2008;36: 554. doi:10.1007/s10439-007-9426-3

110. Xiao Y, Li Y, Han J, Pan Y, Tie L, Li X. Transgelin 2 participates in lovastatin-induced anti-angiogenic effects in endothelial cells through a phosphorylated myosin light chain-related mechanism. PloS One. 2012;7: e46510. doi:10.1371/journal.pone.0046510

111. Nair RR, Solway J, Boyd DD. Expression cloning identifies transgelin (SM22) as a novel repressor of 92-kDa type IV collagenase (MMP-9) expression. J Biol Chem. 2006;281: 26424–26436. doi:10.1074/jbc.M602703200

112. Carpentier G. ImageJ contribution: Angiogenesis Analyzer. 2012 Oct.

113. Crabtree B, Subramanian V. Behavior of endothelial cells on Matrigel and development of a method for a rapid and reproducible in vitro angiogenesis assay. In Vitro Cell Dev Biol Anim. 2007;43: 87–94. doi:10.1007/s11626-007-9012-x

114. Khoo CP, Micklem K, Watt SM. A comparison of methods for quantifying angiogenesis in the Matrigel assay in vitro. Tissue Eng Part C Methods. 2011;17: 895–906. doi:10.1089/ten.TEC.2011.0150

115. Sievert W, Tapio S, Breuninger S, Gaipl U, Andratschke N, Trott K-R, et al. Adhesion molecule expression and function of primary endothelial cells in benign and malignant tissues correlates with proliferation. PloS One. 2014;9: e91808. doi:10.1371/journal.pone.0091808

116. Wang Y, Chen Q, Zhang Z, Jiang F, Meng X, Yan H. Interleukin-10 overexpression improves the function of endothelial progenitor cells stimulated with TNF-α through the activation of the STAT3 signaling pathway. Int J Mol Med. 2015;35: 471–477. doi:10.3892/ijmm.2014.2034

117. Kanehisa M, Goto S. KEGG: Kyoto Encyclopedia of Genes and Genomes. Nucleic Acids Res. 2000;28: 27.

118. Arganda-Carreras I, Fernández-González R, Muñoz-Barrutia A, Ortiz-De-Solorzano C. 3D reconstruction of histological sections: Application to mammary gland tissue. Microsc Res Tech. 2010;73: 1019–1029. doi:10.1002/jemt.20829

119. R Development Core Team. R: a language and environment for statistical computing [Internet]. Vienna, Austria; 2011. Available: http://www.R-project.org/

120. Debnath J, Muthuswamy SK, Brugge JS. Morphogenesis and oncogenesis of MCF-10A mammary epithelial acini grown in three-dimensional basement membrane cultures. Methods San Diego Calif. 2003;30: 256–268.

121. Abcam. Anti-alpha Tubulin antibody (DM1A) [Internet]. 2017. Available: http://www.abcam.com/alpha-tubulin-antibody-dm1a-loading-control-ab7291.html

122. Winfree S, Khan S, Micanovic R, Eadon MT, Kelly KJ, Sutton TA, et al. Quantitative Three-Dimensional Tissue Cytometry to Study Kidney Tissue and Resident Immune Cells. J Am Soc Nephrol. 2017; ASN.2016091027. doi:10.1681/ASN.2016091027

123. Cell Signaling Technology. Phospho-Histone H3 (Ser10) Antibody #9701 [Internet]. 2017. Available: https://www.cellsignal.com/products/primary-antibodies/phospho-histone-h3-ser10-antibody/9701

124. Gavvovidis I, Rost I, Trimborn M, Kaiser FJ, Purps J, Wiek C, et al. A Novel MCPH1 Isoform Complements the Defective Chromosome Condensation of Human MCPH1-Deficient Cells. PLOS ONE. 2012;7: e40387. doi:10.1371/journal.pone.0040387

125. Schindelin J, Arganda-Carreras I, Frise E, Kaynig V, Longair M, Pietzsch T, et al. Fiji: an open-source platform for biological-image analysis. Nat Methods. 2012;9: 676–682. doi:10.1038/nmeth.2019

126. Jacobs CR, Yellowley CE, Davis BR, Zhou Z, Cimbala JM, Donahue HJ. Differential effect of steady versus oscillating flow on bone cells. J Biomech. 1998;31: 969–976. doi:10.1016/S0021-9290(98)00114-6

127. Young SRL, Hum JM, Rodenberg E, Turner CH, Pavalko FM. Non-Overlapping Functions for Pyk2 and FAK in Osteoblasts during Fluid Shear Stress-Induced Mechanotransduction. PLoS ONE. 2011;6. doi:10.1371/journal.pone.0016026

128. Liu ZQ. Scale space approach to directional analysis of images. Appl Opt. 1991;30: 1369–1373.

129. Directionality. In: ImageJ [Internet]. [cited 5 Apr 2017]. Available: https://imagej.net/Directionality

130. Zhang W, Wu Y, Du L, Tang DD, Gunst SJ. Activation of the Arp2/3 complex by N-WASp is required for actin polymerization and contraction in smooth muscle. Am J Physiol - Cell Physiol. 2005;288: C1145–C1160. doi:10.1152/ajpcell.00387.2004

131. Generalized Additive Models: An Introduction with R. In: CRC Press [Internet]. 27 Feb 2006 [cited 13 Mar 2017]. Available: https://www.crcpress.com/Generalized-Additive-Models-An-Introduction-with-R/Wood/p/book/9781584884743

132. Varberg KM, Winfree S, Chu C, Tu W, Blue EK, Gohn CR, et al. Kinetic analyses of vasculogenesis inform mechanistic studies. Am J Physiol Cell Physiol. 2017; ajpcell.00367.2016. doi:10.1152/ajpcell.00367.2016

133. Zon LI. Hematopoiesis: A Developmental Approach. Oxford University Press; 2001.

134. Prasain N, Lee MR, Vemula S, Meador JL, Yoshimoto M, Ferkowicz MJ, et al. Differentiation of human pluripotent stem cells to cells similar to cord-blood endothelial colony-forming cells. Nat Biotechnol. 2014;32: 1151–1157. doi:10.1038/nbt.3048

135. Handsley MM, Edwards DR. Metalloproteinases and their inhibitors in tumor angiogenesis. Int J Cancer. 2005;115: 849–860. doi:10.1002/ijc.20945

136. Cooper GM. Actin, Myosin, and Cell Movement. 2000; Available: https://www.ncbi.nlm.nih.gov/books/NBK9961/

137. Amano M, Ito M, Kimura K, Fukata Y, Chihara K, Nakano T, et al. Phosphorylation and activation of myosin by Rho-associated kinase (Rho-kinase). J Biol Chem. 1996;271: 20246–20249.

138. Ramachandran C, Patil RV, Combrink K, Sharif NA, Srinivas SP. Rho-Rho kinase pathway in the actomyosin contraction and cell-matrix adhesion in immortalized human trabecular meshwork cells. Mol Vis. 2011;17: 1877–1890.

139. Ishizaki T, Uehata M, Tamechika I, Keel J, Nonomura K, Maekawa M, et al. Pharmacological properties of Y-27632, a specific inhibitor of rho-associated kinases. Mol Pharmacol. 2000;57: 976–983.

140. Haile Y, Nakhaei-Nejad M, Boakye PA, Baker G, Smith PA, Murray AG, et al. Reprogramming of HUVECs into Induced Pluripotent Stem Cells (HiPSCs), Generation and Characterization of HiPSC-Derived Neurons and Astrocytes. PLoS ONE. 2015;10. doi:10.1371/journal.pone.0119617

141. Casella JF, Flanagan MD, Lin S. Cytochalasin D inhibits actin polymerization and induces depolymerization of actin filaments formed during platelet shape change. Nature. 1981;293: 302–305. doi:10.1038/293302a0

142. Bray M-A, Carpenter AE. CellProfiler Tracer: exploring and validating high-throughput, time-lapse microscopy image data. BMC Bioinformatics. 2015;16: 368. doi:10.1186/s12859-015-0759-x

143. Allier CP, Vinjimore Kesavan S, Coutard J-G, Cioni O, Momey F, Navarro F, et al. Video lensfree microscopy of 2D and 3D culture of cells. 2014. p. 89471H–89471H–9. doi:10.1117/12.2038098

144. Carpenter AE, Jones TR, Lamprecht MR, Clarke C, Kang IH, Friman O, et al. CellProfiler: image analysis software for identifying and quantifying cell phenotypes. Genome Biol. 2006;7: R100. doi:10.1186/gb-2006-7-10-r100

145. WimTube [Internet]. 2014. Available: https://www.wimasis.com/en/products/13/WinTube

146. Simons M, Alitalo K, Annex BH, Augustin HG, Beam C, Berk BC, et al. State-of-the-Art Methods for Evaluation of Angiogenesis and Tissue Vascularization: A Scientific Statement From the American Heart Association. Circ Res. 2015;116: e99-132. doi:10.1161/RES.0000000000000054

147. Davies PF. How Do Vascular Endothelial Cells Respond to Flow? Physiology. 1989;4: 22–25.

148. Steward R, Tambe D, Hardin CC, Krishnan R, Fredberg JJ. Fluid shear, intercellular stress, and endothelial cell alignment. Am J Physiol Cell Physiol. 2015;308: C657-664. doi:10.1152/ajpcell.00363.2014

149. Koskinen M, Hotulainen P. Measuring F-actin properties in dendritic spines. Front Neuroanat. 2014;8. doi:10.3389/fnana.2014.00074

150. Hamilton SJ, Chew GT, Watts GF. Therapeutic regulation of endothelial dysfunction in type 2 diabetes mellitus. Diab Vasc Dis Res. 2007;4: 89–102. doi:10.3132/dvdr.2007.026

151. Sawada N, Jiang A, Takizawa F, Safdar A, Manika A, Tesmenitsky Y, et al. Endothelial PGC-1α mediates vascular dysfunction in diabetes. Cell Metab. 2014;19: 246–258. doi:10.1016/j.cmet.2013.12.014

152. Cao L, Arany PR, Kim J, Rivera-Feliciano J, Wang Y-S, He Z, et al. Modulating Notch signaling to enhance neovascularization and reperfusion in diabetic mice. Biomaterials. 2010;31: 9048–9056. doi:10.1016/j.biomaterials.2010.08.002

153. Pajvani UB, Shawber CJ, Samuel VT, Birkenfeld AL, Shulman GI, Kitajewski J, et al. Inhibition of Notch signaling ameliorates insulin resistance in a FoxO1-dependent manner. Nat Med. 2011;17: 961–967. doi:10.1038/nm.2378

154. Lin C-L, Wang F-S, Hsu Y-C, Chen C-N, Tseng M-J, Saleem MA, et al. Modulation of notch-1 signaling alleviates vascular endothelial growth factor-mediated diabetic nephropathy. Diabetes. 2010;59: 1915–1925. doi:10.2337/db09-0663

155. Sasso FC, Torella D, Carbonara O, Ellison GM, Torella M, Scardone M, et al. Increased vascular endothelial growth factor expression but impaired vascular endothelial growth factor receptor signaling in the myocardium of type 2 diabetic patients with chronic coronary heart disease. J Am Coll Cardiol. 2005;46: 827–834. doi:10.1016/j.jacc.2005.06.007

156. Schwartz MA. Integrins and Extracellular Matrix in Mechanotransduction. Cold Spring Harb Perspect Biol. 2010;2. doi:10.1101/cshperspect.a005066

157. Estrach S, Cailleteau L, Franco CA, Gerhardt H, Stefani C, Lemichez E, et al. Laminin-binding integrins induce Dll4 expression and Notch signaling in endothelial cells. Circ Res. 2011;109: 172–182. doi:10.1161/CIRCRESAHA.111.240622

158. Collett JA, Mehrotra P, Crone A, Shelley WC, Yoder MC, Basile DP. Endothelial colony forming cells ameliorate endothelial dysfunction via secreted factors following ischemia-reperfusion injury. Am J Physiol - Ren Physiol. 2017; ajprenal.00643.2016. doi:10.1152/ajprenal.00643.2016

159. Kristiansen S, Jørgensen LM, Guldberg P, Sölétormos G. Aberrantly methylated DNA as a biomarker in breast cancer. Int J Biol Markers. 2013;28: 141–150. doi:10.5301/jbm.5000009

160. Momparler RL, Côté S, Momparler LF, Idaghdour Y. Epigenetic therapy of acute myeloid leukemia using 5-aza-2'-deoxycytidine (decitabine) in combination with inhibitors of histone methylation and deacetylation. Clin Epigenetics. 2014;6: 19. doi:10.1186/1868-7083-6-19

161. Sayar N, Karahan G, Konu O, Bozkurt B, Bozdogan O, Yulug IG. Transgelin gene is frequently downregulated by promoter DNA hypermethylation in breast cancer. Clin Epigenetics. 2015;7: 104. doi:10.1186/s13148-015-0138-5

162. Shields JM, Rogers-Graham K, Der CJ. Loss of transgelin in breast and colon tumors and in RIE-1 cells by Ras deregulation of gene expression through Raf-independent pathways. J Biol Chem. 2002;277: 9790–9799. doi:10.1074/jbc.M110086200

163. Wulfkuhle JD, Sgroi DC, Krutzsch H, McLean K, McGarvey K, Knowlton M, et al. Proteomics of human breast ductal carcinoma in situ. Cancer Res. 2002;62: 6740–6749.

164. Yang Z, Chang Y-J, Miyamoto H, Ni J, Niu Y, Chen Z, et al. Transgelin functions as a suppressor via inhibition of ARA54-enhanced androgen receptor transactivation and prostate cancer cell growth. Mol Endocrinol Baltim Md. 2007;21: 343–358. doi:10.1210/me.2006-0104

165. Li Q, Shi R, Wang Y, Niu X. TAGLN suppresses proliferation and invasion, and induces apoptosis of colorectal carcinoma cells. Tumour Biol J Int Soc Oncodevelopmental Biol Med. 2013;34: 505–513. doi:10.1007/s13277-012-0575-0

166. Prasad PD, Stanton J-AL, Assinder SJ. Expression of the actin-associated protein transgelin (SM22) is decreased in prostate cancer. Cell Tissue Res. 2010;339: 337–347. doi:10.1007/s00441-009-0902-y

167. Lin Y, Buckhaults PJ, Lee JR, Xiong H, Farrell C, Podolsky RH, et al. Association of the actin-binding protein transgelin with lymph node metastasis in human colorectal cancer. Neoplasia N Y N. 2009;11: 864–873.

168. Yeo M, Park HJ, Kim D-K, Kim YB, Cheong JY, Lee KJ, et al. Loss of SM22 is a characteristic signature of colon carcinogenesis and its restoration suppresses colon tumorigenicity in vivo and in vitro. Cancer. 2010;116: 2581–2589. doi:10.1002/cncr.25003

169. Zhang Y, Ye Y, Shen D, Jiang K, Zhang H, Sun W, et al. Identification of transgelin-2 as a biomarker of colorectal cancer by laser capture microdissection and quantitative proteome analysis. Cancer Sci. 2010;101: 523–529. doi:10.1111/j.1349-7006.2009.01424.x

170. Rho J-H, Roehrl MHA, Wang JY. Tissue proteomics reveals differential and compartment-specific expression of the homologs transgelin and transgelin-2 in lung adenocarcinoma and its stroma. J Proteome Res. 2009;8: 5610–5618. doi:10.1021/pr900705r

171. Dvorakova M, Nenutil R, Bouchal P. Transgelins, cytoskeletal proteins implicated in different aspects of cancer development. Expert Rev Proteomics. 2014;11: 149–165. doi:10.1586/14789450.2014.860358

172. Thompson O, Moghraby JS, Ayscough KR, Winder SJ. Depletion of the actin bundling protein SM22/transgelin increases actin dynamics and enhances the tumourigenic phenotypes of cells. BMC Cell Biol. 2012;13: 1. doi:10.1186/1471-2121-13-1

173. Assinder SJ, Stanton J-AL, Prasad PD. Transgelin: an actin-binding protein and tumour suppressor. Int J Biochem Cell Biol. 2009;41: 482–486. doi:10.1016/j.biocel.2008.02.011

174. Ren F, Tang R, Zhang X, Madushi WM, Luo D, Dang Y, et al. Overexpression of MMP Family Members Functions as Prognostic Biomarker for Breast Cancer Patients: A Systematic Review and Meta-Analysis. PLOS ONE. 2015;10: e0135544. doi:10.1371/journal.pone.0135544

175. Yoder MC. Differentiation of pluripotent stem cells into endothelial cells. Curr Opin Hematol. 2015;22: 252–257. doi:10.1097/MOH.0000000000000140

176. Broxmeyer HE, Lee M-R, Hangoc G, Cooper S, Prasain N, Kim Y-J, et al. Hematopoietic stem/progenitor cells, generation of induced pluripotent stem cells, and isolation of endothelial progenitors from 21- to 23.5-year cryopreserved cord blood. Blood. 2011;117: 4773–4777. doi:10.1182/blood-2011-01-330514

177. Alphonse RS, Vadivel A, Zhong S, McConaghy S, Ohls R, Yoder MC, et al. The isolation and culture of endothelial colony-forming cells from human and rat lungs. Nat Protoc. 2015;10: 1697–1708. doi:10.1038/nprot.2015.107

178. Avogaro A, Albiero M, Menegazzo L, de Kreutzenberg S, Fadini GP. Endothelial dysfunction in diabetes: the role of reparatory mechanisms. Diabetes Care. 2011;34 Suppl 2: S285-290. doi:10.2337/dc11-s239

179. Alvarado-Moreno JA, Hernandez-Lopez R, Chavez-Gonzalez A, Yoder MC, Rangel-Corona R, Isordia-Salas I, et al. Endothelial colony-forming cells: Biological and functional abnormalities in patients with recurrent, unprovoked venous thromboembolic disease. Thromb Res. 2016;137: 157–168. doi:10.1016/j.thromres.2015.11.005

180. Versteeg HH, Heemskerk JWM, Levi M, Reitsma PH. New Fundamentals in Hemostasis. Physiol Rev. 2013;93: 327–358. doi:10.1152/physrev.00016.2011

181. Roumenina LT, Rayes J, Frimat M, Fremeaux-Bacchi V. Endothelial cells: source, barrier, and target of defensive mediators. Immunol Rev. 2016;274: 307–329. doi:10.1111/imr.12479

182. Hansen NW, Hansen AJ, Sams A. The endothelial border to health: Mechanistic evidence of the hyperglycemic culprit of inflammatory disease acceleration. IUBMB Life. 2017;69: 148–161. doi:10.1002/iub.1610

183. Borghesi A, Garofoli F, Cabano R, Tzialla C, Bollani L, Stronati M. Circulating endothelial progenitor cells and diseases of the preterm infant. Minerva Pediatr. 2010;62: 21–23.

CURRICULUM VITAE

Kaela Margaret Varberg

EDUCATION

2012 B.S. Biochemistry; Minor: Physics of Medicine
Rockhurst University
Kansas City, MO

2017 Ph.D. Physiology; Minor: Life Science
Indiana University
Department of Cellular & Integrative Physiology
Indianapolis, IN
Mentor: Laura S. Haneline, M.D.

Doctoral Dissertation
Kinetic Analyses of Vasculogenesis Inform Mechanistic Studies

Research Committee

Laura S. Haneline, M.D. – Professor, Indiana University School of Medicine, Department of Cellular & Integrative Physiology

Matthias A. Clauss, Ph.D. – Professor, Indiana University School of Medicine, Department of Cellular & Integrative Physiology

Richard N. Day, Ph.D. – Professor, Indiana University School of Medicine, Department of Cellular & Integrative Physiology

Maureen A. Harrington, Ph.D. – Professor, Indiana University School of Medicine, Department of Biochemistry

Edward F. Srour, Ph.D. – Professor, Indiana University School of Medicine, Department of Microbiology and Immunology

RESEARCH FUNDING

Fellowships

2014-2017 NIH T32 Training Grant Fellowship "Basic Science Studies on Gene Therapy of Blood Diseases"

Grants

National Heart, Lung, and Blood Institute of The National Institutes of Health under Award # T32 HL007910

TEACHING EXPERIENCE

Lectures

Biology of Women N200, IUPUI, Indianapolis, IN (Fall 2015)

Service/Outreach

Program Leader; Girls, Inc., Indianapolis, IN (2016)
Lab Volunteer; Susan G. Komen Tissue BioBank, Indianapolis, IN (2015-2017)
Student Mentor; IBMG Program, Indiana University School of Medicine Graduate Division, Indianapolis, IN (2013-2017)
Student Ambassador; IBMG Recruitment, Indiana University School of Medicine Graduate Division, Indianapolis, IN (2013-2017)

Mentoring

Undergraduate Lab Assistant, Biology Department, Indiana University-Purdue University Indianapolis, Indianapolis, IN (2015-2017)
Bioengineering Undergraduate Student, Summer Research Program, Indiana University School of Medicine, Indianapolis, IN (Summer 2014)

PROFESSIONAL ORGANIZATIONS

Memberships

American Physiological Society, 2016-present
North American Vascular Biology Organization, 2016-present
Indiana Physiological Society, 2015-present
International Society for Experimental Hematology, 2014-2015

PUBLICATIONS

Manuscripts

1) K. Varberg, R. Garretson, E.K. Blue, L.S. Haneline. Elevated Transgelin1 is sufficient to induce dysfunction in endothelial colony forming cells from gestational diabetic pregnancies. 2017. In preparation.

2) K. Varberg, S. Winfree, C. Chu, W. Tu, E.K. Blue, C. Gohn, K.W. Dunn, L.S. Haneline. Kinetic analyses of vasculogenesis inform mechanistic studies. 2017. Am. J. Physiol. Cell Physiol. PMID 28100488

3) C. Gohn, E.K. Blue, B. Sheehan, **K. Varberg**, L.S. Haneline. Mesenchyme Homeobox 2 enhances migration of endothelial colony forming cells exposed to intrauterine diabetes mellitus. 2016. J. Cell. Physiol. PMID 27966787

4) E.K. Blue, B. Sheehan, Z. Nuss, F. Boyle, C. Hocutt, C. Gohn, **K. Varberg**, J. McClintick, L.S. Haneline. Epigenetic regulation of PLAC8 contributes to altered function of endothelial colony forming cells exposed to intrauterine gestational diabetes mellitus. 2015. Diabetes. 64(7):2664-75. PMID 25720387

PRESENTATIONS

Oral Presentations

1) **Varberg, K.**, Winfree, S., Chu, C., Tu, W., Blue, E.K., Gohn, C., Dunn, K.W., Haneline, L.S. (2016, February). Kinetic Vasculogenic Analyses of Endothelial Colony-Forming Cells. Oral presentation, 6th Annual Meeting of the Indiana Physiological Society, Greencastle, IN

Poster Presentations

1) **Varberg, K**., Naida, R., Blue, E.K., Haneline, L.S. (2016, October). Elevated Transgelin 1 reduces function of gestational diabetes mellitus exposed neonatal endothelial colony forming cells. Poster presented at the International Vascular Biology Meeting, Boston, MA.

2) **Varberg, K**., Winfree, S., Chu, C., Blue, E.K., Gohn, C., Dunn, K.W., Haneline, L.S. (2016, October). Kinetic vasculogenic analyses of endothelial colony forming cells exposed to intrauterine diabetes. Poster presented at the Developmental Origins of Health and Disease, Detroit, MI.

3) **Varberg, K**., Naida, R., Blue, E.K., Haneline, L.S. (2016, May). Elevated Transgelin 1 reduces function of gestational diabetes mellitus exposed neonatal endothelial colony forming cells. Poster presented at the Riley Hospital for Children Pediatric Scholars Day, Indianapolis, IN.

4) **Varberg, K**., Naida, R., Blue, E.K., Haneline, L.S. (2016, April). Elevated Transgelin 1 reduces function of gestational diabetes mellitus exposed neonatal endothelial colony forming cells. Poster presented at the IUPUI Research Day, Indianapolis, IN.

5) **Varberg, K**., Winfree, S., Chu, C., Blue, E.K., Gohn, C., Dunn, K.W., Haneline, L.S. (2016, February). Kinetic vasculogenic analyses of endothelial colony forming cells exposed to intrauterine diabetes. Poster presented at the Indiana Physiological Society Annual Meeting, Greencastle, IN.

6) **Varberg, K**., Haneline, S. (2015, February). Inflammation and diabetes: The impact on vascular progenitor cells in angiogenesis. Poster presented at the Indiana Physiological Society Annual Meeting 2015, Indianapolis, IN.